Development of a parametric model to distinguish between specific tissue types

For the application in a radiofrequency ablation catheter

by

L.C. Mulder

A Master Thesis in partial fulfillment of the requirements for the degree of

Master of Science
In Mechanical Engineering

at the Delft University of Technology,
Department of BioMechanical Engineering

May 9, 2022

Daily Supervisor:	Prof. Dr. B.H.W. Hendriks
Graduation Committee:	Prof. Dr. J. Dankelman
	Dr. M. Jelvehgaran Esfahani

Preface

This Master Thesis is written to obtain a Master of Science in Mechanical Engineering at the Delft University of Technology. My interest in medical technology and my eagerness to learn new things lead me to choose the topic addressed in this Master Thesis. In addition to that, I wanted to do something that had the potential to be later used in a real application. Approximately one year of hard work lead to the accomplishment of this Master Thesis. The entire project was one big learning process. I got to enhance skills such as academic writing, problem solving and gained specific knowledge about impedance spectroscopy and parametric modelling. Furthermore, I gained practical skills by performing impedance measurements on real porcine hearts.

During my research, I have had support from various people, whom I would like to thank. First of all, I would like to thank my supervisor Prof. Dr. B.H.W. Hendriks for the supervision, guidance and help in defining my goals. In addition, I would like to thank Prof. Dr. J. Dankelman for the feedback and for being part of my graduation committee. Furthermore, I would like to thank Dr. M. Jelvehgaran Esfahani for explaining to me how to work with the impedance analyzer and S. Azizian Amiri for making the electrosurgical knife available. Lastly, I would like to thank my family and friends for supporting me throughout my entire thesis.

Larissa Mulder
Delft, May 2022

Abstract

In the Netherlands, 362.000 people suffered from atrial fibrillation in 2019. During a catheter intervention, the tissue that causes atrial fibrillation is destroyed by heat generated by an alternating current exerted from an ablation catheter. Two problems of this treatment are over-ablation of the heart tissue and the non-contingent surrounding of scar tissue around the pulmonary veins. Better surgical outcomes can be obtained if an extra imaging technique is added to prevent these problems from occurring. Impedance spectroscopy has potential, it is already widely used for measurements and food characterization and it enables the measurement of the distinct dielectric properties and impedance of different tissue types. Based on the dielectric properties and impedance, different tissue types can be distinguished from each other and the surgeon can adapt his procedure according to this information.

The goal of this Master Thesis is to distinguish different tissue types in the radiofrequency range with impedance spectroscopy during a cardiac ablation procedure. Impedance data for this Master Thesis are gathered via impedance measurements on three porcine hearts with two-needle electrodes over a frequency range from 100 Hz to 1 MHz. Ablated lesions are created with an electrosurgical knife in fulguration and pure cut mode. To distinguish between different tissue types with impedance spectroscopy there is a need for a parametric model that can parameterize the impedance spectra. This enables the comparison of different tissue types based on a couple of parameters instead of a complete spectrum. A parametric model is fitted to the measured impedance spectra and the resulting best-fit parameters are evaluated. The parametric model that is used is a series combination of a CPE model and a two-pole Cole impedance model. The CPE model models the electrode polarization contribution to the impedance spectrum. This way no a-priory knowledge regarding the electrode polarization is needed. The two-pole Cole impedance model models the tissue contribution to the impedance spectrum.

In the measurements that are performed in this Master Thesis, an increase in impedance is seen after ablation. The differences between the healthy and ablated measurements are mostly described by (significant) differences in the parameters of the CPE model (K and m) and the second Cole term (R_2, t_2 and a_2). The mean values of R_2 and a_2 increased after ablation, while the values of t_2, K and m decreased after ablation for most measurements. Classification of healthy and ablated tissue is performed based on a formula consisting of a combination of these model parameters. The sensitivity and specificity are both around the 80%. This classification serves as a first impression, with the results indicating that discrimination of healthy from ablated tissue is possible with parametric modeling.

Contents

Nomenclature

AF	Atrial fibrillation
ANOVA	Analysis Of Variance Test
CM	Cell membrane
CPE	Constant phase element
dRC	Distributed RC
ECF	Extracellular fluid
EEC	Electrical equivalent circuit
EP	Electrode polarization
FN	False negative
FP	False positive
ICF	Intracellular fluid
LA	Left atrium
LV	Left ventricle
MSE	Mean Squared Error
NPV	Negative predictive value
PPV	Positive predictive value
RF	Radiofrequency
TN	True negative
TP	True positive

List of Figures

List of Tables

1 Introduction

Atrial fibrillation (AF) is the most common type of arrhythmia. An AF results in a very fast and irregular heartbeat. 362.700 people suffered from an AF in the Netherlands in 2019 alone and in 2020 81 people a day were hospitalized as a result of AF [1]. In the United States, this number is even higher, in 2010 there were 5.1 million cases and this number is estimated to be twice as high by 2030 [2]. If an AF is left untreated it can lead to heart failure, stroke or even death [3].

Often, AF can be treated with radiofrequency ablation. During this medical intervention, the heart structure that is causing the irregular and fast heartbeat is destroyed by an ablation catheter exerting radiofrequency energy. The ablation catheter is guided to the heart via the femoral veins [4]. It is of great importance that all heart tissue with abnormal electrical activity is destroyed, to prevent the arrhythmia from returning. At the same time, no excessive tissue must be destroyed since this can damage surrounding structures such as the esophagus and the major nerves [4][5][6].

1.1. Problem statement

Currently, it is still a challenge to ablate the correct amount of heart tissue during the treatment of AF [6]. Furthermore, the patient is exposed to radiation during the intervention for the tracking of the catheter. To obtain better surgical outcomes, a real-time imaging technique that can follow the lesion formation and distinguish between different tissue types is required. Impedance spectroscopy might be a promising technique. It is already widely used in other fields and it enables the measurement of tissue's distinct dielectric properties [7][8]. Changes in tissue's condition lead to changes in the impedance and dielectric properties of the tissue [8][9]. To distinguish between different tissue types with impedance spectroscopy there is a need for parametric models that can parameterize the impedance spectra. This enables the comparison of the different tissue types based on a couple of parameters instead of the complete spectrum [10]. According to a literature study by Mulder (2021), there is currently no model that is directly suited for the application in a cardiac ablation procedure [11]. Therefore, a parametric model is needed for the description of the impedance spectra of heart tissue.

1.2. Objective

As a first step of the implementation of impedance spectroscopy, for the distinction between different tissue types during a cardiac ablation procedure, the main research question of this Master

Thesis is:

'How can different tissue types be distinguished in the radiofrequency range with impedance spectroscopy during a cardiac ablation procedure?'

To obtain an answer to this main question, three sub-questions will be answered:

1. How can the impedance of heart tissue be modelled?
2. Can different parts of the heart be distinguished from each other with modelling?
3. How can healthy and ablated heart tissue be distinguished with modelling?

1.3. Thesis outline

To obtain an answer to the main and sub-questions, this master thesis has been separated into seven chapters.

Chapter 2. Theory
The second chapter contains the background information that is required for this Master Thesis. This information is gathered during a previously performed literature study. The theory is divided into four sections: the clinical picture and intervention of atrial fibrillation, an introduction to impedance and the dielectric properties of tissue, an overview of parametric impedance models and background information on fitting techniques.

Chapter 3. Methodology
Chapter three elaborates on the methods that are used in this Master Thesis. It is divided into the measurement methodology, the fitting methodology and the classification methodology.

Chapter 4. Parametric description of heart tissue
In this chapter, parametric models for the description of tissue regarding the ablation procedure for the treatment of atrial fibrillation are evaluated. In the end, the optimal model combination for the description of heart tissue is determined.

Chapter 5. Measurements and results
In this chapter, the measurements of porcine hearts for the collection of impedance data are discussed. The parametric model that is found to be most promising according to chapter four will be used for the modelling of the measured impedance spectra. The best-fit parameters are evaluated and a classification is performed to conclude about the discrimination between healthy and ablated tissue.

Chapter 6. Discussion and recommendations
This chapter contains the discussion and recommendations for future research.

Chapter 7. Conclusions
This final chapter includes the most important conclusions of this Master Thesis.

2

Theory

Previous to this Master Thesis a literature study has been performed [11]. The conclusions of this literature study together with important theoretical background information are given in this chapter [1]. Firstly, an in-depth explanation is given about the disease and the corresponding intervention that are the reason for this research. Then, the concept of impedance (spectroscopy) and dielectric properties is discussed, as these form the basis on which different tissue types will be distinguished. Furthermore, the parametric models that can be used for the description of these properties are discussed. Lastly, background information on fitting techniques is given.

2.1. Clinical picture and intervention

A cardiac arrhythmia is an abnormality or perturbation of the heart rhythm [3]. There are many types of cardiac arrhythmias ranging from benign to very serious. One of the most common types is atrial fibrillation (AF). AF can be treated with a cardiac ablation intervention. However, this intervention has some shortcomings. This section consists of three parts. First, the anatomy of the heart is briefly explained. Then a detailed explanation of atrial fibrillation is given. This is followed by an explanation of the cardiac ablation intervention and its shortcomings.

2.1.1. Anatomy of the heart

The locations of the left ventricle (LV) and left atrium (LA) are displayed in figure 2.1. The left ventricle consists of a thick myocardial wall that consists of branches of myocytes resulting in a complex three-dimensional fibrous network with an anisotropic structure. The inside of the ventricle consists of irregular trabeculae. These trabeculae are muscular ridges of myocytes. The mitral valve is a fibro collagenous surface that separates the left ventricle from the left atrium. It is connected to the papillary muscle by chordae tendineae. The papillary muscles are bulges from the ventricular wall, while the chordae tendineae are cords of fibrous inelastic tissue [12]. The inside of the ventricle is thus a nonflat surface.

The left atrium is muscular consisting of myocardial fibers with alternating thickness. The inner layer of the myocardium (endocardium) is smooth. The outer layer of the myocardium (epicardium) is covered with fatty tissue [13]. The left atrium has a left atrial appendage that consists of muscle bundles. The pulmonary veins are connected to the left atrium and this area contains fibro-fatty tissue [14]. The left and right atrium are separated by the atrial septum.

[1] This chapter has been (partly) graded before

2.1.2. Atrial fibrillation

In a healthy heart, the blood flow is regulated by the contraction of the four heart chambers. These contractions are regulated by a circuit of electrical impulses that are sent out by the sinus node at the start of every heartbeat. An electrical impulse from the sinus node leads to contraction of the atria (upper chambers of the heart). Resulting in blood flow to the ventricles (lower chambers of the heart). Meanwhile, the electrical impulse reaches the atrioventricular node that delays the signal to give the ventricles time to fill with blood. Later the signal is sent to the ventricles resulting in contraction and a blood flow leaving the heart [15]. See figure 2.1a for a visualization of this circuit of impulses.

During atrial fibrillation (AF), parts of the heart with abnormal conductivity disturb the heart rhythm by chaotic circuits of impulses. This leads to fast and uncoordinated contractions of the atrium [16]. These chaotic circuits can have three main causes: cells with enhanced automaticity, triggered activity or re-entry circuits [3]. The groups of cells in the heart with enhanced automaticity are called ectopic foci. These sites can send up to 600 impulses per minute. The AV-node filters out most of these signals and the heartbeat does not transcend 150 beats per minute. Ectopic foci are often located in the atrial muscle and around the pulmonary veins. Re-entry circuits, for example, lead to an impulse not leaving the right atrium. The normal and disturbed circuits of electrical impulses are shown in figure 2.1b.

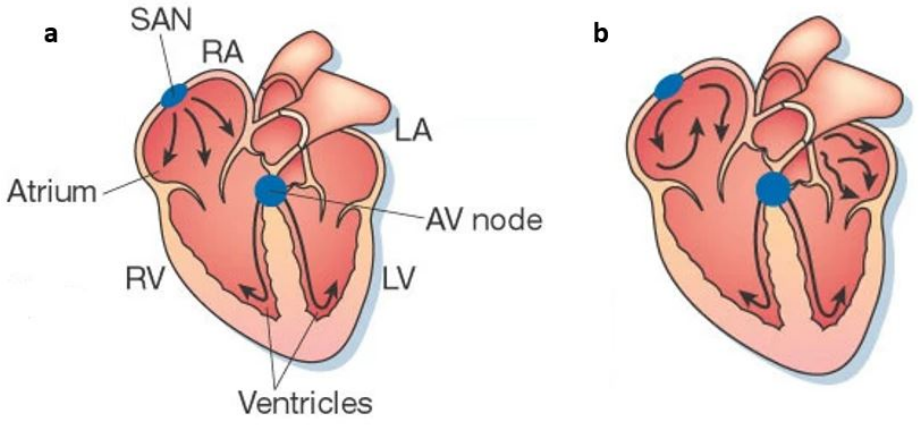

Figure 2.1: Impulses during a normal (**a**) and a disturbed (**b**) heart rhythm [17]

2.1.3. Cardiac ablation intervention

Atrial fibrillation can be treated with a cardiac ablation intervention. There are other treatment options as well, but advantages of cardiac ablation over these treatments are: no need for exercise restrictions after the intervention, no chronic drugs use and fewer break-through episodes resulting in fewer hospital visits [18].

Radiofrequency ablation is a common procedure for the treatment of AF. During this intervention, an ablation catheter is placed in the heart via the femoral veins. It is brought in direct contact with the parts of the heart that disturb the electrical circuit of impulses. Radiofrequency energy, with a frequency ranging from 1 kHz to 1 MHz, is exerted by electrodes on the catheter [6]. The exerted radiofrequency energy increases the tissue temperature to approximately 100 degrees, resulting in permanent tissue damage [19]. This is called ablation. There are different ablation patterns as can be seen in figure 2.2. Such as pulmonary vein ablation (i), where the pulmonary veins are isolated

as these are areas with a high amount of enhanced automaticity. Compartmentalization of the left and right atrium (ii) can be used to suppress reentry circuits. Specific cells responsible for reentry circuits or with enhanced automaticity can be ablated separately as well (iii).

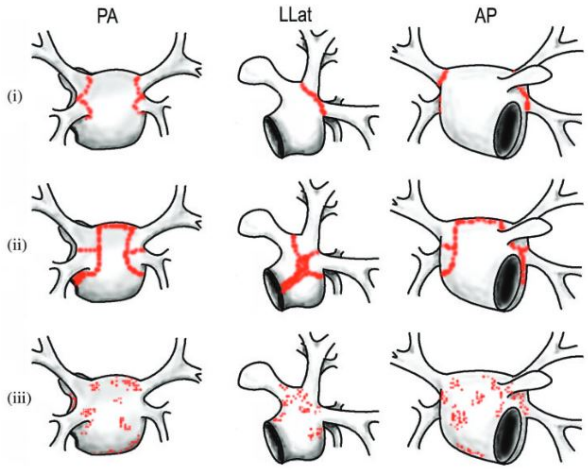

Figure 2.2: Ablation patterns in the heart for the treatment of atrial fibrillation [6]

To map the location of the ablation catheter during the intervention, mapping catheters are inserted into the heart to track the location of the ablation catheter. Current methods that are used for this tracking are: fluoroscopic imaging [20], intracardiac echocardiography [21], electroanatomical mapping systems, dielectric imaging, sometimes in combination with an MRI or CT scan previous to the intervention [22].

It is important that the correct tissue area is destroyed but several problems can occur. Firstly, not all abnormal heart tissue may be ablated, for example by the non-contiguous surrounding of the pulmonary veins. This can lead to a recurrence of the AF. Secondly, ablation of excessive heart tissue is undesired as this results in damage to the normal electrical system of the heart. Lastly, critical structures such as the esophagus can be damaged during the intervention. For better surgical outcomes there is a need for a real-time imaging technique to prevent these problems from occurring. Impedance spectroscopy might have potential as it enables the measurement of dielectric properties of tissue. Based on the dielectric properties, different tissue types can be distinguished from each other. This can be used for the recognition of critical structures and to follow the lesion formation during the intervention.

2.2. Impedance and dielectric properties

This section gives background information about impedance and the dielectric properties of tissue, the application in electrical impedance spectroscopy and the occurrence of electrode polarization.

2.2.1. Impedance and dielectric properties of tissue

On the macroscopic level, tissue consists of conductors and capacitors. This is a result of the structure of the tissue. It consists of combinations of cells that have a similar function. These cells have an intracellular fluid (ICF), sometimes including cell organelles and are surrounded by a cell membrane (CM). All cells are located within the extracellular fluid (ECF) [23]. Both the ICF and the ECF are composed of electrically conducting materials and therefore act as conductors. The CM consists

of two layers of conducting proteins that are separated by an insulating layer. It is not conducting as it is impermeable to ions but it contains proteins that can transport particles across the membrane [24]. The CM causes charge separation and acts as a capacitor. Besides cells, tissue consists of free charges and dipole molecules. In the presence of an electric field, the free charges move until they are blocked or until the interior electric field is zero. Dipoles cannot move freely but they rotate under the presence of an electric field to align their charge centers. The rotation of dipoles creates a polarization of the material and results in an opposing electric field [8]. The net electric field reduces due to this opposing electric field and this reduction is characterized by the relative permittivity (ϵ_r).

Tissue can be described with its dielectric properties (including conductivity and permittivity). These properties determine the response of a tissue to an applied electric field and can change due to pathological conditions. Conductivity is the ability to transport charges and permittivity is the ability to store charges or to rotate dipole molecules. They can both be measured in terms of changes in the impedance. The complex impedance is the frequency-dependent resistance to an AC current flow. When a DC current is used, only the resistance is taken into account. This gives a distorted vision as tissue is not purely resistive. The complex impedance consists of a real and an imaginary part, as can be seen in equation 2.1. According to Naranjo-Hernández (2019) [25]: 'R is described as the opposition of the medium to the flow of electric current and is inversely proportional to the conductance and X can be defined as the opposition of the medium to a change in electric current'.

$$Z = R_s + jX_s, \quad C_s = -\frac{1}{\omega X_s} \tag{2.1}$$

The reciprocal of the impedance is the admittance (Y), see equation 2.2. The admittance consists of the conductance (G) and susceptance (B) that can be rewritten into the capacitance (C). These terms can be rewritten into the conductivity and relative permittivity with the electrode configuration.

$$Y = G_p + jB_p, \quad C_p = \frac{B_p}{\omega} \tag{2.2}$$

Both conductivity and permittivity are complex values and these are written as σ^* and ϵ^* respectively. The equations for the complex conductivity and permittivity are given in equations 2.3 and 2.4. ϵ' (also ϵ_r) is called the relative permittivity or dielectric constant and this represents the ability of a tissue to store energy. ϵ" indicates the dielectric losses, i.e. the dissipation of energy into heat by frictional motion of the charge carrying elements [26].

$$\sigma^* = (\sigma + j\omega\epsilon) = j\omega\epsilon^* \tag{2.3}$$

$$\epsilon^* = \epsilon' - j\epsilon" = \epsilon_r - \frac{j\sigma}{\omega\epsilon_0} \tag{2.4}$$

2.2.2. Application in electrical impedance spectroscopy

Electrical impedance spectroscopy is a technique that can be used to gain knowledge about cells and tissues by measuring the complex impedance over a range of frequencies, resulting in an impedance spectrum. This is relevant as the impedance and dielectric properties are frequency-dependent.

During impedance spectroscopy, a small amplitude AC current is applied and the voltage over the electrodes is measured. The impedance, Z(f), can then be calculated by dividing the measured voltage, V(f), by the applied current, I(f) [11].

Frequency dependence

The frequency dependence of the relative permittivity is called a dispersion [8]. Depending on the tissue type multiple dispersion regions can be distinguished. A dispersion region is characterized as a gradual decrease in permittivity as the frequency increases and is caused by a polarization mechanism with a single time constant (the relaxation time). However, dispersion regions can be extended due to the contributions of multiple relaxation mechanisms. The relaxation time represents the delayed polarization because polarization does not always occur instantaneously [24]. For electrons and small dipoles, it happens faster than for interfacial polarization. In figure 2.3, the frequency dependence of the conductivity and permittivity is shown. The conductivity increases as the frequency increases. Because charge carriers travel smaller distances at higher frequencies resulting in a lower chance to get trapped at interfaces and the cell membrane becomes conductive for high frequencies. The permittivity decreases as the frequency increases, due to the inability of tissues to react to the quick changes of the electric field [8].

By measuring the impedance over a wide frequency range, phenomena that are dominating in certain frequency ranges can be characterized with impedance spectroscopy [7]. Three main dispersion regions can be distinguished for biological tissues. Firstly, the α-dispersion is present from Hz till kHz and is caused by the counterion polarization that surrounds the cell membranes. Secondly, the β-dispersion occurs in the frequency range from 10 kHz to 100 MHz and is caused by the polarization of the cell membranes and the formation of electric double layers at the membrane surfaces. Thirdly, the γ-dispersion occurs in the GHz range and is due to the polarization of water molecules. Each of these dispersion regions is indicated in figure 2.3. The γ-dispersion is sometimes followed by a smaller δ-dispersion because of bound water molecules and cell organelles [27].

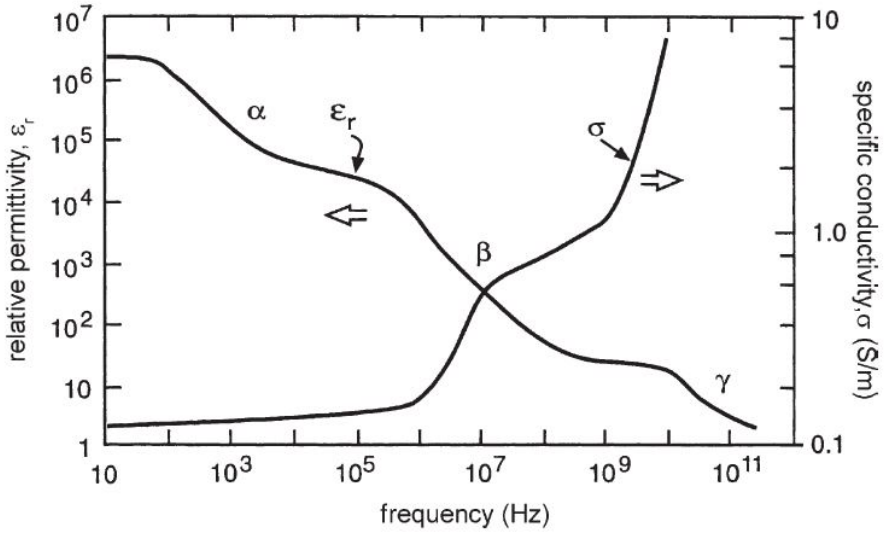

Figure 2.3: Frequency dependence of the dielectric properties and impedance, three dispersion regions are visible: α-, β- and γ-dispersion [8]

Rewriting impedance data

The impedance can be represented by a series or parallel equivalent circuit. Both representations can be measured with an impedance analyzer. The series impedance parameters are the resistance (R_s) and reactance (X_s) as given in equation 2.1. The parallel impedance parameters are the capacitance (C), susceptance (B) and conductance (G) as given in equation 2.2. It does not matter which parameters are measured because they can be rewritten into each other. In this Master Thesis, the series mode is used. The output of the series mode is the complex impedance. In this mode, the modulus and angle of the impedance are measured. These values are rewritten into the real and imaginary part of the impedance according to the rules for a complex number. These rules are given in equations 2.5, 2.6 and 2.7.

$$Z = a + b \cdot j \tag{2.5}$$

$$a = Re(Z) = cos(\angle Z) \cdot |Z| \tag{2.6}$$

$$b = Im(Z) = sin(\angle Z) \cdot |Z| \tag{2.7}$$

2.2.3. Electrode polarization

Electrode polarization (EP) is a phenomenon that occurs in the low-frequency range. It is caused by the accumulation of free charges from the sample around the measuring electrodes. This leads to the formation of ionic double layers on the electrode surface that act as capacitors. These capacitors result in an electrode impedance. This electrode impedance can be 10^6 times larger than the tissue impedance and can therefore mask the latter completely in the low-frequency range. Both impedances interfere with each other and this is undesired. The frequency range that is affected by EP and the amount of EP that is present depend on several factors. These factors are among others: the measured sample, the electrode properties such as material, radius, structure, surface and shape, the electrode distance, the temperature and the current density [28][29][30][31][32]. Samples with high conductivity have more pronounced electrode polarization, this is also the case for electrodes with a smaller radius [28].

2.2.4. Frequency range affected by electrode polarization

The electrode polarization must be removed from the impedance spectrum completely without influencing the impedance of the tissue itself. Therefore, it is necessary to know the frequency range in which the electrode polarization is present.

Electrode polarization range according to literature

Electrode polarization is present up to higher frequencies in measurements on (high conductive) cell suspensions than it is in samples with a lower conductivity such as tissue. Muscle is a tissue with an intermediate conductivity in comparison to other tissue types [8].

According to Sanchez et al. (2011), electrode polarization influences the measurements of cardiac tissue below 1 kHz, when measuring in a four-electrode configuration with platinum-iridium electrodes [33]. Miklavcic et al. (2006) mention the same influence for the measurement of in vivo tissue when measuring in a two-electrode configuration with platinum electrodes [8]. Gabriel et al. (1996) mention that the effects of electrode polarization are present up to 1 kHz and are significant below 100 Hz when the data is measured with a coaxial probe [34]. Teixeira et al. (2020) mention that a four-electrode configuration circumvents electrode polarization at frequencies below 1 kHz

in impedance spectra of tissue [35]. According to Stoneman et al. (2007), electrode polarization influences the measurements of tissue from 1 Hz up to 1 MHz when measuring with two coaxial platinum electrodes [36]. For cell suspensions, the frequency range for electrode polarization is assumed to be higher. According to Miklavcic et al. (2006), the spectrum of a cell suspension is affected by electrode polarization up to 100 kHz [8]. Bordi et al. (2001) mention slightly higher affected frequencies of 100 kHz till 1 MHz [30]. According to Wolf et al. (2011), the affected frequencies range up to the MHz range for biological matter and up to 1 MHz for blood plasma [31]. According to Zhuang et al. (2011), the spectra of the relative permittivity and the conductivity of conductive cell suspensions are affected by electrode polarization up to 1 MHz and 100 kHz, respectively [32]. Chassagne et al. (2016) assume that electrode polarization is typically present up to 100 kHz for electrolyte solutions [37]. There can be concluded that there is a wide frequency range up to which the electrode polarization might be present in a measured spectrum. For tissue, the limit ranges from 1 kHz up to 1 MHz.

Impedance plateau of heart tissue
Measured spectra of porcine heart tissue in a two-electrode configuration are investigated and compared to data in the literature to investigate the influence of electrode polarization. In the data, there are steep increases and decreases visible in the low-frequency range before the data reaches an approximately stable value. These increases and decreases are not visible in the data from literature where the electrode polarization is partly removed. The large peaks in the low-frequency range of the measured data are present up to approximately 1 to 50 kHz. The real part of the impedance is affected up to lower frequencies than the imaginary part of the impedance.

Conclusion frequency range influenced by electrode polarization
The frequency range in which there must be accounted for electrode polarization ranges from 100 Hz to approximately 50 kHz. This is the range where the data show large peaks in comparison to the literature. These peaks in impedance, permittivity and conductivity values can be assigned to electrode polarization. After this frequency range, a plateau with the tissue impedance is assumed to be left. It is complex to compare the exact values of these plateaus because the amount of EP shows a large difference between locations. Also, the influence of the electrode polarization is not equal for all variables.

2.3. Parametric models for the description of impedance

During impedance spectroscopy, the impedance or dielectric properties are measured over a range of frequencies resulting in a measured spectrum. Instead of this spectrum, it is desired to describe the tissue according to a couple of parameters. This way all information of the impedance spectrum is summarized by a couple of parameters. The spectrum can be parameterized by the fitting of a parametric model to the measurement data.

In this section, an overview of the most promising parametric models according to the literature study by Mulder (2021) is given [11]. The parametric models are separated into the general parametric models and the approaches for the elimination of electrode polarization.

2.3.1. Overview of general parametric models

General parametric models are models that describe the impedance or dielectric properties of tissue. These models can be divided into different categories: the theoretical models, the cell models,

the mixture equations, the equivalent circuits and others. An extended overview of these models is given in a literature study by Mulder (2021) [11]. In this section, only the parametric models that are of most interest for the application in a cardiac ablation procedure are discussed. However, none of these models is directly suited for the implementation in an ablation catheter.

Cole-Cole model The Cole-Cole model is a widely known theoretical model that describes the dielectric relaxations in tissue and other media. A distribution parameter α accounts for distribution of relaxation times and thus a broadening of the dispersion curve. The model describes the relative permittivity, as can be seen in equation 2.8. The parameters have the following meaning: ϵ_0 is the permittivity of free space, ϵ_s is the permittivity at a low-frequency ($\omega\tau \ll 1$), ϵ_∞ is the permittivity at a very high frequency ($\omega\tau \gg 1$), ω is the angular frequency, τ is the relaxation time and σ_i is the static ionic conductivity. The Cole-Cole model is a very promising theoretical model. According to Gabriel et al. (1996) the (four-pole) Cole-Cole model can describe a wide variety of tissues and blood in the frequency range from 10 Hz - 100 GHz [10]. The data by Gabriel et al. (1996) are often used as a reference for the suitability of other models [10]. The measured frequency range has a great impact on the choice of a model because this relates to the number of dispersion regions that will be present. Often tissue is more appropriately described by a multi-pole Cole-Cole model.

$$\hat{\epsilon} = \epsilon_\infty + \frac{\epsilon_s - \epsilon_\infty}{1 + (j\omega\tau)^{(1-\alpha)}} + \frac{\sigma_i}{j\omega\epsilon_0} \tag{2.8}$$

Debye model The Debye model is a simplification of the Cole-Cole model and is given by equation 2.9. Multiple papers state that the Debye model cannot describe blood in the frequency range below 1 MHz [31][38]. However, Simicevic and Haynie (2005) contradict this by mentioning that blood can be described with a Debye model in the frequency range from 100 kHz to 100 GHz [39]. Tissue types such as muscle and fat can be described with a multi-pole Debye model in the frequency range from 10 Hz to 10 GHz [40].

$$\hat{\epsilon} = \epsilon_\infty + \frac{\epsilon_s - \epsilon_\infty}{1 + j\omega\tau} + \frac{\sigma_i}{j\omega\epsilon_0} \tag{2.9}$$

Raicu model The Raicu model is used to represent any polarization mechanism in the audio and radiofrequency range. The proposed formula for the complex permittivity is shown in equation 2.10. λ, μ and ν are real constants with a value between 0 and 1 [41]. For choosing specific values of these parameters, this model can be simplified to a Debye, Cole-Cole or Cole-Davidson model [42]. According to Raicu (1999), this is the most general formula and it can properly simulate the low and high frequencies of a frequency range [42]. The model can be used with good accuracy over a wide frequency range (several kHz to 100 MHz) for different tissue types.

$$\epsilon* = \epsilon_\infty + \frac{\Delta\epsilon}{[(j\omega\tau)^\lambda + (j\omega\tau)^{1-\mu}]^\nu} + \frac{\sigma_i}{j\omega\epsilon_0} \tag{2.10}$$

Cole impedance model The Cole impedance model is the impedance version of the Cole-Cole model. It describes a single ideal dispersion by equation 2.11. Z is the impedance, R_∞ is the resistance at a very high frequency, R_0 is the resistance at a very low-frequency, ω is the angular

frequency, τ is the characteristic time constant and α is a constant. As long as α is constant, $(j\omega\tau)^{\alpha}$ represents a CPE model [43]. The value for α varies between 0 and 1, the smaller the value the wider the dispersion region [44]. The Cole impedance model is able to describe a suspension of erythrocytes in the frequency range from 100 kHz to 1 MHz [45].

$$Z = R_{\infty} + \frac{R_0 - R_{\infty}}{1 + (j\omega\tau)^{\alpha}} \tag{2.11}$$

Shunting-C model This model is part of the equivalent circuits and it is made with a focus on the modelling of blood. The basis of this model is the Fricke equivalent circuit. A shunting capacitor is added to this circuit to describe blood more accurately [46]. The shunting-C model is shown in figure 2.4a. According to Zhbanov and Yan (2017), the circuit can describe blood in the frequency range from 40 Hz to 110 MHz [46].

Zhbanov model This model is part of the equivalent circuits. It is an extension of the shunting-C model as a parallel combination of a resistor and a capacitor is added to eliminate the stray capacitance and electrode polarization effect. The circuit is shown in figure 2.4b. Zhbanov and Yan (2017) mention that the model can accurately describe blood in the frequency range from 40 Hz to 110 MHz [46]. In equivalent circuits, it is quite simple to add new elements to describe the tissue more adequately. The Fricke and Lapicque equivalent circuits are basic equivalent circuits that are not able to model tissue on their own. However, an extended version of these equivalent circuits might be able to describe tissue accurately. Both models should therefore be considered and are shown in figure 2.4.

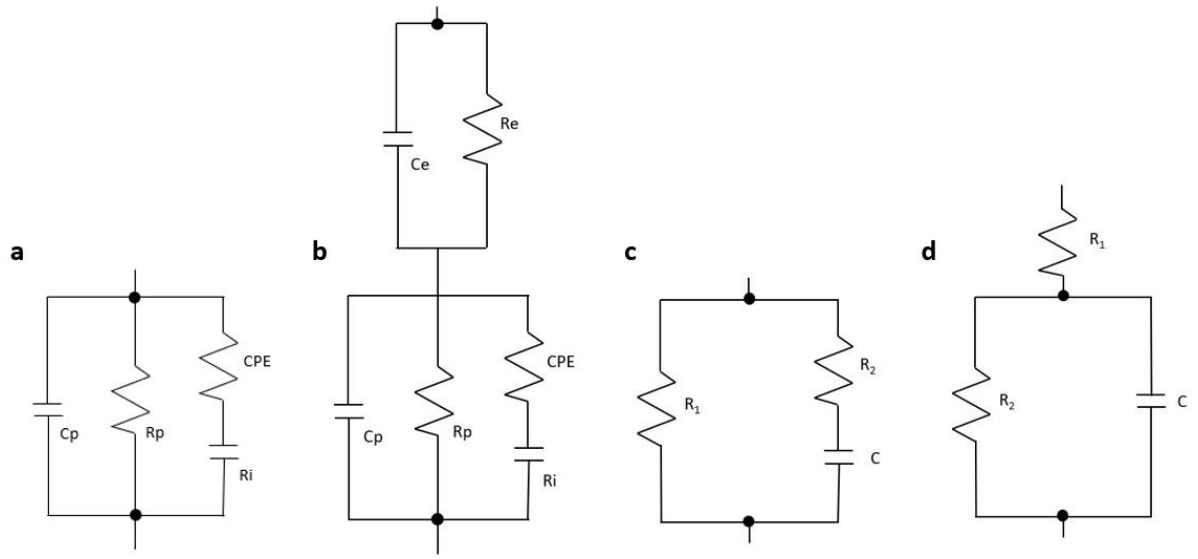

Figure 2.4: Electrical equivalent circuits for the description of tissue: EEC of the shunting capacitor model (**a**), Zhbanov model (**b**), Fricke model (**c**) and Lapicque model (**d**) [47][48]

2.3.2. Overview of electrode polarization approaches

Electrode polarization (EP) covers the tissue impedance in the low-frequency range as is explained in subsection 2.2.3. It can be removed either via a hardware modification or a theoretical approach. None of these methods completely removes the EP effect. In this section, only the approaches that

are of most interest for the application in a cardiac ablation procedure are discussed. A more complete overview of other approaches can be found in the literature study by Mulder (2021) [11].

Hardware modifications
Hardware modifications can be separated into comparison methods and self-correction methods. For the application in a cardiac ablation procedure, self-correction methods are preferred over comparison methods. Comparison methods are undesired as they might need to be repeated between all interventions due to alterations in the sample or changes in the electrode surface which makes it time-consuming. Two self-correction methods of interest are the four-electrode configuration and the choice of a specific electrode material. The EP effect is also limited when a large electrode distance is used, although limited space might be available on a catheter. Moreover, an increase in current density leads to a decrease in EP impedance but also to a decreased lifetime of the electrodes due to enhanced corrosion [49]. However, in an ablation catheter often high current densities are used so this should not be a problem.

Four-electrode configuration: the measurements are performed in a four-electrode configuration instead of a two-electrode configuration. This way the electrodes that measure the voltage are different than the electrodes that exert the current. Therefore, most EP will occur at the current applying electrodes and the influence of EP on the measuring electrodes is limited. However, a disadvantage is that the four-electrode configuration leads to additional electrical artifacts such as stray fields.

Electrode material: a good electrode material can limit the amount of EP. A material with a low impedance and one that increases the surface area is desired as this reduces the electrode polarization impedance. Platinum black is a good example of such material. When using the probe in vivo one must be careful that the material is not harmful to the patient.

Theoretical approaches
The ionic double layer that is formed during EP can be modelled such that the EP effect can be removed from the tissue impedance. An equivalent circuit is an interesting method for the correction of EP since these are self-correcting and can easily be added in series to the admittance of the tissue. Two models have shown potential for the removal of EP. These are a CPE model and a distributed RC circuit. It is however difficult to describe the formed microlayer completely and to be sure that the EP effect is removed correctly.

A *CPE* model is a good and often mentioned model for the modeling of the EP contribution. According to Wolf et al. (2011) and Zhbanov and Yan (2017), it works for the correction of the spectrum of blood [31][46]. Another equivalent circuit that provides a nearly perfect fit with the EP contribution is the *distributed RC circuit* [31]. Wolf et al. (2011) prefer a distributed RC circuit over a CPE model because the parameters of the first have more physical meaning than the latter while they are both able to accurately model the EP contribution [31]. The CPE model however has a simpler formula and is mentioned as a method for removing EP in many articles [29][30][31][46][50].

2.4. Fitting basics

A model can be fitted to measurement data with a fitting algorithm. This fitting algorithm changes the parameters of the model until the best fit with the measurement data is found. The best fit is defined by the minimization of an objective function, also called the merit function. The merit

function measures the agreement between the data and the fitted model. Often the nonlinear least squares method is used. This method calculates the error between the data points and the fitted model according to equation 2.12 [25][51][52]. In this equation e stands for the error function that has to be minimized, y_{data} for the measured impedance data and y_{model} for the impedance of the model. The function is minimized until the gradient becomes zero. A disadvantage of the nonlinear least squares method is that it is sensitive to outliers [53].

$$min \sum e_i^2 = min \sum (y_{data_i} - y_{model_i})^2 \tag{2.12}$$

The use of the nonlinear least squares method requires an iterative method for the change in parameters of the model function. Different algorithms are suitable for objective functions of the least squares type. These are for example the Nelder-Mead simplex method, the trust-region-reflective algorithm and the Levenberg-Marquardt algorithm.

- The Nelder-Mead simplex method is one of the most widely used direct search methods. It does not use derivatives and is assumed to be robust, effective and computationally compact. A geometric figure (simplex) is adapted to the shape of the function and contracts to find a minimum [54]. A small number of function evaluations is used per iteration [55].
- The trust-region-reflective algorithm approximates the function through a simplification. This simplification should reflect the function behaviour in the trust region (neighbourhood). It is well suited for large-scale problems [56].
- The Levenberg-Marquardt algorithm uses the gradient descent and the Gauss-Newton method. When the solution is far away from the desired solution the gradient descent method is used, otherwise the Gauss-Newton method. The sum of least squares is reduced by calculating the derivative and moving away from the direction of the steepest descent. This algorithm is well suited for medium-scale problems [57].

3

Methodology

To answer the research questions and achieve the goal of finding a parametric model for the description and differentiation of heart tissue, a methodology has been drafted. This methodology is discussed in this chapter with the main goal to present and discuss the steps, tools and methods used in this research to answer the main research question:

'How can different tissue types be distinguished in the radiofrequency range with impedance spectroscopy during a cardiac ablation procedure?'

First, the measuring method is discussed because impedance measurements must be performed to collect the data for this Master Thesis. Secondly, the fitting method is discussed. Multiple potentially interesting parametric models are investigated based on their fits to the impedance spectra. The best model is used for the parameterization of all measured spectra and the resulting best-fit parameters will be evaluated. Lastly, the classification method is discussed as this is the final step in the distinction between healthy and ablated heart tissue. All these steps are summarized in figure 3.1.

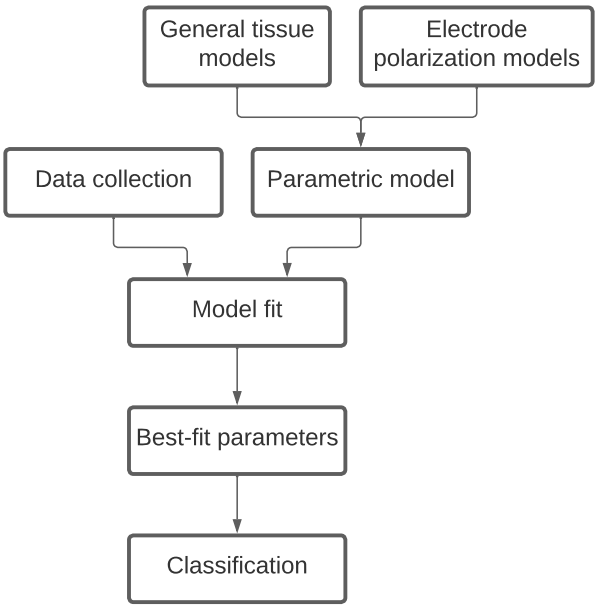

Figure 3.1: Methodology framework including all steps of this Master Thesis

3.1. Measuring method

The impedance measurement setup (see figure 3.2) consists of a 4192A LF HP impedance analyzer connected to a measuring probe. The software LabVIEW is used to save the data from the impedance analyzer to a laptop. In appendix A, the installation of Labview is explained. The impedance is measured in terms of the angle and the absolute value of the impedance and is afterwards rewritten into the real and imaginary part of the impedance using the software Matlab. The measurement probe that is used (see figure 3.2) consists of four electrodes. However, the probe is used in a two-electrode configuration with electrodes two and three. Electrode two is connected to the low potential output of the impedance analyzer and electrode three to the high potential output. The lengths of the electrodes are 5 mm, the diameters are 1mm and the inter-electrode distance is 5mm.

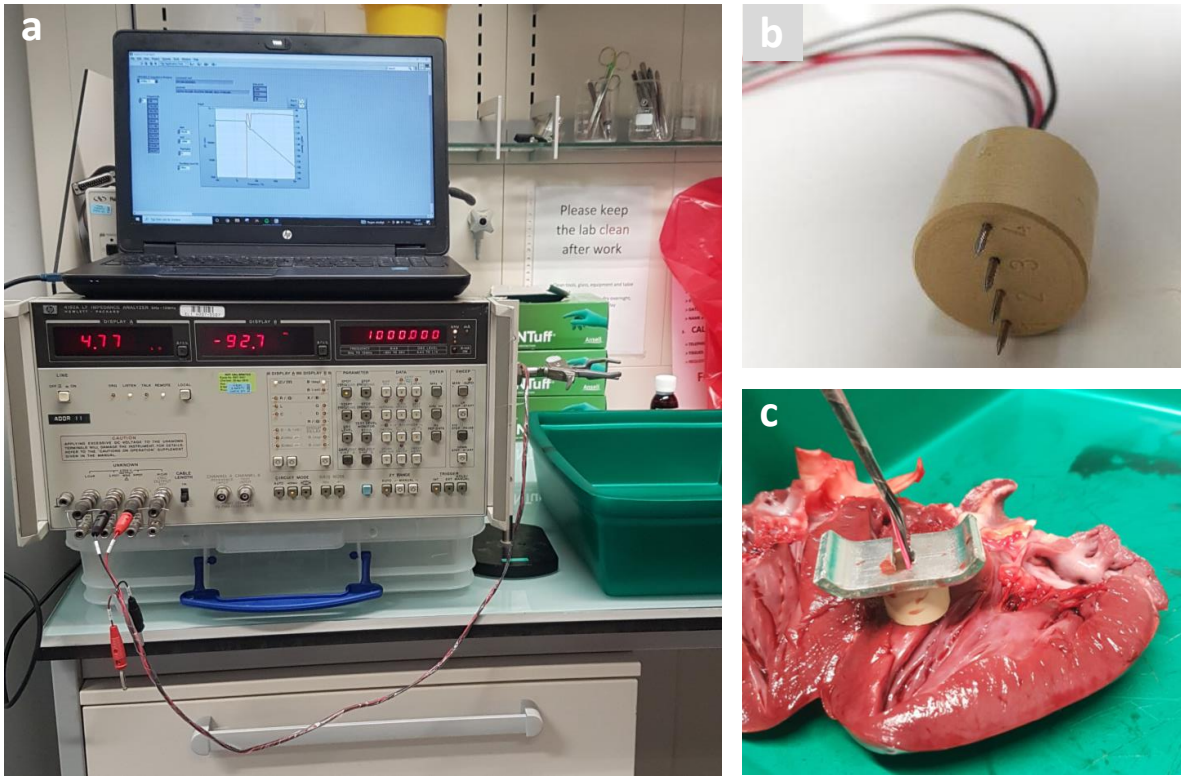

Figure 3.2: The measurement setup including 4192A LF HP impedance analyzer (**a**), measurement probe [58] (**b**) and fixation in the heart tissue (**c**)

The impedance analyzer must be warmed up for 30 minutes before the measurements are performed. The measurements are performed over a frequency range from 100 Hz to 1 MHz and 51 samples are taken. Each measurement is repeated five times. The electrodes are cleaned with soap and 96 % alcohol before and between the measurements. The measurements are performed at room temperature and the tissue temperature is measured with a cooking thermometer. To ensure complete contact between the probe and the tissue, a weight of 35 grams is placed on the probe (see figure 3.2) and the wires are supported during the measurements. For the setting up of this method, experiments on saline and tofu are performed to gain an understanding of how a reliable impedance measurement can be performed. More information on these experiments is given in appendices B and C.

All measurements are performed on porcine hearts as these hearts have similar properties to human hearts and are easier to collect. All vessels are dissected from the hearts and the hearts are frozen directly after excision from the thoracic content. Approximately 24 hours before the measurements, the hearts are thawed by placing them in the fridge and later at room temperature.

Ablated lesions are created with an electrosurgical knife with a blade because an ablation catheter is not available. The electrosurgical knife is used in combination with the ValleyLab Force FX electrosurgical generator. Two different ablation settings are used. Setting one uses the fulguration mode and the tissue is touched with the blade tip over a circle of approximately 6mm with a power of 35 Watt for 20 seconds. Setting two uses the pure cut mode with a power of 15 Watt for 25 seconds with one-second rest after in total 10 and 15 seconds. The complete surface of the blade is kept in touch with the tissue. During ablation, the tissue must be placed on a return electrode pad. To know the coagulation depth, all ablation lesions must be investigated after the impedance measurements.

3.2. Fitting method

A parametric model is to be fitted to the measured impedance spectra. The nonlinear least squares method will be used in this Master Thesis as this is a commonly used method for fitting a model to data. It is used in combination with the *fminsearchbnd* function in Matlab. The function *lsqcurvefit* is also considered, the tradeoff between these two methods is given in appendix D. *Fminsearchbnd* iteratively changes the parameter values with the Nelder-Mead simplex (direct search) method until a minimum is found according to the least squares method. The least squares are taken of the complex impedance as in equation 3.1. Where $Z_{im,data}$ is the measured imaginary part of the impedance, $Z_{re,data}$ is the measured real part of the impedance, w is the sample number, $Z_{im,model}$ is the model fit to the imaginary part of the impedance and $Z_{re,model}$ is the model fit to the real part of the impedance.

$$MSE = \sum (Z_{im,data}(w) - Z_{im,model}(w))^2 + \sum (Z_{re,data}(w) - Z_{re,model}(w))^2 \tag{3.1}$$

The accuracy of the model fit is determined based on the MSE of the real and imaginary part of the impedance and the robustness of the parameters. Two sets of initial parameters are used and the fit is repeated with the best-fit parameters until the lowest MSE for both the real and imaginary part of the impedance are found. However, if the MSE improves with a value smaller than 5 at the expense of a parameter, the fit is stopped. The parameter bounds are set at 0 (minimum) and infinity (maximum) for all parameters except for the exponents. For the exponents, the upper bounds are set at 1.

A model fit from literature is repeated. This is the fit from the widely known Cole-Cole model to the data on heart tissue measured by Gabriel et al. (1996) and serves as a benchmark for the other model fits that are performed in this Master Thesis [34]. This is discussed in appendix E.

Statistical analysis

Statistical analyses are performed using Matlab software. The data is presented in boxplots. These give a clear indication of the spread of the parameters. They indicate the median, a box with the 25th and 75th percentile and the most extreme data that are not considered outliers are indicated by the whiskers. T-tests are used for the assessment of the differences between two sample sets. A

p-value smaller than 0.05 is considered to be statistically significant. Most t-tests assume that the data comes from a population with a normal distribution. Whether this is the case or not is tested with the Kolmogorov-Smirnov test. When the data comes from a normal distribution, the one-way analysis of variance test (ANOVA) is used. When this is not the case the Wilcoxon rank-sum test is used as this test is more robust to outliers and skew datasets. Therefore, the samples do not have to come from a population with a normal distribution. For the comparison of the parameters of healthy and ablated tissue from the same heart, a paired t-test must be used. When the data does not come from a population with a normal distribution, the Wilcoxon signed-rank test is used. The test is performed between corresponding measurement locations.

3.3. Classification method

As a final step in this Master Thesis, a classification is performed for the distinction between healthy and ablated heart tissue. This classification serves as a first impression. Ideally, a training data set and a validation data set are used. However, in this study, one data set is used.

A formula consisting of a combination of multiple parameters of the parametric model is used for the classification. This formula is determined based on the results of the model fit and the (significant) differences between the parameters for healthy and ablated tissue. Based on this formula a threshold value is set that divides the measurements into measurements of healthy tissue and measurements of ablated tissue.

Statistical analysis

The performance of the classification is described with a confusion matrix. The confusion matrix of this study is shown in figure 3.3. Ablated tissue is categorized as positive and healthy tissue as negative. Based on the values of the confusion matrix (true positive (TP), true negative (TN), false positive (FP) and false negative (FN)) other measures for the evaluation can be determined. The measures that are used in this Master Thesis are the positive predictive value (PPV), the negative predictive value (NPV), the specificity, the sensitivity, the accuracy and the Matthews correlation coefficient (MCC). The explanations and formulas of these measures are summarized in appendix F.

		Actual	
		Ablated	Healthy
Predicted	Ablated	True positive (TP)	False positive (FP)
	Healthy	False negative (FN)	True negative (TN)

Figure 3.3: Confusion matrix

The accuracy indicates the ratio between the number of correctly classified samples and the total number of samples. When the number of samples per group (healthy and ablated) is not equal this is not taken into account in the accuracy and it can give a skew indication [59]. However, the MCC is a reliable measure that gives a score based on all four segments of the confusion matrix. The MCC is used as a measure for the quality of the classification with a value between *1* (excellent classification) and *-1* (worse classification indicating no agreement between actual and predicted data) [59][60].

4

Parametric description of heart tissue

During impedance spectroscopy the impedance or dielectric properties of tissue are measured over a certain frequency range, resulting in a spectrum. This spectrum contains all measured data points. Instead of comparing the tissues based on a spectrum with many points, it is better to quantify the spectrum by writing it in a couple of parameters. To do so, a dimension reduction must be done. This results in a reduced parameter space. It is important to keep an understanding of these parameters. Therefore, it is preferred to use a parametric model based on theories for the dimension reduction of the spectrum. This way tissues can be distinguished based on parameters that are understood and this can lead to useful insights. This is not the case for parameters that are found using e.g. big data and machine learning as with these processes the understanding behind the parameters is lost. The parametric models that are discussed in section 2.3 are investigated in this chapter with as goal to answer the first sub-question of this master thesis:

'How can the impedance of heart tissue be modelled?'

The goal of this chapter is to find a parametric model that provides a good fit with the impedance spectra of heart tissue. The spectra consist of an electrode polarization contribution and a tissue contribution. Because the exact amount of electrode polarization and the affected frequency range are unknown, the electrode polarization impedance and tissue impedance are modeled in series. This way no a-priory knowledge of the electrode polarization is needed. The two models together represent the complete spectrum and insight into the contribution of electrode polarization will be gained. Before modelling both contributions in series, the two contributions are fitted separately to the impedance spectrum. Thereafter, the most promising models are modelled in series. Lastly, conclusions are drawn based on these fits and the sub-question is answered.

4.1. Electrode polarization modelling

In the upcoming subsections, two models for the description of electrode polarization are evaluated. These models are the CPE model and the distributed RC (dRC) circuit. The fitting is performed

according to the fitting method described in chapter 3. To find the optimal fit some factors are varied. These are: the initial parameter values, the merit function, the frequency range and the part of the spectrum (real, imaginary or complex) that the least squares is taken of. The correctness of the fit is determined based on the value of the MSE, the lower this error the better the model performs [2]. The heart data that is used is measured on the sidewall of an excised porcine heart with the measuring setup described in chapter 3. The measured frequency ranges from 100 Hz to 1 MHz.

4.1.1. CPE model

The CPE model is mentioned in many articles for the modelling of electrode polarization with as main application blood. A CPE model is a frequency-dependent component consisting of a combination of a resistor and a capacitor. Its impedance is given in equation 4.1. According to Sanabria and Miller (2006) the parameter K represents the ion concentration at the electrode-tissue contact and the parameter m is related to the surface roughness of the electrodes [61]. For specific values of m the model acts as a pure resistor or capacitor [8].

$$Z_{CPE} = K(j\omega)^{-m} \tag{4.1}$$

The best fit was fitted to the imaginary part of the impedance and resulted in an MSE of 2.53e6 and 524 for the real part and imaginary part of the impedance respectively. This fit described the imaginary part of the impedance spectrum quite accurately. The real part, however, has the correct shape but there is an offset between the measured spectrum and the model fit. Due to this offset and the fact that the MSE is not normalized, the MSE value is very large. The offset between the model and data of the real part of the impedance is caused by the missing contribution of the tissue impedance. When a resistor was added in series to the CPE model, the fit for the real part of the impedance improved. Both fits are shown in figure 4.1 [3].

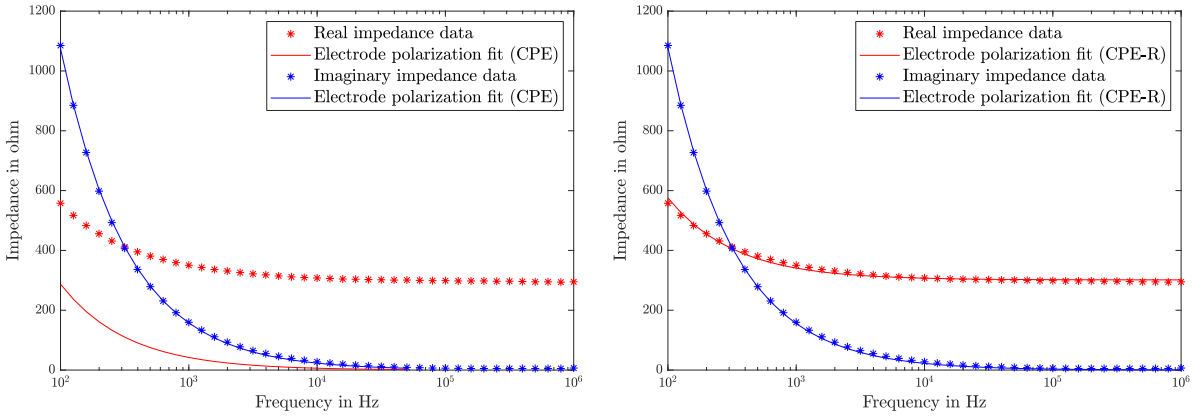

Figure 4.1: Optimal fits to heart tissue data for the description of electrode polarization by a CPE model (left) and by a CPE model in series with a resistor (right)

4.1.2. Distributed RC circuit

The distributed RC (dRC) circuit can be used for the modelling of electrode polarization in the impedance spectrum. It is a circuit consisting of a resistor and capacitor in parallel where there

[2] The MSE is not normalized because all the MSEs in this Master Thesis are taken over the same frequency range

[3] The imaginary part of the impedance is multiplied by -1 for better visualization together with the real part of the impedance in this Master Thesis

is accounted for a distribution of relaxation times. The impedance of a dRC circuit is given in equation 4.2.

$$Z_{dRC} = \frac{R}{(1 + (j\omega RC)^{1-a})^b} \tag{4.2}$$

The best fit was fitted to the imaginary part of the impedance and resulted in an MSE of 2.53e6 and 526 for the real part and imaginary part of the impedance respectively. The fit is similar to the fit of the CPE model.

4.1.3. Conclusion EP model

The results of the previous subsections are summarized in table 4.1. The CPE model and the distributed RC circuit give similar results. The imaginary part of the spectrum can be modeled accurately but the real part of the impedance cannot. The offset of the model from the real part of the spectrum is caused by the contribution of the tissue impedance and should therefore not be described with the EP model. The MSE values for both models are of the same order. A disadvantage of the dRC circuit is that it consists of more parameters than the CPE model. Fewer parameters are preferred to prevent overfitting. Physical meaning is mentioned for both models by Wolf et al. (2011) and Sanabria et al. (2006) [31][61]. The CPE model is mentioned in many studies as a good approach for the elimination of electrode polarization.

To conclude, the CPE model and the dRC circuit have similar performance for the description of the impedance spectrum in the low-frequency range. However, the CPE model consists of fewer parameters and is a widely used model for the description of electrode polarization. Therefore, the CPE model will be used in the assessment in series with a general model.

Model	**MSE Re(Z)**	**MSE Im(Z)**	**# parameters**
CPE model	2.53e6	524	2
Distributed RC circuit	2.53e6	526	4

Table 4.1: Overview of MSEs per electrode polarization model

4.2. Tissue impedance modelling

In the upcoming subsections, the general parametric models that are discussed in chapter 2.3 are examined to see which of these models is suitable for the description of the impedance of heart tissue. These parametric models are the Cole-, Debye-, Raicu impedance models and the Shunting-C and Zhbanov equivalent circuits. The fitting is performed according to the fitting method described in chapter 3. To find the optimal fit some factors are varied. These are: the initial parameter values, the merit function, the frequency range and the part of the spectrum (real, imaginary or complex) that the least squares are taken of. The correctness of the fit is determined based on the value of the MSE, the lower this error the better the model performs.

4.2.1. Cole impedance model

The Cole impedance model is part of the theoretical models and describes the tissue impedance. It is similar to the Cole-Cole model, except for the fact that the Cole-Cole model describes the permittivity. This type of model is mentioned in many articles and is widely used for the description of

different tissue types. The impedance of the Cole impedance model is given in equation 4.3. The distribution parameter a accounts for a distribution of relaxation times and allows a broadening of the dispersion curve. The parameters of the model do not have a physical meaning, although some articles have tried to assign it. There can be accounted for multiple relaxation mechanisms by adding extra Cole terms. The measured spectrum ranges from 100 Hz to 1 MHz and is expected to contain two dispersions (α and β). Therefore, an one-pole and a two-pole Cole impedance model will be discussed.

$$Z_{Cole} = R_\infty + \frac{R_0 - R_\infty}{1 + (j\omega\tau)^a} \tag{4.3}$$

The best fit that is performed with a two-pole Cole impedance model was fitted to the complex part of the impedance. The model can quite accurately describe a complete impedance spectrum of heart tissue and has an MSE of 311 and 316 for the real and imaginary part of the impedance respectively. The MSE values for the high-frequency range (10 kHz - 1 MHz) are 99 and 33. One Cole term describes the EP contribution, while the other Cole term describes the tissue contribution to the spectrum. The fit of the two-pole Cole impedance model and the contributions of the two terms are shown in figure 4.2.

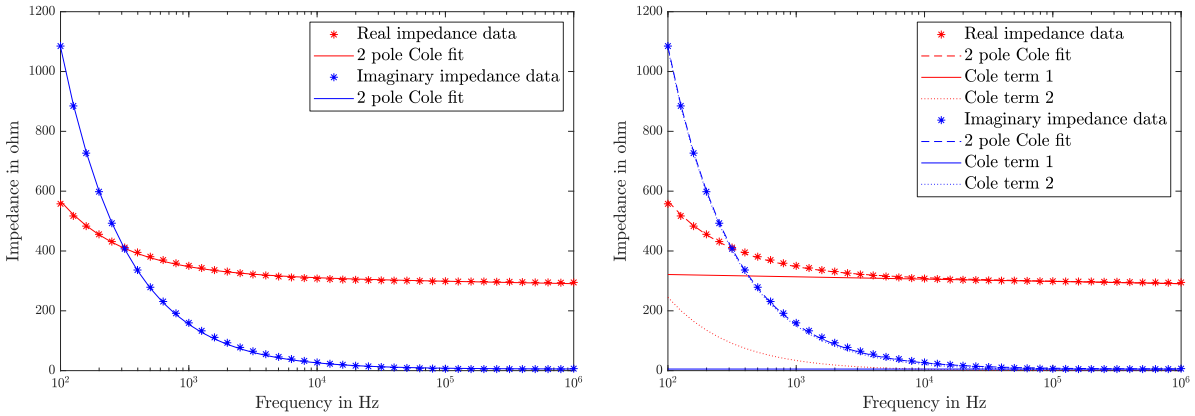

Figure 4.2: Optimal fit to heart tissue data for the description of the tissue impedance with a two-pole Cole impedance model (left) with the contributions of the two Cole terms displayed (right)

To purely describe the tissue impedance, an one pole Cole model is fitted to the spectrum. This resulted in a good fit for the high-frequency range. The MSE values are 1.7e3 and 777 for the real and imaginary part of the impedance respectively. For the high-frequency range (10 kHz - 1 MHz) the errors are 200 and 329. To improve the fit in the high-frequency range, the frequency range of the fit is limited from 10 kHz to 1 MHz. The best results for a fit with the focus on the high-frequency range results in an MSE of 44 and 76 for the real and imaginary part of the impedance respectively. For a specific value of R_∞, the fit results in a horizontal line for both the real and imaginary part of the impedance. This is what is expected for the tissue impedance since the peak in the low-frequency range is caused by the electrode polarization.

4.2.2. Debye model

The Debye model is part of the theoretical models and is a simplification of the Cole impedance model. It does not account for a distribution of relaxation times and describes a medium with a

single relaxation mechanism that is characterized by one single time constant (the relaxation time). The model assumes that the medium relaxes towards a new equilibrium as a first-order process. Similar to the Cole impedance model, the parameters of the model do not have physical meaning and there can be accounted for multiple relaxation mechanisms by adding extra Debye terms. The impedance of the Debye model is given in equation 4.4. The measured spectrum ranges from 100 Hz to 1 MHz and is expected to contain two dispersions(α and β). Therefore, a two-pole Debye model is used.

$$Z_{Debye} = R_\infty + \frac{R_0 - R_\infty}{1 + (j\omega\tau)} \tag{4.4}$$

Unlike the two-pole Cole impedance model, the two-pole Debye model cannot describe the complete spectrum accurately. The MSE values are 2.3e3 and 2.2e3 for the real and imaginary part of the impedance respectively. For the high-frequency range (10 kHz - 1 MHz) the errors are 285 and 603. To improve the fit in the high-frequency range, the frequency range of the fit is limited from 10 kHz to 1 MHz. The best fit with a focus on the high-frequency range results in a low MSE of 24 and 25 for the real and imaginary part of the impedance respectively. Because the fit with a two-pole Debye model is very accurate in this range, an one-pole Debye model is used for the fitting as well. This results in MSE values of 128 and 197.

4.2.3. Raicu model

The Raicu model is also part of the theoretical models. The Cole impedance model and the Debye model are simplifications of the Raicu model. The parameters of the model do not have physical meaning and there can be accounted for multiple relaxation mechanisms by adding extra Raicu terms. The impedance of the Raicu model is given in equation 4.5. The measured spectrum ranges from 100 Hz to 1 MHz and is expected to contain two dispersions(α and β). Therefore, a two-pole Raicu model is used as a start.

$$Z_{Raicu} = R_\infty + \frac{R_0 - R_\infty}{[(j\omega\tau)^\lambda + (j\omega\tau)^{1-\mu}]^\nu} \tag{4.5}$$

The best fit that is performed with a two-pole Raicu model can accurately describe the complete spectrum of the heart tissue and has an MSE of 128 and 198 for the real and imaginary part of the impedance respectively. For the high-frequency range (10 kHz - 1 MHz) the MSEs are 55 and 32. There can be concluded that a two-pole Raicu model might be too extended for the description of purely heart tissue. To purely describe the tissue impedance, an one-pole Raicu model is fitted to the spectrum. This still resulted in quite a good fit for the high-frequency range, the MSEs are 172 and 309. For the complete spectrum the errors were higher: 2.5e3 and 729 for the real and imaginary part of the impedance respectively. To improve the fit in the high-frequency range, the frequency range of the fit is limited from 10 kHz to 1 MHz. The best results for a fit with the focus on the high-frequency range results in an MSE of 44 and 76 for the real and imaginary part of the impedance respectively.

4.2.4. Shunting-C model

The shunting-C model is part of the equivalent circuits. It consists of a series and parallel combination of resistors, a capacitor and a CPE element. The impedance of the circuit is given in equation

4.6. The circuit is used to model the impedance of blood in a measuring cell. Therefore, the parameters have a physical meaning that is focused on blood. R_p is the plasma resistance in the presence of erythrocytes, the CPE element represents the cell membrane capacitance and R_i is the interior resistance of the erythrocytes [46]. The capacitor C_p is added for a more convenient fit.

$$Z_{Shunting-C} = \left(j\omega C_p + \frac{1}{R_p} + \frac{1}{R_i + K(j\omega)^{-a}} \right)^{-1} \tag{4.6}$$

The Shunting-C circuit cannot model the complete spectrum of the heart tissue accurately. The MSE values are 1.6e3 and 626 for the real and imaginary part of the impedance respectively. For the high-frequency range (10 kHz - 1 MHz) the errors are slightly lower: 354 and 163. To purely describe the tissue impedance, the fit should be accurate for the high-frequency range where the electrode polarization impedance has disappeared. To improve the fit in the high-frequency range, the frequency range of the fit is limited from 10 kHz to 1 MHz. The best fit with the focus on the high-frequency range results in an MSE of 17 and 5 for the real and imaginary part of the impedance respectively.

4.2.5. Zhbanov model

The Zhbanov model is part of the equivalent circuits. It consists of a series and parallel combination of resistors, capacitors and a CPE element. It is an extension of the Shunting-C circuit as a parallel combination of a resistor and a capacitor is added to enable more accurate modelling of the impedance of blood in a measuring cell. The extra resistor and capacitor represent the electrode polarization. Therefore, the Zhbanov circuit should model the complete spectrum of heart tissue from 100 Hz to 1 MHz. The impedance of the circuit is given in equation 4.7. An advantage of an equivalent circuit is that it is easier to give physical meaning to the parameters.

$$Z_{Zhbanov} = \frac{1}{\frac{1}{R_e} + j\omega C_e} + \left(j\omega C_p + \frac{1}{R_p} + \frac{1}{R_i + K(j\omega)^{-a}} \right)^{-1} \tag{4.7}$$

The circuit cannot describe the complete spectrum of the heart tissue and results in an MSE of 3.5e4 and 1.8e4 for the real and imaginary part of the impedance respectively. As this circuit already includes elements for the description of electrode polarization it is not necessary to look at the high-frequency fit.

4.2.6. Conclusion tissue modelling

The results of the previous subsections are summarized in table 4.2. First of all, the Zhbanov circuit is eliminated because of the large errors of the fit with this circuit. Because the Zhbanov circuit contains elements for the description of electrode polarization, it should be able to fit a complete spectrum accurately and not just the high-frequency range. The Shunting-C circuit, on the other hand, is used for the description of the tissue impedance and can model the spectrum accurately in the high-frequency range. This is also the case for the one and two-pole Cole impedance model, the two-pole Debye model and the one-pole Raicu model. The number of parameters of these models is of the same order, ranging from four to six. The one-pole Debye model is eliminated because it results in higher MSE values than the other models. The two-pole Raicu model is eliminated

because it contains five more parameters than the one-pole Raicu model which also results in an accurate fit.

Model	**MSE [Re(Z), Im(Z)]**			**# parameters**
	Fit 1 [4]	**Fit 2** [5]	**Fit 3** [6]	
2-pole Cole model	311, 316	99, 33	8, 10	7
1-pole Cole model	1.7e3, 777	200, 329	44, 76	4
2-pole Debye model	2.3e3, 2.2e3	285, 603	25, 25	5
1-pole Debye model	x	x	128, 197	3
2-pole Raicu model	128, 198	55, 32	x	11
1-pole Raicu model	2.5e3, 729	172, 309	44, 76	6
Shunting-C circuit	1.6e3, 626	354, 163	17, 5	5
Zhbanov circuit	3.5e3, 1.8e4	x	x	7

Table 4.2: Overview of MSEs per general model

To conclude, the one and two-pole Cole impedance model, the two-pole Debye model, the one-pole Raicu model and the Shunting-C circuit will be examined in series with a CPE model to verify whether the combination can accurately describe a complete impedance spectrum.

4.3. Combining electrode polarization and tissue impedance modelling

For a complete evaluation of the measured impedance spectrum, the spectrum is modeled as a series combination of an EP model and a general model. This way, there is accounted for the (undesired) electrode polarization impedance and the tissue impedance without having to know the exact amount of electrode polarization a-priory. Also, the two contributions can be separated because two different models are used.

The most promising models according to the conclusions in subsections 4.1.3 and 4.2.6 are used for this evaluation. For the modelling of the EP contribution this is a CPE model and for the modelling of the tissue impedance these are: the one and two-pole Cole impedance model, two-pole Debye model, one-pole Raicu model and the Shunting-C circuit. The series combinations of these models are investigated in this section. This is done by fitting the models to multiple impedance spectra that resulted from measurements on the sidewall of a porcine heart, these spectra are displayed in appendix G. The MSE values of the fits are evaluated, together with the number and robustness of the parameters and the contribution of the electrode polarization and tissue model to the fit.

CPE model in series with an one-pole Cole impedance model

The model contains six parameters and is fitted to the complex part of the impedance over the complete frequency range from 100 Hz to 1 MHz. A standard merit function containing the least squares method is used and the upper and lower bounds are *infinity* and *0* for all parameters. This results in an MSE of 24 and 217 for the real and imaginary part of the impedance respectively. The CPE model describes the low-frequency range and especially the steep increase that is associated with electrode polarization. The Cole model describes the high-frequency part of the fit, which

[4] Fit over the complete frequency range

[5] Fit over the complete frequency range, but the error is calculated over the frequency range from 10 kHz - 1 MHz

[6] Fit over the high-frequency range from 10 kHz - 1 MHz

is the tissue impedance. However, these contributions do change when the initial parameters are changed. None of the parameters tends to go towards their bounds. The model is not able to model a selection of other impedance spectra accurately. Some fits resulted in large errors, such as an MSE of 487 and 651.

CPE model in series with a two-pole Cole impedance model

The model contains nine parameters and is fitted to the complex part of the impedance over the complete frequency range from 100 Hz to 1 MHz. A standard merit function containing the least squares method is used and the upper and lower bounds are *infinity* and *0* for all parameters. This results in an MSE of 22 and 69 for the real and imaginary part of the impedance respectively. The fit of the model and the contributions of the CPE model and Cole impedance model are shown in figure 4.3. Just as for the previous combination the CPE model describes the low-frequency range and the Cole model the high-frequency part of the fit. However, these contributions do change when the initial parameters are changed. None of the parameters tends to go towards their bounds. The model is able to model a selection of other impedance spectra as well, resulting in an MSE of 35 and 138.

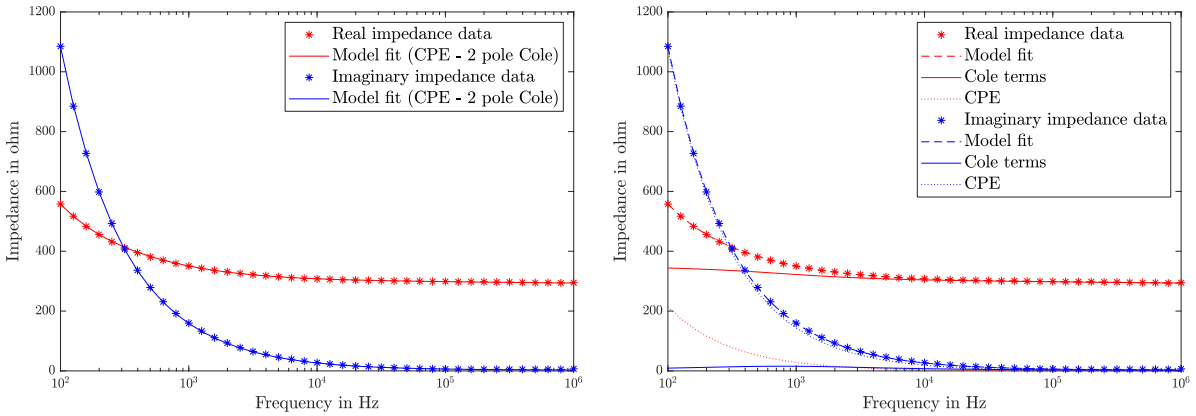

Figure 4.3: Optimal fits to heart tissue data by a series combination of a CPE model and a two-pole Cole impedance model (left) with the contributions of the different elements displayed (right)

CPE model in series with a two-pole Debye model

The model consists of seven parameters and is fitted to the complex part of the impedance over the complete frequency range from 100 Hz to 1 MHz. A standard merit function containing the least squares method is used and the upper and lower bounds are *infinity* and *0* for all parameters. This results in an MSE of 64 and 187 for the real and imaginary part of the impedance respectively. The contribution of the CPE model disappears for higher frequencies and does almost completely describe the spectrum in the low-frequency range. The Debye model forms a horizontal line that describes the high-frequency range of the spectrum. However, these contributions do change when the initial parameters are changed. None of the parameters tends to go towards their bounds. For the model to describe other measurements as well, the initial parameters have to be changed. However, this still resulted in larger errors, such as an MSE of 123 and 225.

CPE model in series with an one-pole Raicu model

The model consists of eight parameters and is fitted to the complex part of the impedance over the complete frequency range from 100 Hz to 1 MHz. A standard merit function containing the least squares method is used and the upper and lower bounds are *infinity* and *0* for all parameters. This

results in an MSE of 25 and 128 for the real and imaginary part of the impedance respectively. Similar to the one-pole Cole impedance model, the Raicu model describes the graph in the high-frequency range but is present in the low-frequency range as well. The CPE model contribution disappears for higher frequencies but does not describe the entire spectrum in the low-frequency range. However, these contributions do change when the initial parameters are changed. None of the parameters tends to go towards their bounds. For the model to describe other measurements as well, the initial parameters have to be changed. However, this still resulted in larger MSE values of 152 and 277.

CPE model in series with a Shunting-C equivalent circuit

The model contains seven parameters and is fitted to the complex part of the impedance over the complete frequency range from 100 Hz to 1 MHz. A standard merit function containing the least squares method is used and the upper and lower bounds are *infinity* and *0* for all parameters. This results in an MSE of 153 and 307 for the real and imaginary part of the impedance respectively. The CPE model describes the low-frequency range and especially the steep increase that is likely to be associated with electrode polarization. The Shunting-C circuit describes the high-frequency part of the fit, which is likely to be the tissue impedance. None of these parameters tends to go towards their bounds. For the model to describe other measurements as well, the initial parameters have to be changed. However, this still resulted in larger MSE values of 167 and 291.

The MSE values for two fits and the number of model parameters are summarized in table 4.3 for all model combinations.

Measurement 1			
Model	**MSE Re(Z)**	**MSE Im(Z)**	**# parameters**
CPE-Cole (1)	24	127	6
CPE-Cole (2)	22	69	9
CPE-Debye (2)	64	187	7
CPE-Raicu (1)	25	128	8
CPE-Shunting C	153	307	7
Measurement 2			
Model	**MSE Re(Z)**	**MSE Im(Z)**	**# parameters**
CPE-Cole (1)	487	651	6
CPE-Cole (2)	35	138	9
CPE-Debye (2)	123	225	7
CPE-Raicu (1)	152	277	8
CPE-Shunting C	167	291	7

Table 4.3: Overview of MSEs per series combination of a CPE model and a general model

4.4. Conclusions

How can the impedance of heart tissue be modelled?

The impedance of heart tissue can be modelled by a parametric model. Parametric models can reduce the dimensions of a measured spectrum and they contribute to an understanding of the parameters in which the spectrum is quantified. The fitting method is verified with a benchmark fit to the data of Gabriel (1996) [34]. This showed that a good model fit with the data can be found using least squares optimization. The Matlab function *fminsearchbnd* is used with the Nelder-Mead

Simplex algorithm.

For a complete evaluation of the measured impedance spectrum, the spectrum is modeled as a series combination of an electrode polarization model and a general model. This way, the (undesired) electrode polarization impedance and the tissue impedance are accounted for, without a-priori knowledge of the exact amount of electrode polarization. There are many types of general parametric models for the description of tissue impedance. The first filtering step was already performed in the literature study of Mulder (2021) [11]. Resulting from this study, six parametric models were left for the modelling of the tissue impedance. These parametric models are the Cole-, Debye- and Raicu impedance models and the shunting C- and Zhbanov equivalent circuits. The electrode polarization impedance can be modeled by a CPE model or a distributed RC circuit. However, the CPE model is chosen as the performance of both models is equal and the CPE model consists of fewer parameters and is widely used.

The series combinations of these models are fitted to heart tissue data that is measured according to the methodology discussed in chapter 3. The fits of the CPE model in series with the two-pole Debye model and Shunting-C circuit result in large errors, therefore these are excluded. When the spectra differ a bit, the combinations with the one-pole Cole impedance model and the one-pole Raicu model result in larger errors as well. From the fits, there can be concluded that the overall performance based on the MSE values is best for the CPE model in series with the two-pole Cole impedance model. Because this model results in a low MSE for the real and imaginary part of the impedance with robust parameters and can describe a variety of spectra, it is chosen as the default model for this Master Thesis. These benefits compensate for the downside of the large number of parameters present in this model. Also, the CPE element describes the low-frequency range and the general part (two-pole Cole impedance model) mostly describes the high-frequency range. This is as expected since electrode polarization is mostly present for low frequencies.

5

Measurements and results

In this chapter, the measurements that are performed on porcine hearts for the collection of impedance data are discussed. The parametric model that is found to be most promising according to the conclusions of chapter 4 (a series combination of a CPE model and a two-pole Cole impedance model), is used for the parameterization of these measured impedance spectra. The parameter values of the fits are investigated to see whether a distinction between different parts of the heart and between ablated and healthy heart tissue can be made based on these fitting parameters. In the end, a classification is performed based on a combination of model parameters for the discrimination between healthy and ablated tissue. By doing so, answers to the following sub-questions can be given:

'Can different parts of the heart be distinguished from each other with modelling?'

'How can healthy and ablated heart tissue be distinguished with modelling?'

5.1. Measurements on porcine heart

This section discusses the impedance measurements on porcine hearts. The measurements are performed according to the method discussed in chapter 3. Two porcine hearts (H1 and H2) are measured and the lesions are created with an electrosurgical knife in fulguration mode (ablation setting one as discussed in chapter 3). The times between all measurements are recorded such that potential dehydration of the tissue over time can be taken into account. The time between the first and last measurement of heart H1 was approximately 2.5 hours. For heart H2 this was 1.5 hours. The measurements are performed at a room temperature of 20 degrees Celsius. Heart H1 had a temperature of 15 degrees Celsius at the beginning of the measurements and 18 degrees Celsius at the end of the measurements. Heart H2 had a constant temperature of 19 degrees Celsius during the measurements.

In both hearts a frontal section is made and three locations are measured. These locations are the sidewall of the left ventricle (sw LV), the inside of the left ventricle (ins LV) and the inside of the

left atrium (LA). At each location, multiple measurements are performed and each measurement is repeated five times. The left atrium is measured because this is the part of the heart that is often ablated during catheter ablation. Because this part is a non-flat surface, the flat sidewall of the left ventricle is measured as well. For comparison, the inside of the left ventricle is measured.

In total 70 healthy measurements divided over 14 locations are performed on heart H1 and 50 healthy measurements divided over 10 locations on heart H2. The measured locations of healthy tissue for heart H2 are shown in a schematic overview in figure 5.1. A number of these locations are ablated and measured again. The coagulation depths of all ablated lesions are investigated after the impedance measurements and are presented in appendix H.

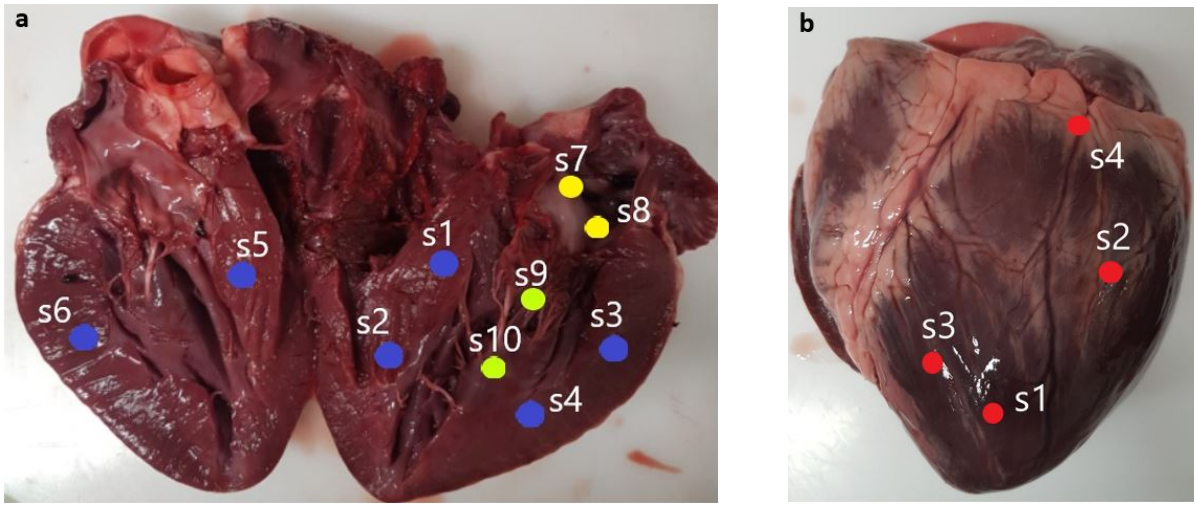

Figure 5.1: Measured locations of heart H2 (**a**). Blue: measurements on the sidewall of the ventricle. Green: measurements on the inside of the ventricle. Yellow: measurements on the inside the atrium. Measured locations of heart H3 (**b**). Red: measurements on the outside of the ventricle

Afterwards, a control experiment is performed on another porcine heart (H3) to verify the results of the previous measurements. A frontal section is made and two locations are measured. These locations are the outside of the left ventricle and the sidewall of the left ventricle. The outside of the ventricle is measured because this location is measured in a study by Yamaguchi et al. (2021) which is used for the comparison of the results [9]. Because this part is a non-flat surface, the flat sidewall of the left ventricle is measured as well. In total 50 healthy measurements divided over 10 locations are performed on heart H3. Each of these locations is ablated with ablation setting two, as discussed in chapter 3. Because a different ablation setting is used than in the previous measurements, the created lesions are different. In figure 5.2, sections of the two lesions types are shown. The coagulation depths of all ablation lesions are investigated after the impedance measurements and are presented in appendix H. The time between the first and last measurement of heart H3 was approximately 2.5 hours. The heart had a constant temperature of 20 degrees Celsius during the measurements.

5.2. Model fitting

A series combination of a CPE model and a two-pole Cole impedance model is fitted to the measured impedance spectra. The formula of this parametric model is given in equation 5.1. The fit is performed according to the fitting method discussed in chapter 3. The two sets of initial parameter

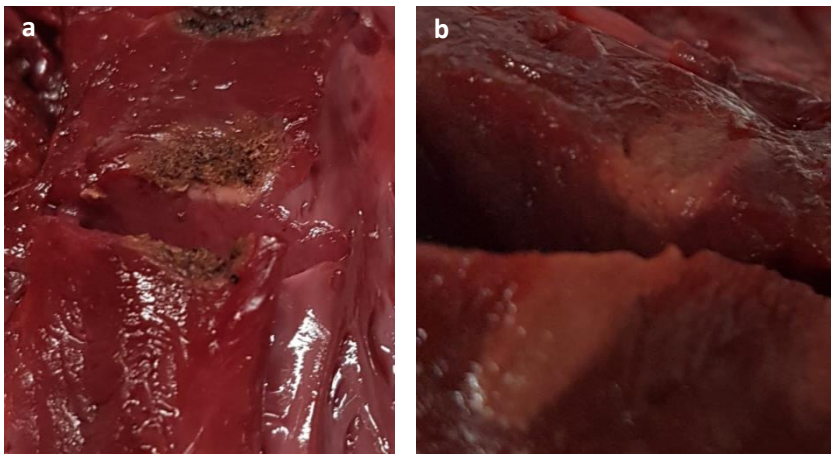

Figure 5.2: Ablation lesions created with fulguration mode (**a**) and pure cut mode (**b**)

values that are used are ([R_1, t_1, a_1, R_2, t_2, a_2, K, m, R_∞]): [101, 3e-4, 0.7, 253, 1e-8, 0.8, 2.5e-6, 0.9, 188] and [45, 9.6e-5,0.7, 225, 3.6e-9, 0.8, 2.5e-6, 0.7, 175].

$$Z = R\infty + \frac{R_1}{1+(j\omega t_1)^{a_1}} + \frac{R_2}{1+(j\omega t_2)^{a_2}} + \frac{1}{K(j\omega)^m} \tag{5.1}$$

The MSE of both the real and imaginary part of the impedance is about 100 with fits resulting in slightly higher and slightly lower errors. Although for a couple of measurements, the fit resulted in very large MSEs (> 1000). This was the case for deviating measurement data with exceptional high real and imaginary part of the impedance. The parametric model had difficulties providing an accurate fit for these measurements. In these cases, the contribution of the CPE term disappeared especially for the real part of the impedance that led to the spectrum being completely described by the Cole terms. This resulted in an incomplete description of the spectra and different parameter values. For example, $R\infty$ could become very small over multiple iterations while the MSE improves only very little. The opposite happened for R_1.

In figure 5.3 one of the fits is displayed. The different contributions of the electrode polarization part and the general part of the model are shown. A similar combination of these two parts is seen for most other fits as well. The EP part describes the increase in the spectrum in the low-frequency range for both the real and imaginary part of the impedance. The contribution of the term disappears for frequencies above 50 kHz. The general part describes the data in the high-frequency range. The first Cole term has only a small contribution, while the second Cole term and the $R\infty$ parameter have a large contribution. The second Cole term describes the slight decrease for the real part of the impedance and the slight increase for the imaginary part of the impedance in the high-frequency range.

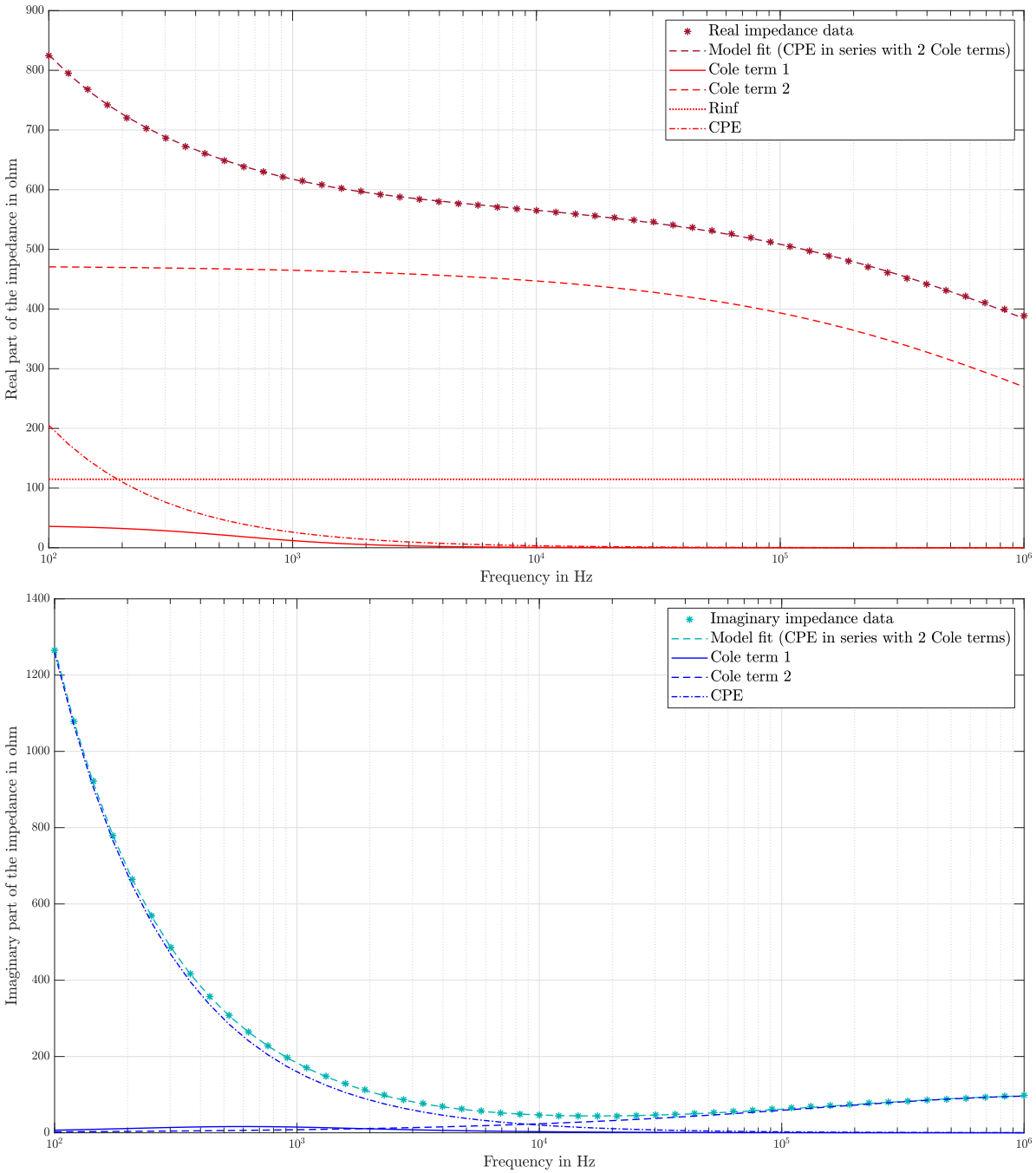

Figure 5.3: Fit of a CPE model in series with a 2-pole Cole impedance model to an impedance spectrum. The contributions of all elements of the parametric model are displayed (R_∞, the first Cole term, the second Cole term and the CPE term) for the real and imaginary part of the impedance

5.3. Parameter evaluation

The measured impedance spectra and best-fit parameters are investigated with the main goal to investigate whether there is a difference between healthy and ablated tissue. Furthermore, the differences between multiple hearts and between different locations of one heart are investigated.

Comparison of different parts of the heart

The three different locations that are measured at hearts H1 and H2 are compared. For all parameters, differences are present between the cardiac chambers. Some of these differences are statistically significant while others are not. In figure 5.4, the boxplots of the parameters a_1 and R_2 are displayed. In these boxplots, the differences between the three locations in the heart are visualized for hearts H1 and H2. These differences are not constant and equal for both hearts. For example, for parameter a_1 the value of the left atrium is smaller than for the other locations at heart H1 but the opposite is true for heart H2. Also, it is remarkable that the values within one location for R_2 are divided into two parts, resulting in a large variability. This is also the case for the other parameters that are measured on the left atrium and the inside of the left ventricle. Lastly, the parameters that model the electrode polarization show (significant) differences between the different locations and hearts. An overview of the differences between all parameters is given in appendix I.

In heart H3, the outside of the left ventricle is measured. This results in deviating spectra in comparison to the other locations that are measured. The values for the real part of the impedance are much higher in comparison to the other locations while the imaginary part of the impedance does not show such an increase. Also, there are large differences in the height of the real part of the impedance between the different measurements in this location. In appendix I the impedance spectra and parameter values of these measurements are shown.

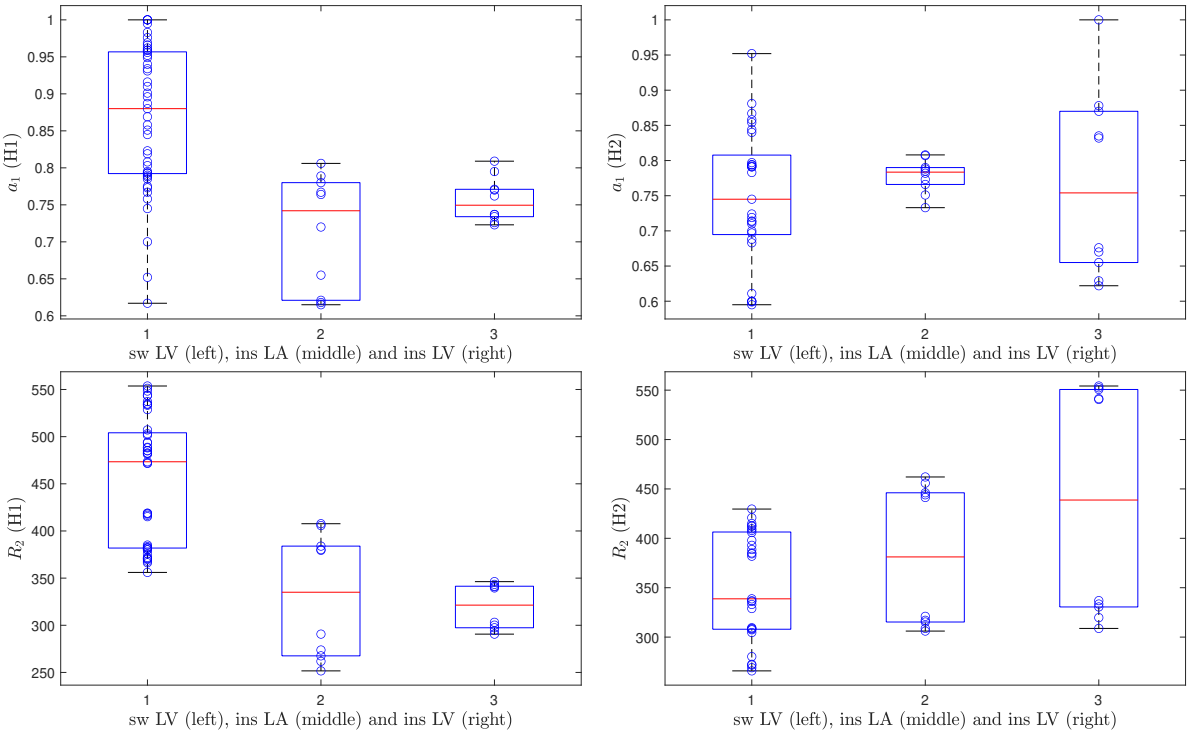

Figure 5.4: Boxplots of the parameters a_1 and R_2 for the different locations of hearts H1 and H2

Comparison of healthy and ablated heart tissue

After ablation in fulguration mode (setting one), the real and imaginary part of the impedance increase. This increase is shown in figure 5.5 for the measurements on the sidewall of the left ventricle. The solid lines represent the measurements of healthy tissue and the dotted lines the measurements of ablated tissue. Only for one set of measurements on the inside of the ventricle of heart H2 and for

one set of measurements on the atrium of heart H1 a decrease in impedance occurs. For the other locations, the increase in impedance is characterized by two parts. The first part is the increase in the low-frequency range for both the real and imaginary part of the impedance. The second part is the flattened decrease that is present in the high-frequency range of the real part of the impedance. These two parts are described by the parameters of the CPE model and the second Cole term, see figure 5.3. The impedance spectra of heart H3 show quite some variation. However, an increase in impedance is observed in most measurements after ablation in pure cut mode (setting two) as well.

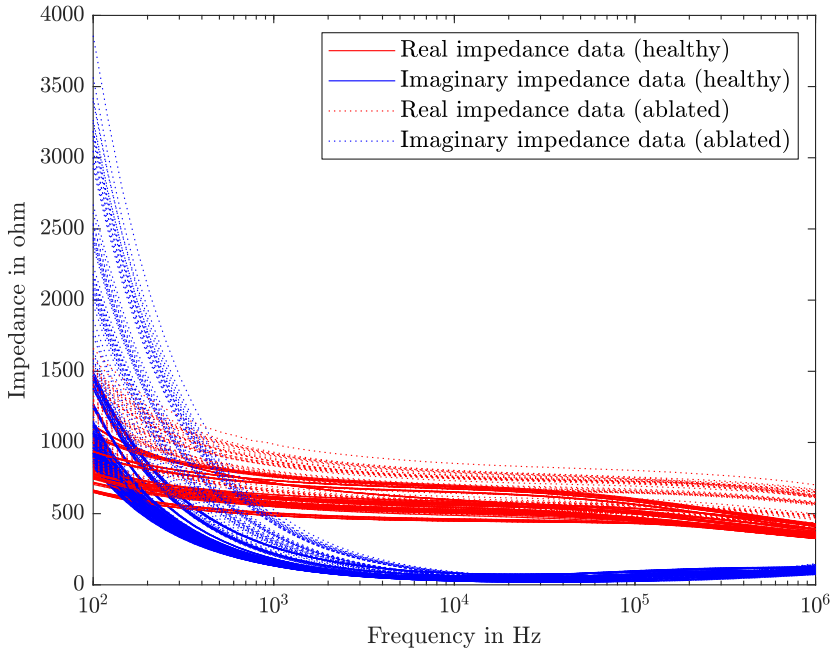

Figure 5.5: Impedance spectra of healthy and ablated sidewall ventricle measurements on hearts H1 and H2. Healthy spectra are indicated with the solid lines and the ablated spectra with the dotted lines

The change in impedance spectra and especially the impedance increase after ablation result in a change in parameters. Figure 5.6 shows the parameter values of R_2, t_2, a_2 and K that were determined from the impedance spectra of the sidewall of the ventricle of heart H1. Each parameter is displayed individually for both the healthy and ablated measurements, clear differences are visible. The mean values of R_1, t_1, R_2 and a_2 increased after ablation, while the values of $R\infty$, a_1, t_2, K and m decreased after ablation. However, some measurements show several different changes in parameter values before and after ablation for example the measurements on the inside of the left ventricle. Also, t_1 increases only for halve of the measured locations. In appendix J an overview of the changes per location is given.

A Wilcoxon signed-rank test shows significant differences at a significance level of 5% for all parameters except R_1 when assessing all measurement locations for hearts H1, H2 and H3 together (only the measurements on the outside of the LV of H3 are left out). However, when the different locations were assessed separately the significance changed. For the measurements on the sidewall of the ventricle of heart H1, all parameters showed significant differences except for parameter t_1. For the same location of heart H2, only R_1 did not show a significant difference. While for the measurements of the atrium of heart H1 only a_1 and a_2 showed a significant difference. In appendix J the outcomes of the Wilcoxon signed-rank test for all locations and hearts are shown.

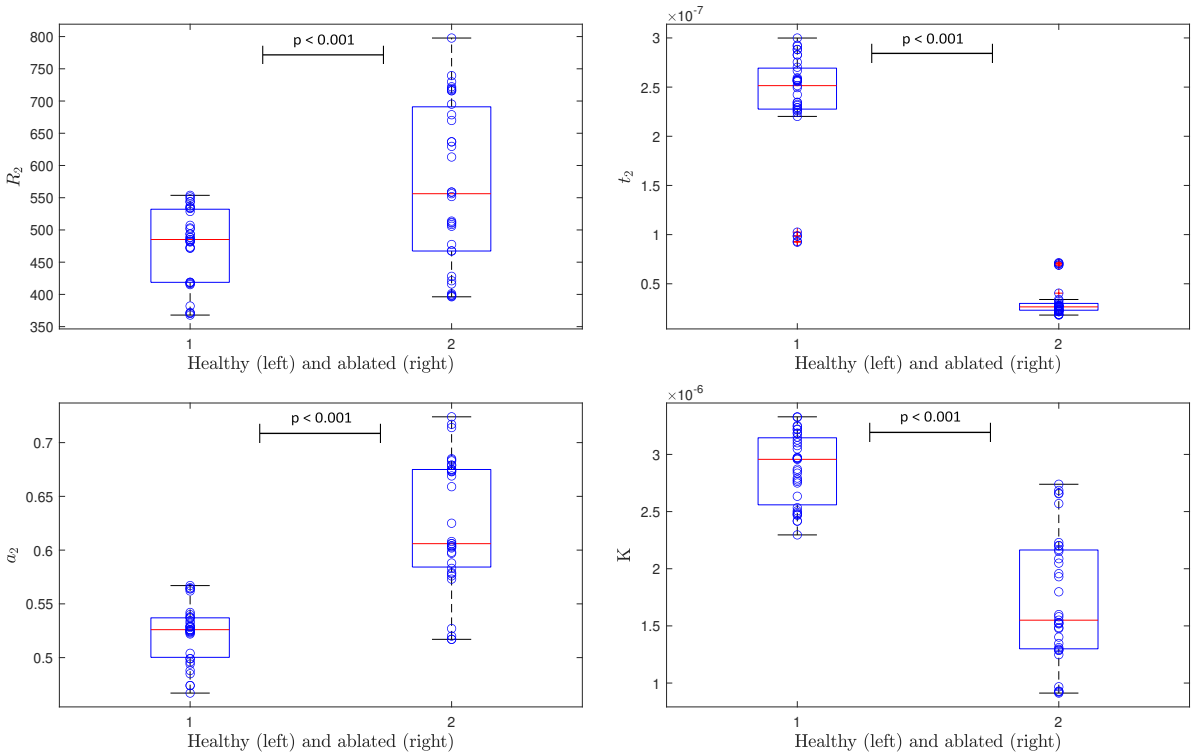

Figure 5.6: Boxplots of R_2, t_2, a_2 and K of healthy and ablated sidewall ventricle measurements of heart H1 derived from the model fit including the p-values of the Wilcoxon signed rank test

5.4. Tissue classification

A classification of healthy and ablated tissue is made based on a formula consisting of a combination of the model parameters. This formula, shown below as equation 5.2, consists of parameters R_2 and t_2. These parameters are used because they have a significant difference between healthy and ablated tissue for most of the measured locations. Furthermore, they belong to one of the terms of the parametric model that describes a deviant part of the impedance spectra. The combination of these parameters results in an optimal difference between healthy and ablated heart tissue because for all parameters a similar decrease or increase occurs after ablation for most of the measured locations.

$$\text{Classification formula:} \quad \frac{R_2}{t_2^2} \tag{5.2}$$

The threshold value is set at $0.120 \cdot 10^{18}$, all values lower than this value are categorized as healthy heart tissue and all values higher than this value are categorized as ablated heart tissue. The threshold value (indicated by the green line) is displayed in boxplots containing all healthy and ablated tissue data in figure 5.7.

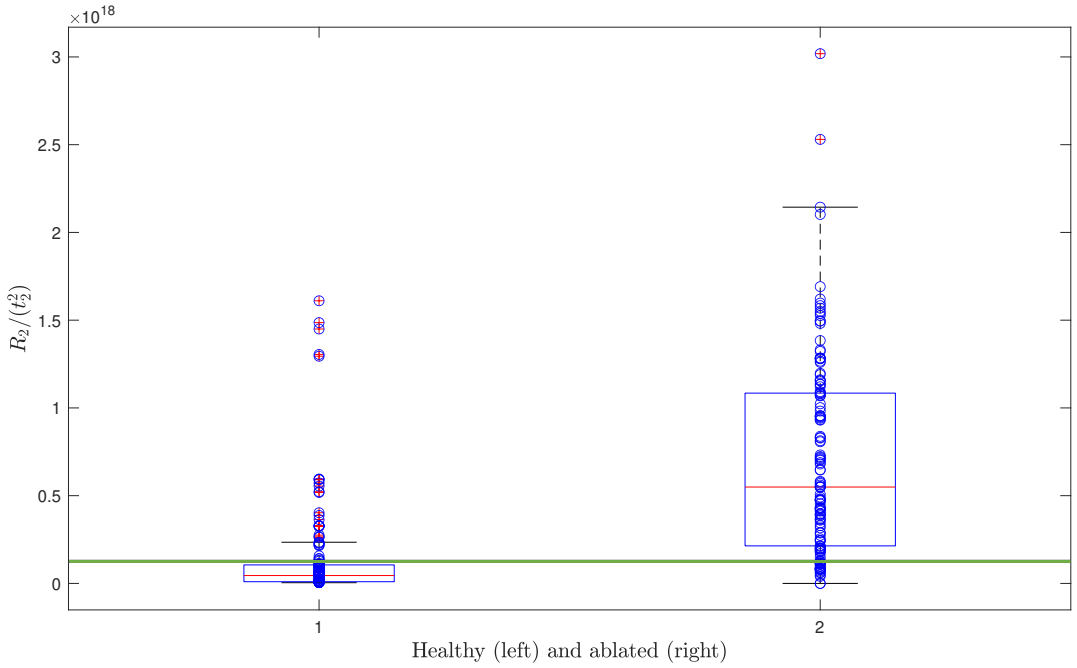

Figure 5.7: Boxplots of healthy and ablated tissue of formula $\frac{R_2}{t_2^2}$ with a classification threshold value $0.120 \cdot 10^{18}$ (green line)

The classification results for healthy and ablated heart tissue are summarized in table 5.1. They indicate that accurate discrimination of healthy and ablated heart tissue might be possible. The achieved sensitivity is slightly higher than the specificity but both values are around 80%. The accuracy is 0.813 and the MCC is 0.629.

Threshold value	**MCC**	**ACC**	**Sensitivity**	**Specificity**	**PPV**	**NPV**	**TP**	**FN**	**FP**	**TN**
$0.120 \cdot 10^{18}$	0.629	0.813	84.4	78.6	77.8	85.0	119	22	34	125

Table 5.1: Classification results for discrimination between healthy and ablated heart tissue

6

Discussion and recommendations

This chapter contains the overall discussion of this Master Thesis and the recommendations for future research are given.

6.1. Discussion

In the upcoming subsections, the results of this Master Thesis and the research limitations are discussed.

6.1.1. Most important results

Comparison of different parts of the heart

There are significant differences in found parameter values between various locations of the heart and between similar locations of different hearts. However, these differences are not always consistent. The heart being a heterogeneous and anisotropic organ explains that inconsistency. Besides the overall nature of the heart leading to inconsistency, the alternating thickness of the myocardium of the heart chamber and the possible presence of a layer of fat can impact the results. Lastly, other structures such as the trabaculae and chordae tendineae can have an impact. These factors result in differences in the impedance spectra. Moreover, differences between the multiple hearts can be caused by different hydration levels, temperature differences and different physical conditions of the pig to which the heart belonged. This is in agreement with findings in the literature: different regions in the heart can vary considerably and the inter-patient variation of the same region can be large [8][62][63].

Other factors that add to the differences are measurement uncertainties and uncertainties in the model fit. Impedance measurements are sensitive to outside effects. For example, incomplete contact between the electrodes and the tissue can result in relatively large fluctuations of the impedance spectrum. Most factors that can influence the impedance measurements are kept constant in this Master Thesis. Such as the contact force by adding a weight for the fixation of the probe. The uncertainties due to the model fit are discussed later in this section.

Some parameter values of the measurements within one location (i.e. the inside of the atrium and the inside of the ventricle) are divided into two groups. These groups are also visible in the impedance spectra. A cause for this clustering can be found in the fact that the measurements for these locations are only performed in two spots resulting in a large variability due to differences in

the tissue within these locations.

The electrode polarization parameters (*K* and *m)* are not constant over the measurements indicating that the electrode polarization contribution is not constant. In the impedance spectra, the peaks in the low-frequency range of the spectra have different heights. However, the repeated measurements on one location show equal peaks. Several factors have an influence on the amount of electrode polarization. These factors are among others: the measured sample, the electrode properties such as material, radius, structure, surface and shape, the electrode distance, the temperature and the current density [28][29][30][31][32]. The factors regarding the electrode material and probe constants are assumed to be constant over the measurements. The temperature of heart H1 changed by three degrees Celsius over the measurements, however, the temperature of heart H2 was constant and fluctuations were present as well. Therefore, the change in temperature is assumed to have no influence. The differences in electrode polarization contributions are thus likely to be caused by differences in the sample between the measurement locations just as these influence the other parameters. The electrode polarization contribution disappears before 100 kHz for all measurements, on average around 50 kHz. This range is in agreement with findings in the literature [31][33][34][35][36].

The measurements on the outside of the ventricle of heart H3 showed a remarkable increase in the real part of the impedance in comparison to the other locations. Also, there was a large difference between the measurements in this location. These differences can be caused by the nonuniform layer of fat that covers the outside of the ventricle. Furthermore, uncertainties in the measurements can have attributed to the differences as it was difficult to ensure a stable measuring position due to the curvature of the ventricle.

Comparison of healthy and ablated heart tissue

An increase in impedance is observed for the measurements taken after ablation in this Master Thesis. This increase in impedance is characterized by two parts. The first part is an increase in the peak value of the low-frequency range. This peak is described by the CPE element of the parametric model which indicates that it is caused by electrode polarization. After ablation, an increase in conductivity is expected mainly in the low-frequency range due to irreversible changes to the cells such as damaged cell membranes [64]. As electrode polarization is more pronounced in samples with high conductivity, the peak in the impedance can be caused by increased electrode polarization impedance [28]. This contribution will then overlap the tissue impedance.

The second part of the increase in impedance is present in the high-frequency range. For healthy tissue, a decrease in the real part of the impedance is visible around 100 kHz. For some measurements, this is more pronounced than for others. However, after ablation, this decrease has flattened. This small decrease in the spectrum of healthy tissue might be caused by the fact that for higher frequencies the current flows through the cell membrane and intracellular fluid instead of only through the extracellular fluid. The cell membranes can be damaged by ablation resulting in a smaller difference between impedance in the high and low-frequency range. Furthermore, after ablation with fulguration mode, the formation of coagulum and desiccation might contribute to an impedance increase. The flattening can also be caused by tissue dehydration due to loss of moisture over the measurements.

In the literature, a drop in the tissue impedance is mentioned during and after catheter ablation

instead of an increase as in this Master Thesis [9][65][66]. In the papers by Martin et al. (2018) and Das et al. (2021), the impedance is measured during ablation in the presence of blood [65][66]. During ablation, there is an increase in tissue temperature resulting in increased ion mobility that might explain the impedance drop. But in a recently published paper by Yamaguchi et al. (2021), an impedance drop is measured after ablation without the presence of a fluid [9]. The presence of electrode polarization can be a reason for the increase in the low-frequency range in this Master Thesis. Also, differences in ablation and measurement methods are possible causes for the differences as these vary in all studies. In this Master Thesis, an electrosurgical knife is used in fulguration and pure cut mode and the impedance is measured by needle electrodes. While in the literature some lesions are created with an ablation catheter and others with an electrosurgical knife in soft coagulation mode and the measurements are performed with a catheter. All these factors contribute to the differences in the results.

The ablation method with fulguration mode leads to the occurrence of tissue charring, vaporization, desiccation and formation of a coagulum leading to a layer with a high resistance that can be a reason for an increase in impedance instead of a decrease. This is in accordance with findings in the literature [67][68][69][70]. Ablation without tissue charring results in the degeneration of the tissue due to the high temperature resulting in the loss of structure and damage of the cell membranes that give rise to a decrease in resistance. However, the control experiment with ablation with the pure cut mode shows an increase in impedance although it does not lead to tissue charring. Therefore, the increase in impedance that was visible after ablation in hearts H1 and H2 cannot be completely dedicated to the presence of a coagulum. According to Leondes (2003), the cell membranes get damaged due to the stopping of blood flow after excision resulting in a straight line for the real part of the impedance [63]. This can be a reason for the lack of impedance drop because the cell membranes might be already damaged before the ablation. On the other hand, the increase in impedance can be (partly) attributed to the moisture loss over the measurement period and the increase in electrode polarization due to damage to the cell membranes. The use of needle electrodes results in the fact that the exerted current does not only pass through the ablated tissue but also through the healthy tissue. Therefore, these influences are measured as well.

An increase in impedance is not present for one set of measurements on the inside of the ventricle of heart H2 and for one set of measurements on the atrium of heart H1. This is not purely caused by less effective ablation, as not for all measurements on these locations the ablation depth was superficial (see appendix H). Measurement errors due to the inhomogeneity and irregularities of the measurement locations in the LA and LV might have added to the differences in the results. A flattening in the decrease of the impedance in the high-frequency range is visible for these measurements just as for the measurements in other locations.

Parametric model

The parametric model can fit most impedance spectra accurately. The MSEs between the data and model are limited, the parameters are robust and do not go towards their boundaries. Also, the contributions of the electrode polarization part (CPE element) and the general part of the model (Cole terms) are as expected. The CPE element describes the increase in impedance in the low-frequency range. The contribution of the EP term disappears around 50 kHz, which is in agreement with findings in literature [31][34][35][36]. The first Cole term has only a negligible contribution to the impedance spectrum while the second Cole term is responsible for the description of the data

in the high-frequency range. However, some deviating spectra cannot be accurately described by the parametric model. In some cases, the general model tends to fit the complete frequency range even though still a small peak that is likely to be caused by EP is present. This results in divergent parameter values that are indicated as outliers. For example, the value of $R\infty$ becomes very small, but the contribution of the first Cole term (mostly due to an increase in R_1) increases. This can be partly prevented by stopping the fitting process early. Other outliers are caused by deviating impedance spectra that might be the result of measurement errors such as incomplete electrode-tissue contact.

Parameter evaluation

The changes in the impedance spectra resulted in a change in parameter values. These changes were similar for most of the measured locations, however, there were some exceptions. These different changes are mostly present for the parameters of the first Cole term. This term only has a small contribution to the impedance spectra and therefore the difference between its contribution to the healthy and ablated spectrum are varying. An example is t_1 which decreases for half of the locations after ablation while it increases for the other locations. Another cause for the differences is the variation in impedance between different measured locations as is explained at the beginning of this chapter.

Depending on the location, the parameter differences were significant ($p < 0.05$) or not ($p > 0.05$) according to the Wilcoxon signed-rank test. In some cases, the lack of significance is due to the limited number of measurements. This is for example the case for the best-fit parameters of the fits of the left atrium for heart H2. There is a difference between the parameters for healthy and ablated tissue but due to the limited number of measurements, this difference is not significant.

The parameters of the CPE element and the second Cole term describe the two deviant parts in the spectra of healthy and ablated tissue. The change of the tissue impedance is of interest and not the change due to electrode polarization impedance. Hence, the focus is on the parameters belonging to the second Cole term. To elaborate on these parameters, each parameter is discussed separately.

$R\infty$

The $R\infty$ parameter decreases after ablation for all locations. This decrease led to significantly different values between healthy and ablated tissue for the measurements on the sidewall of the LV and the inside of the LV of heart H1. Also, for the sidewall of the LV of heart H2, the difference was significant. For all other locations, the differences were not significant. According to Grimnes and Martinsen (2005), $R\infty$ represents the resistance at a very high frequency [43]. This seems to match the contribution in the spectrum. Because $R\infty$ is a horizontal line in the spectrum of the real part of the impedance and for a frequency of 1 MHz the spectrum does not reach the level of the $R\infty$ parameter. However, the parameter might not be meaningful in a frequency range with a maximum frequency of 1 MHz [67].

R_2

The value for R_2 increases after ablation except for the inside of the left ventricle of heart H2 and the sidewall of heart H3. This increase led to significantly different values between healthy and ablated tissue for all measurements except for the measurements on the atria of hearts H1 and H2, the inside of the ventricle of heart H2 and the sidewall of heart H3. The parameters of the latter show large variability. The parameter R_2 belongs to the second Cole term which has a large contribution

to both the real and imaginary part of the impedance. It describes the jumps in the impedance in the high-frequency range. For the real part of the impedance this is a slight decrease and for the imaginary part of the impedance this is a slight increase in the impedance spectrum. Mainly the slight decrease in the real part of the impedance is important because this decrease flattens after ablation. According to Grimnes and Martinsen (2005) and Haemmerich et al. (2003), R_2 represents the difference between the resistance at a very low frequency (the resistance of the ECF) and the resistance at a very high frequency (R_∞) [43][67]. An increase in the value for R_2, would then indicate that the difference between these two resistances has increased by either an increase in resistance for the low frequencies, by a decrease in the resistance for the high frequencies or by a combination of the two.

t_2

The value for t_2 decreases after ablation for the measurements on all locations. This decrease led to significantly different values between healthy and ablated tissue for all measurements except for the measurements on the atria and the outside of the ventricle. Just as for parameter R_2, t_2 belongs to the second Cole term. Haemmerich et al. (2003) mention that the approximation of this parameter might be poor due to the limited frequency range [67]. However, it is interesting to investigate the physical meaning of this parameter. According to Grimnes and Martinsen (2005) t_2 represents the characteristic time constant of the tissue [43]. More specifically, this is the relaxation time constant of dipolar orientation [71]. The relaxation time represents the delayed polarization because polarization does not always occur instantaneously. The second Cole term describes the spectrum in the region where β-dispersion (10 kHz to 100 MHz) occurs. β-dispersion is caused by the polarization of the cell membranes and the formation of electric double layers at the membrane surfaces. Thus the decrease in t_2 might indicate that there is less polarization of the cell membranes due to damage caused by ablation.

a_2

The value for a_2 increases after ablation for all locations except for the inside of the ventricle of heart H2. This increase led to significantly different values between healthy and ablated tissue for all measurements except for the inside of the ventricle and atrium of heart H2 and the outside of the ventricle of heart H3. Just as for parameters R_2 and t_2, a_2 belongs to the second Cole term. There are very divergent meanings given to this parameter. Haemmerich et al. (2013) mention that it is a distribution parameter that accounts for the distribution of relaxation times. The higher the value, the larger the spread in relaxation frequencies. Furthermore, they mention that a_2 might give a poor approximation due to the limited frequency range [67]. Grimnes and Martinsen (2005) mention that it is just a constant [43]. While González-Correa et al. (2019) mention that a_2 indicates the imperfections of the cell membrane [72]. So there is not one clear physical meaning that can be given to this parameter.

Classification evaluation

The formula on which the classification is based consists of the parameters R_2 and t_2. The combination of these parameters optimizes the difference between healthy and ablated tissue. Furthermore, these parameters are chosen because they describe the deviant part of the spectrum in the high-frequency range that is associated with a change in tissue impedance. The deviant part in the low-frequency range is likely to be caused by electrode polarization and this should not be included in the classification. Therefore, the parameters of the CPE element are not included in

the classification formula. The formula lacks physical meaning as it is a random combination of model parameters. However, physical meaning is tried to be given to the separate parameters in the previous paragraphs.

Because there is an overlap between the values of healthy and ablated tissue (see figure 5.7), a trade-off had to be made between the number of false positives and the number of false negatives of the classification to set the threshold value. A false positive (healthy tissue that is indicated as ablated tissue) increases the chance of a recurrence of the AF and a need for another catheter intervention. While a false negative (ablated tissue that is indicated as healthy tissue) increases the chance of over-ablation with a risk of damaging surrounding structures and the normal electrical circuit in the heart. In a normal procedure over-ablation happens less frequently than ablation of too little tissue resulting in the returning of the arrhythmia [5][6]. Thus it is desired that the number of false positives is low because ablation of too little tissue has a quite high probability of occurrence. On the other hand, the number of false negatives must be as low as possible because a false negative can have a high impact. Therefore, the threshold value is set such that the number of false negatives and false positives are as low as possible with to a lesser extent the goal to get the number of false negatives as low as possible.

The classification results show that discrimination of healthy from ablated tissue might be possible. However, this classification serves as a first impression. A sensitivity of 84.4% indicates a high true positive rate which is desired. The specificity of 78.6% is also quite high. According to the MCC (0.629), the quality of the classification is not bad since the value is closer to *1* (indicating excellent classification) than to *0* (indicating a classification similar to random performance). These results are promising. But before implementation in a clinical application, this method should be improved further to satisfy the requirements belonging to clinical applications.

6.1.2. Research limitations

Useful results are obtained, although there are some limitations of this research that must be mentioned. First of all, the impedance measurements are performed on ex vivo porcine hearts while in the real application in vivo human hearts are measured. The differences between in vivo and ex vivo measurements e.g. the presence of blood, the tissue temperature and the level of dehydration must be taken into account when studying the results. Furthermore, the probe used for the measurements contains needle electrodes while in the real application a catheter is used. This can result in differences in the measured impedance spectra. However, for the application in this Master Thesis, the difference between healthy and ablated tissue is important and not the exact value of the impedance. Needle electrodes measure a larger contribution of healthy tissue than a catheter which makes the difference between healthy and ablated tissue less pronounced. Also, the ablation method of this Master Thesis was greatly based on the availability of equipment. An electrosurgical knife and electrosurgical generator with limited settings were used. While in reality an ablation catheter is used.

6.2. Recommendations

This section contains the recommendations for further research.

Perform experiments as in a real application
So far, the classification is performed based on data that is measured on ex vivo porcine tissue with needle electrodes and lesions created by an electrosurgical knife. This leads to differences with the real application. Therefore, it is recommended to perform future experiments that are more similar to the real application e.g. finally by performing the measurements on human heart tissue (in vivo) with an ablation catheter.

Explore the increase in impedance
In this Master Thesis, an increase in impedance is shown that was not present in other studies. Therefore, it is recommended to investigate the cause of this increase in more detail. The time interval between excision and the experiments is suspected to be one of the causes for this difference. Therefore, a recommendation would be to start with performing multiple measurements at different times after excision. This way, the influence of the lack of blood flow and dehydration on the measurements can be studied. The increase can also be caused by the measurement and ablation methods. Therefore, it is recommended to compare different measurement methods i.e. measurements performed with an ablation catheter and in a two-electrode configuration and different ablation methods i.e. ablation with an ablation catheter and an electrosurgical knife.

Investigate the limitations of the parametric model
In this research, the parametric model has been able to accurately describe most impedance spectra. However, for deviating spectra the model fit gets less optimal. Therefore, the limitations of the parametric model should be investigated in more detail. Also, the CPE model should be verified as an accurate measure for the description of the electrode polarization, to make sure that the correct amount of electrode polarization is described and removed. Lastly, the physical meaning of the model parameters must be investigated in more detail.

Improve the classification method
This thesis gives a promising first impression of the possibilities offered by a classification based on model parameters for healthy and ablated heart tissue. A next step would be to extend this research by collecting training and validation sets. Furthermore, it is recommended to look into other classification methods. An example of an interesting method is to perform a principal component analysis (PCA).

Use the technique for other applications
The technique of this Master Thesis shows the potential to distinguish healthy from ablated heart tissue. However, it might be useful in other applications as well. For example for the distinction between tumors and healthy tissue or to distinguish nerves and blood vessels from tissue.

7

Conclusion

How can the impedance of heart tissue be modelled?

The impedance of heart tissue can be modelled by a parametric model which reduces the dimensions of a measured spectrum. Parametric models contribute to an understanding of the parameters in which the spectrum is quantified. The model fit is made using least squares optimization with the Matlab function *fminsearchbnd* that uses the Nelder-Mead Simplex algorithm. For a complete evaluation of the measured impedance spectrum, the spectrum is modeled as a series combination of an electrode polarization model and a general model. This way, the (undesired) electrode polarization impedance and the tissue impedance are accounted for, without a-priori knowledge of the exact amount of electrode polarization. Different models are investigated but there can be concluded that the overall performance is best for a series combination of a CPE model and a two-pole Cole impedance model. This model results in a low MSE for the real and imaginary part of the impedance with robust parameters and can describe a variety of spectra. In this combination, the CPE model describes the low-frequency range and the Cole impedance model mostly describes the high-frequency range. This is as expected since electrode polarization is mostly present for low frequencies. To conclude, the impedance of heart tissue can be modelled accurately by this parametric model.

Can different parts of the heart be distinguished from each other with modelling?

There are significant differences in impedance spectra and found parameter values between various locations of the heart and between similar locations of different hearts. However, these differences are not always consistent. Also, the electrode polarization contribution fluctuates over the measurements. These fluctuations are likely to be caused by variations in the tissue as other factors that can have an influence are kept constant. Due to the inconsistent differences between locations in the heart and between hearts, it is not possible to distinguish between different locations and different hearts based on the model parameters. However, this distinction is not necessary for the application of an ablation catheter. The goal of the addition of impedance to the procedure is not to distinguish between locations and hearts but to investigate the differences between healthy and ablated tissue at one specific location. Therefore, not the absolute parameter values of the heart tissue itself, but the delta in the parameter values between the healthy and ablated tissue are crucial.

How can healthy and ablated heart tissue be distinguished with modelling?

The difference between measurements before and after ablation is characterized by an increase in impedance for ablation in pure cut and fulguration mode. However, in the literature, an impedance

drop is mentioned. This difference might be caused by the ablation and measurement methods but also by the fact that the heart is measured some time after excision and by the presence of electrode polarization. The differences between the healthy and ablated measurements are mostly described by (significant) differences in the parameters of the CPE model (K and m) and the second Cole term (R_2, t_2 and a_2). The mean values of R_2 and a_2 increased after ablation, while the values of t_2, K and m decreased after ablation for most measurements. Classification of healthy and ablated tissue is made based on a formula consisting of a combination of the model parameters R_2 and t_2. With both sensitivity and specificity values of around 80%, the classification, that serves as a first impression, shows promising results. To conclude, this study shows that parametric modeling in combination with impedance spectroscopy is a promising method for the discrimination of healthy from ablated heart tissue.

Bibliography

[1] Hartstichting, Bekijk de cijfers over hart- en vaatziekten. [Online]. Available: https://www.hartstichting.nl/hart-en-vaatziekten/feiten-en-cijfers-hart-en-vaatziekten (visited on 07/13/2021).

[2] S. Colilla, A. Crow, W. Petkun, D. E. Singer, T. Simon, and X. Liu, "Estimates of current and future incidence and prevalence of atrial fibrillation in the U.S. adult population", The American journal of cardiology, vol. 112, no. 8, pp. 1142–1147, 2013.

[3] D. Fu, "Cardiac Arrhythmias: Diagnosis, Symptoms, and Treatments", Cell Biochem Biophys, vol. 73, pp. 291–296, 2015.

[4] Hartstichting, Alles over ablatie. [Online]. Available: https://www.hartstichting.nl/hart-en-vaatziekten/behandelingen/ablatie (visited on 04/26/2022).

[5] Melbourne Heart Rhythm, Atrial Fibrillation Ablation - Risks. [Online]. Available: https://www.melbourneheartrhythm.com.au/learn/procedures/13-atrial-fibrillation-ablation?start=4 (visited on 04/26/2022).

[6] J. P. Joseph and K. Rajappan, "Review Radiofrequency ablation of cardiac arrhythmias: past, present and future", QJM, vol. 105, pp. 303–314, 2012.

[7] O. Kanoun, Impedance Spectroscopy Advanced Applications: Battery Research, Bioimpedance, System Design. 2019.

[8] D. Miklavčič, N. Pavšelj, and F. X. Hart, "Electric Properties of Tissues", in Wiley Encyclopedia of Biomedical Engineering, John Wiley and Sons, Inc., 2006.

[9] T. Yamaguchi, E. Ogawa, and A. Ueno, "Short-Time Impedance Spectroscopy Using a Mode-Switching Nonsinusoidal Oscillator: Applicability to Biological Tissues and Continuous Measurement", Sensors 2021, vol. 21, no. 21, p. 6951, 2021.

[10] S. Gabriel, R. W. Lau, and C. Gabriel, "The dielectric properties of biological tissues: III. Parametric models for the dielectric spectrum of tissues", Physics in Medicine and Biology, vol. 41, no. 11, pp. 2271–2293, 1996.

[11] L. Mulder, "Literature study. models for the dielectric properties of biological tissue: A systematic review", 2021.

[12] S. Whiteman, Y. Alimi, M. Carrasco, J. Gielecki, A. Zurada, and M. Loukas, "Anatomy of the cardiac chambers: A review of the left ventricle", Translational Research in Anatomy, vol. 23, p. 100 095, 2021.

[13] S. Y. Ho, K. P. McCarthy, and F. F. Faletra, "Anatomy of the left atrium for interventional echocardiography", European Journal of Echocardiography, vol. 12, no. 10, pp. i11–i15, 2011.

[14] S. Whiteman, E. Saker, V. Courant, S. Salandy, J. Gielecki, A. Zurada, et al., "An anatomical review of the left atrium", Translational Research in Anatomy, vol. 17, p. 100 052, 2019.

[15] Mayo Clinic, Tachycardia - Symptoms and causes. [Online]. Available: https://www.mayoclinic.org/diseases-conditions/tachycardia/symptoms-causes/syc-20355127 (visited on 03/15/2021).

[16] J. Thomas, Facts and Statistics About Atrial Fibrillation. [Online]. Available: https://www.healthline.com/health/living-with-atrial-fibrillation/facts-statistics-infographic.

[17] S. Nattel, "New ideas about atrial fibrillation 50 years on", Nature, vol. 415, no. 6868, pp. 219–226, 2002.

[18] A. M. Dubin and G. F. Van Hare, "Radiofrequency Catheter Ablation: Indications and Complications", Pediatric Cardiology, vol. 21, pp. 551–556, 2000.

[19] A. Finelli, J. C. Rewcastle, and M. A. Jewett, "Cryotherapy and radiofrequency ablation: Pathophysiologic basis and laboratory studies", Current Opinion in Urology, vol. 13, no. 3, pp. 187–191, 2003.

[20] National Institute of Biomedical Imaging and Bioengineering, Magnetic Resonance Imaging (MRI). [Online]. Available: https://www.nibib.nih.gov/science-education/science-topics/magnetic-resonance-imaging-mri (visited on 03/18/2021).

[21] Q. Sha, M. Velleca, L. L. Goldstein, L. M. Boo, and K. Bains, "The Value of Intracardiac Echocardiography in Catheter Ablation of Cardiac Arrhythmias: Insights from Recent Clinical Studies", EMJ Cardiology, vol. 8, pp. 2–9, 2020.

[22] A. Tognolini, A. Al-Ahmad, P. J. Wang, H. H. Hsia, R. J. Herfkens, E. Girard, et al., "Intraprocedure Visualization of the Esophagus Using Interventional C-arm CT as Guidance for Left Atrial Radiofrequency Ablation", Academic Radiology, vol. 18, no. 7, pp. 850–857, 2011.

[23] T. K. Bera, "Bioelectrical impedance methods for noninvasive health monitoring: A review", Journal of Medical Engineering, vol. 5, pp. 1–41, 2014.

[24] J. Jossinet, "Elementary electrodynamics", Technology and Health Care, vol. 16, pp. 465–474, 2008.

[25] D. Naranjo-Hernández, J. Reina-Tosina, and M. Min, "Fundamentals, recent advances, and future challenges in bioimpedance devices for healthcare applications", Journal of Sensors, 2019.

[26] M. Manoufali, S. A. R. Naqvi, and A. M. Abbosh, "Accurate Fourth-Order Debye Model for the Head Tissues Across the 0.1-1 GHz Band Using Metaheuristic Genetic Algorithm", IEEE Journal of Electromagnetics, RF and Microwaves in Medicine and Biology, vol. 2, no. 2, pp. 79–86, 2018.

[27] M. R. Tofighi, "Interaction between electromagnetic waves and biological materials", in Healthcare and Biosensing, 2017, pp. 53–101.

[28] H. Kalvøy, "New Method for Separation of Electrode Polarization Impedance from Measured Tissue Impedance", The Open Biomedical Engineering Journal, vol. 5, no. 1, pp. 8–13, 2011.

[29] P. B. Ishai, M. S. Talary, A. Caduff, E. Levy, and Y. Feldman, "Electrode polarization in dielectric measurements: A review", Measurement Science and Technology, vol. 24, no. 10, p. 102 001, 2013.

[30] F. Bordi, C. Cametti, and T. Gili, "Reduction of the contribution of electrode polarization effects in the radiowave dielectric measurements of highly conductive biological cell suspensions", Bioelectrochemistry, vol. 54, no. 1, pp. 53–61, 2001.

[31] M. Wolf, R. Gulich, P. Lunkenheimer, and A. Loidl, "Broadband dielectric spectroscopy on human blood", Biochimica et Biophysica Acta - General Subjects, vol. 1810, no. 8, pp. 727–740, 2011.

[32] J. Zhuang, W. Ren, Y. Jing, and J. F. Kolb, "Dielectric evolution of mammalian cell membranes after exposure to pulsed electric fields", IEEE Transactions on Dielectrics and Electrical Insulation, vol. 19, no. 2, pp. 609–622, 2012.

[33] B. Sanchez, G. Vandersteen, J. Rosell-Ferrer, J. Cinca, and R. Bragos, "In-cycle myocardium tissue electrical impedance monitoring using broadband impedance spectroscopy", Annual International Conference of the IEEE Engineering in Medicine and Biology Society, vol. 2011, pp. 2518–2521, 2011.

[34] S. Gabriel, R. W. Lau, and C. Gabriel, "The dielectric properties of biological tissues: II. Measurements in the frequency range 10 Hz to 20 GHz", Physics in Medicine and Biology, vol. 41, no. 11, pp. 2251–2269, 1996.

[35] V. S. Teixeira, V. Labitzky, U. Schumacher, and W. Krautschneider, "Use of Electrical Impedance Spectroscopy to Distinguish Cancer from Normal Tissues with a Four Electrode Terminal Setup", Current Directions in Biomedical Engineering, vol. 6, no. 3, pp. 341–344, 2020.

[36] M. R. Stoneman, M. Kosempa, W. D. Gregory, C. W. Gregory, J. J. Marx, W. Mikkelson, et al., "Correction of electrode polarization contributions to the dielectric properties of normal and cancerous breast tissues at audio/radiofrequencies", Physics in medicine and biology, vol. 52, no. 22, pp. 6589–6604, 2007.

[37] C. Chassagne, E. Dubois, M. L. Jiménez, J. P. van der Ploeg, and J. van Turnhout, "Compensating for electrode polarization in dielectric spectroscopy studies of colloidal suspensions: Theoretical assessment of existing methods", Frontiers in Chemistry, vol. 4, 2016.

[38] M. Mrozowski and M. A. Stuchly, "Parameterization of media dispersive properties for FDTD", IEEE Transactions on Antennas and Propagation, vol. 45, no. 9, pp. 1438–1439, 1997.

[39] N. Simicevic and D. T. Haynie, "FDTD simulation of exposure of biological material to electromagnetic nanopulses", Physics in Medicine and Biology, vol. 50, no. 2, p. 347, 2005.

[40] J. Clegg and M. P. Robinson, "A genetic algorithm for optimizing multi-pole Debye models of tissue dielectric properties", Physics in Medicine and Biology, vol. 57, no. 19, pp. 6227–6243, 2012.

[41] P. Bhardwaj, D. V. Rai, M. L. Garg, and B. P. Mohanty, "Potential of electrical impedance spectroscopy to differentiate between healthy and osteopenic bone", Clinical Biomechanics, vol. 57, pp. 81–88, 2018.

[42] V. Raicu, “Dielectric dispersion of biological matter: model combining Debye-type and "universal"responses”, Phys Rev E Stat Phys Plasmas Fluids Relat Interdiscip Topics, vol. 60, no. 4 Pt B, pp. 4677–4680, 1999.

[43] S. Grimnes and Ø. G. Martinsen, “Cole electrical impedance model - A critique and an alternative”, IEEE Transactions on Biomedical Engineering, vol. 52, no. 1, pp. 132–135, 2005.

[44] A. Ivorra, M. Genescà, A. Sola, L. Palacios, R. Villa, G. Hotter, et al., “Bioimpedance dispersion width as a parameter to monitor living tissues”, Physiological Measurement, vol. 26, no. 2, 2005.

[45] Y. Ulgen and M. Sezdi, “Hematocrit dependence of the Cole-Cole parameters of human blood”, Proceedings of the International Conference on Biomedical Engineering Days, pp. 71–74, 1998.

[46] A. Zhbanov and S. Yang, “Electrochemical impedance spectroscopy of blood for sensitive detection of blood hematocrit, sedimentation and dielectric properties”, Analytical Methods, vol. 9, no. 22, pp. 3302–3313, 2017.

[47] N. Brunel and M. C. Van Rossum, “Quantitative investigations of electrical nerve excitation treated as polarization”, Biological Cybernetics, vol. 97, pp. 341–349, 2007.

[48] K. N. Bocan, M. H. Mickle, and E. Sejdic, “Multi-Disciplinary Challenges in Tissue Modeling for Wireless Electromagnetic Powering: A Review”, IEEE Sensors Journal, vol. 17, no. 20, pp. 6498–6509, 2017.

[49] H. P. Schwan, “Linear and nonlinear electrode polarization and biological materials”, Annals of Biomedical Engineering, vol. 20, no. 3, pp. 269–288, 1992.

[50] G. Yoon, “Dielectric properties of glucose in bulk aqueous solutions: Influence of electrode polarization and modeling”, Biosensors and Bioelectronics, vol. 26, no. 5, pp. 2347–2353, 2011.

[51] T. J. Freeborn, “A survey of fractional-order circuit models for biology and biomedicine”, IEEE Journal on Emerging and Selected Topics in Circuits and Systems, vol. 3, no. 3, pp. 416–424, 2013.

[52] D. Ayllon, F. Seoane, and R. Gil-Pita, “Cole equation and parameter estimation from electrical bioimpedance spectroscopy measurements - A comparative study”, Proceedings of the 31st Annual International Conference of the IEEE Engineering in Medicine and Biology Society, 2009, pp. 3779–3782.

[53] Y. Yang, W. Ni, Q. Sun, H. Wen, and Z. Teng, “Improved Cole parameter extraction based on the least absolute deviation method”, Physiological Measurement, vol. 34, no. 10, p. 1239, 2013.

[54] J. A. Nelder and R. Mead, “A Simplex Method for Function Minimization”, The Computer Journal, vol. 7, no. 4, pp. 308–313, 1965.

[55] K. I. M. McKinnon, “Convergence of the Nelder–Mead Simplex Method to a Nonstationary Point”, SIAM Journal on Optimization, vol. 9, no. 1, pp. 148–158, 2006.

[56] MathWorks Benelux, Equation Solving Algorithms. [Online]. Available: `https://nl.mathworks.com/help/optim/ug/equation-solving-algorithms.html` (visited on 04/06/2022).

[57] M. I. A Lourakis, “A Brief Description of the Levenberg-Marquardt Algorithm Implemened by levmar”, Foundation of Research and Technology, 2005.

[58] P. Luik, “DESIGN OF A CARDIAC PHANTOM”, Master’s thesis, Technical University of Delft, 2020.

[59] D. Chicco and G. Jurman, “The advantages of the Matthews correlation coefficient (MCC) over F1 score and accuracy in binary classification evaluation”, BMC Genomics, vol. 21, no. 1, pp. 1–13, 2020.

[60] B. H. Hendriks, A. J. Balthasar, G. W. Lucassen, M. Voort, M. Mueller, V. V. Pully, et al., “Nerve detection with optical spectroscopy for regional anesthesia procedures”, Journal of Translational Medicine, vol. 13, no. 1, pp. 1–11, 2015.

[61] H. Sanabria and J. H. Miller, “Relaxation processes due to the electrode-electrolyte interface in ionic solutions”, Physical Review. E, Statistical, Nonlinear, and Soft Matter Physics, vol. 74, no. 5, 2006.

[62] S. Salahuddin, A. L. Gioia, A. Shahzad, M. A. Elahi, A. Kumar, D. Kilroy, et al., “Demonstration of dielectric heterogeneity of previously assumed homogeneous tissues: Examination of the heart”, in 12th European Conference on Antennas and Propagation, 2018, pp. 1–5.

[63] C. T. Leondes, “Frequency Variation Techniques in Electrical Impedance Tomography”, in Computational Methods in Biophysics, Biomaterials, Biotechnology and Medical Systems. Springer, US, 2002, pp. 1177–1199.

[64] D. Haemmerich, D. Schutt, A. Wright, J. G. Webster, and D. M. Mahvi, “Electrical conductivity measurement of excised human metastatic liver tumours before and after thermal ablation”, Physiological Measurement, vol. 30, no. 5, pp. 459–466, 2010.

[65] C. A. Martin, R. Martin, P. R. Gajendragadkar, P. Maury, M. Takigawa, G. Cheniti, et al., “First clinical use of novel ablation catheter incorporating local impedance data”, Journal of Cardiovascular Electrophysiology, vol. 29, no. 9, pp. 1197–1206, 2018.

[66] M. Das, A. Luik, E. Shepherd, M. Sulkin, J. Laughner, T. Oesterlein, et al., “Local catheter impedance drop during pulmonary vein isolation predicts acute conduction block in patients with paroxysmal atrial fibrillation: initial results of the LOCALIZE clinical trial”, EP Europace, vol. 23, no. 7, p. 1042, 2021.

[67] D. Haemmerich, S. T. Staelin, J. Z. Tsai, S. Tungjitkusolmun, D. M. Mahvi, and J. G. Webster, “In vivo electrical conductivity of hepatic tumours”, Physiological Measurement, vol. 24, no. 2, p. 251, 2003.

[68] D. E. Haines and A. F. Verow, “Observations on electrode-tissue interface temperature and effect on electrical impedance during radiofrequency ablation of ventricular myocardium.”, Circulation, vol. 82, no. 3, pp. 1034–1038, 1990.

[69] M. E. Ring, S. K. Huang, G. Gorman, and A. R. Graham, “Determinants of Impedance Rise During Catheter Ablation of Bovine Myocardium with Radiofrequency Energy”, Pacing and Clinical Electrophysiology, vol. 12, no. 9, pp. 1502–1513, 1989.

[70] F. H. Wittkampf and H. Nakagawa, “RF Catheter Ablation: Lessons on Lesions”, Pacing and Clinical Electrophysiology, vol. 29, no. 11, pp. 1285–1297, 2006.

[71] S. Paulson, S. Jouravleva, and C. N. McLeod, “Dielectric relaxation time spectroscopy”, IEEE Transactions on Biomedical Engineering, vol. 47, no. 11, pp. 1510–1517, 2000.

[72] C. González-Correa, E. Colina-Gallo, and D. Miranda-Mercado, “The alpha parameter of the Cole-Cole model as an indicator of fibromyalgia”, Journal of Physics: Conference Series, vol. 1272, no. 1, S507–S519, 2019.

[73] TU Delft, Installation instruction for Windows LabVIEW 2018 Pro 64-bit. [Online]. Available: `https://software.tudelft.nl/442/` (visited on 08/13/2021).

[74] IT’IS Foundation, Tissue Frequency Chart. [Online]. Available: `https://itis.swiss/virtual-population/tissue-properties/database/tissue-frequency-chart/` (visited on 11/30/2021).

[75] K. Sasaki, K. Wake, and S. Watanabe, “Development of best fit Cole-Cole parameters for measurement data from biological tissues and organs between 1 MHz and 20 GHz”, Radio Science, vol. 49, no. 7, pp. 459–472, Jul. 2014.

[76] A. K. Akobeng and A. K. Akobeng, “Understanding diagnostic tests 1: sensitivity, specificity and predictive values”, Acta Pædiatrica, vol. 96, no. 3, pp. 338–341, 2007.

A

Installation of Labview

For the impedance measurements that are performed during this Master Thesis, the 4192A LF HP impedance analyzer is used. To extract the desired data from the impedance analyzer to a laptop, the software LabVIEW 2018 is used. LabVIEW is a graphical programming tool that can be used in combination with a DAQ hardware device. For this combination to work, LabVIEW and the NI-DAQmx driver must be installed. In this appendix, the installation of LabVIEW 2018 is written out step by step.

For students from the TU Delft LabVIEW 2018 is freely downloadable from the TU Delft Software webpage. Follow the instructions of the LabVIEW 2018 instruction manual that is available by the download itself [73]. The steps that are described in this manual are [73]:

1. Extract LabVIEW 2018 on a laptop and open the folder *LV32* or *LV64* depending on the operating system of the laptop,
2. Run the *setup.exe* file,
3. Click *Decline Support* when there is asked to install *Hardware Support*,
4. Enter the NI account in the NI Licensing Wizard that pops up,
5. Restart the laptop,
6. Open the *NI-DAQmx* folder and run *setup.exe*,
7. Follow the instructions and leave the settings at default,
8. Restart the laptop,
9. Download the NI-488.2 software package. It can be found online on www.ni.com or by googling NI-488 download,
10. The installation of LabVIEW 2018 is finished.

The DAQ hardware device (impedance analyzer) is connected to a laptop via a USB port. An error as in figure A.1a can occur due to an unrecognized connection port. Step 10, (downloading the NI-488.2 software package) should prevent this error from occurring. To check whether the package is downloaded, open NI MAX (My System - Measurement and Automation Explorer) and check if the package is visible under 'Software', as can be seen in figure A.2. When running LabVIEW without connection to the impedance analyzer another error can occur. This error is shown in figure A.1b. Connect the laptop to the impedance analyzer to let the error disappear.

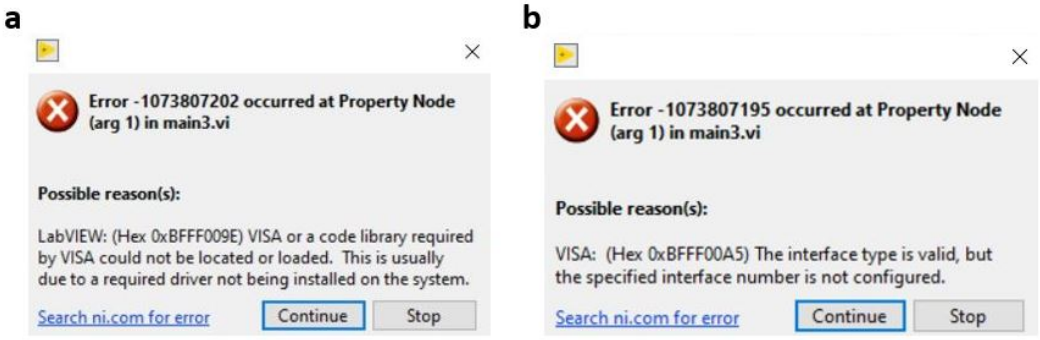

Figure A.1: Possible errors during installation of Labview: a DAQ hardware device error (**a**) and a connection error (**b**)

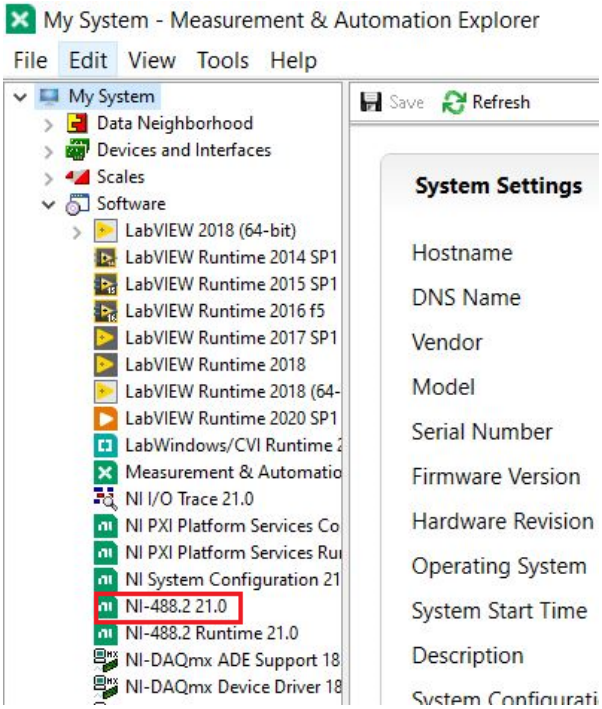

Figure A.2: NI-488.2 software package

B

Saline experiments

In this appendix, the results and main findings of the saline experiments are discussed. These experiments are performed to gain an understanding of how a reliable impedance measurement can be performed. These findings are partly used for the drafting of the methodology for repeatable measurements.

Saline is a homogeneous NaCl solution and is a very common reference liquid with strong frequency-dependent dielectric properties. Furthermore, saline can have similar dielectric properties as some biological tissues. During four identical experiments, five saline solutions are measured. Measurements from literature act as a reference. The saline solutions are made by the dissolution of an 0.9% NaCl solution with demi water and are measured over a frequency range from 10 kHz to 1 MHz. To investigate the measurement variability due to for example differences in room temperature and preparation of the saline, the experiment is repeated four times. To investigate the repeatability of the measurements, each measurement within an experiment is conducted three times. The repeatability shows the amount of variability due to the measurement setup.

The five solutions that are measured are:

1. Solution 1: 100% demi water
2. Solution 2: 0.9% NaCl solution
3. Solution 3: 0.6% NaCl solution
4. Solution 4: 0.45% NaCl solution
5. Solution 5: 0.36% NaCl solution

First, the differences between the four experiments and an experiment in literature by Luik (2020) are investigated [58]. The results of the four experiments are shown in figure B.1. The shape of the spectra is similar to shape of the spectra of the study by Luik (2020) [58]. However, there are some remarkable differences. First of all, there are small differences in the mean conductivity values of approximately 0.1 S/m. These differences cannot be caused purely by errors in the saline concentrations because some solutions are bought. It must thus be caused by outside effects such as room temperature or by the way that the measurements are performed. Secondly, the graphs of experiment 2 are different in the low-frequency range than for the other experiments. The difference is also more pronounced for higher saline concentrations. Electrode polarization and cleaning of the electrodes might be one of the causes since electrode polarization is more pronounced in samples

with higher conductivity. Lastly, the data of the imaginary part of the impedance overlap for all five solutions. A reason for the overlap can be the visualization of the data and the insecurities in the low-frequency range.

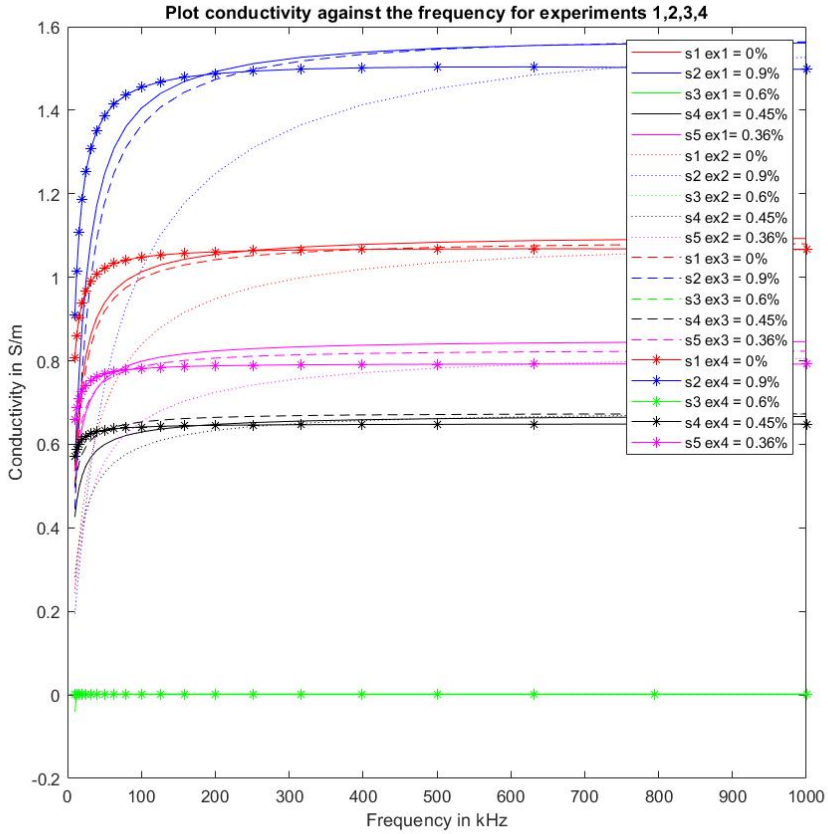

Figure B.1: Conductivity data from saline experiments 1 to 4 for all solutions. In the legend, s stands for the type of solution (1-5) and experiment stands for the number of the experiment (1-4)

In the final application, not the absolute conductivity or impedance values of the heart tissue are important, but the differences between different tissue types during one experiment. Therefore, the repeatability of the measurements is important and this is investigated such that the differences within one experiment are limited. To do so, measurements are performed in a different way than standard. Three factors are changed during the measurements of the five different solutions and each type of measurement is repeated five times. It is important to take into account that there are more influences on the measurements than the factors that are changed during these experiments. The factors that are changed are: measurement by hand or from a stable position, measuring position in the cup and electrode-solution contact. The measuring conditions are displayed in figure B.2.

The first conclusion that can be drawn is that measurements performed from a stable position show more similar results than measurements that are performed by hand (see figures B.2a and B.2b). For the repeatability of the measurements, it is best to perform the measurements from a stable position. Secondly, the influence of the measuring position is tested by placing the probe in the middle of the cup and at the edge of the cup (see figures B.2c and B.2d). The differences between these two

positions are very small. Thirdly, the contact of the electrodes with the solution was changed. In all previously discussed measurements, there is assumed that the complete electrode is in contact with the solution. Incomplete electrode contact results in differences in the measured impedance spectra. It is therefore important that the complete electrodes are in contact with the sample.

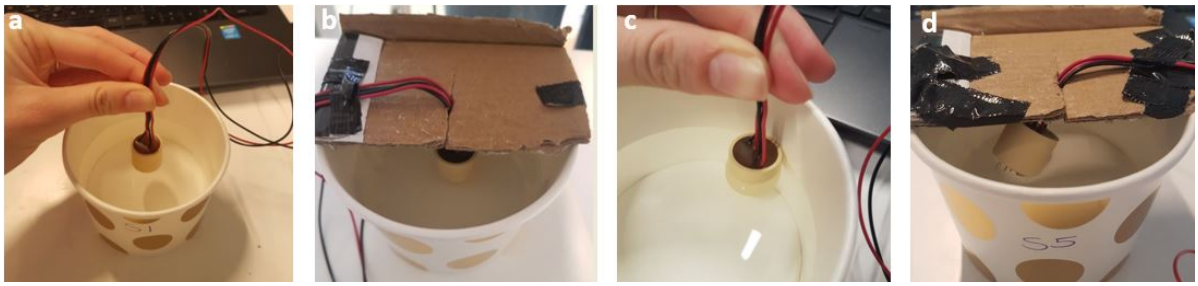

Figure B.2: Different measurement conditions on saline solutions: measurement performed by hand (**a**), measurement performed from a stable position (**b**), measurement performed at the edge of the cup (**c**) and measurement performed with the electrodes partly in contact with the solution (**d**)

C

Tofu experiments

In this appendix, the results and main findings of the tofu experiments are discussed. These findings are partly used for the drafting of the methodology for repeatable measurements. The goal of these measurements is to get familiar with the measurement setup and to test the repeatability of the impedance measurements. This is a follow-up on the saline measurements.

Tofu (AH Biologisch Vegan tofu naturel) is used as this is a solid and mostly homogeneous medium. This makes it more comparable to the measurements of heart tissue than a saline solution. A homogeneous medium is used to make sure that inhomogeneities do not cause any differences in the measurement results. The influence of several factors on the repeatability of impedance measurements is investigated. The investigated factors are: fixation of the probe (including electrode-sample contact), removal of the probe in between the measurements and the height of the measured sample. It is important to note that there are more influences on the impedance measurements than the factors that are changed during these experiments. Each measurement is repeated 10 times. The measurements are performed in agreement with the methods explained in the methodology (chapter 3) and over a frequency range from 100 Hz to 1 MHz, 51 samples are taken.

The way the probe is fixated during measurements influenced the saline measurements. Measurements from a stable position had a smaller variation than measurements performed by hand. Measurements on tofu are performed from three positions. The first (default) position, is a position where the electrodes are placed in the tofu and the cables are supported such that the probe stays in the same place (figure C.1a). Secondly, the electrodes are placed in the tofu and the probe is held in position by hand (figure C.1b), no pressure is executed. Lastly, the electrodes are placed in the tofu and the cables are unsupported (figure C.1c). This results in incomplete contact between the electrodes and the tofu. Measurements performed from the first position are most repeatable. This is in agreement with the conclusion from the saline experiments. Measurements that are performed by hand can be influenced by shaking of the hand and by different amounts of pressure that are exerted on the probe. To ensure complete electrode contact in the default position, a small weight can be added.

Furthermore, the effect of the removal of the probe between the measurements is investigated. During one part of the experiment, the probe is kept in place while repeating the measurements. While during another part, the probe is removed from the tofu between the repeated measurements. The latter results in a larger variability in the measured spectra. Tofu is supposed to be homogeneous, so

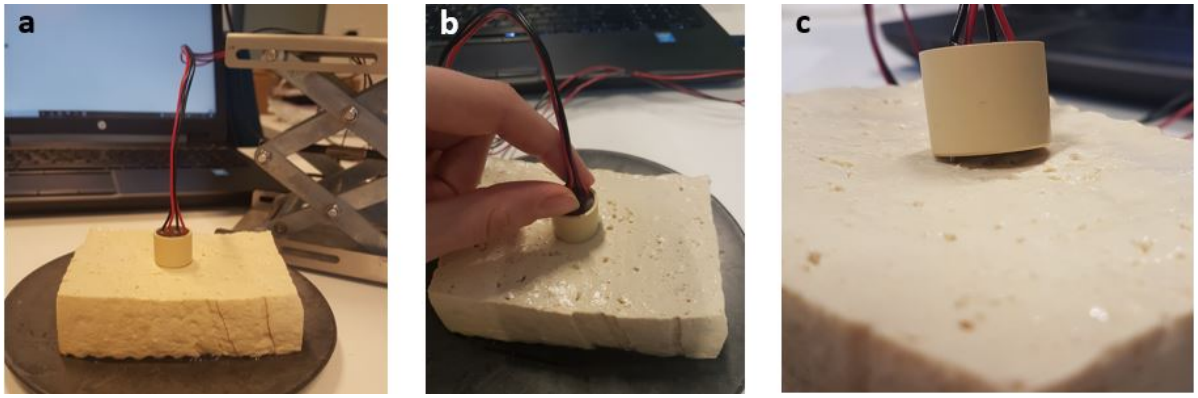

Figure C.1: Different probe fixations during tofu measurements: measurement performed from a stable position with the cables supported (**a**), measurement performed with the probe supported by hand (**b**), measurement performed with the electrodes partly in the sample and the cables not supported (**c**)

the exact position of the measurement should not influence the results. Therefore, for the repeatability, it is better to keep the probe fixated between the measurements.

Lastly, the influence of the height of the sample on the measurement is investigated. In the previous measurements the sample height was approximately 3 cm. For the last measurements this height is reduced to 1 cm, such that the electrodes were still completely inside the tofu. As expected the repeatability of these measurements is comparable to that of part 1 (same fixation but different sample height). Although, the mean values of all variables differ a lot. This can be caused by the thin thickness of the sample but also by the loss of moisture as the two different measurements are performed at the beginning and the end of the experiment.

D

Lsqcurvefit vs fminsearchbnd

In this appendix, the trade-off between *lsqcurvefit* and *fminsearchbnd* is given. The robustness of the two functions is tested on fits of a four-pole Cole-Cole model with initial parameters that are similar to the best-fit parameters provided by Gabriel (1996) [10]. The fit is performed on data that is provided by the IT'IS foundation [74]. Firstly, noise is added to the measurement data. Secondly, the initial parameters are changed.

An addition of 2% noise to the data leads to a deviation of the fit in the high-frequency range. Resulting in an MSE of $1.03 \cdot 10^4$ when the fit is performed with *lsqcurvefit* (see figure D.1). When the function *fminsearchbnd* is used with a similar merit function this results in an MSE of $5.87 \cdot 10^2$ (see figure D.2). The upper bounds of α influence the fit, for the previous fits the upper bounds are set at ∞. When the upper bounds of the exponents are set at 1, this results in a less accurate fit. This difference is larger for *lsqcurvefit* than for *fminsearchbnd*.

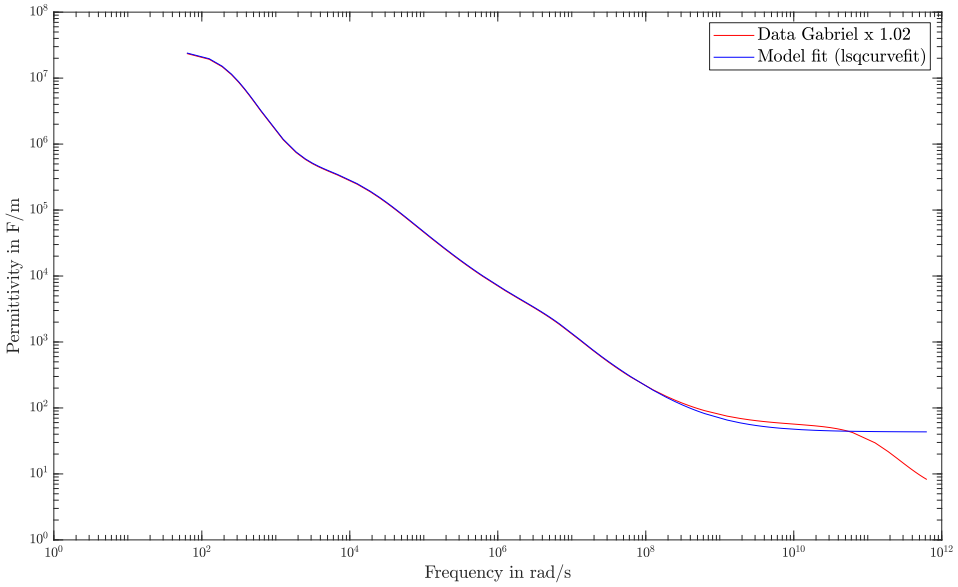

Figure D.1: The fit of a 4 pole Cole-Cole model to the permittivity data of the heart muscle measured by Gabriel with 2% noise added, with lsqcurvefit and all upper bounds set to infinity

Changing the initial parameters by a multiplication of 0.85 leads to a less accurate fit. Resulting in an MSE of $1.86 \cdot 10^{12}$ for the function *lsqcurvefit*. For *fminsearchbnd* with a similar merit function

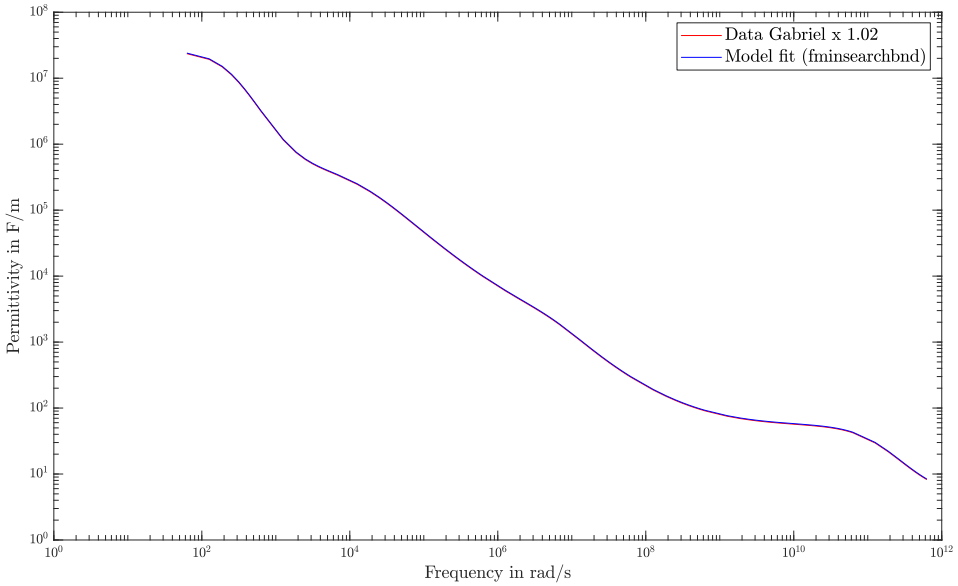

Figure D.2: The fit of a 4 pole Cole-Cole model to the permittivity data of the heart muscle measured by Gabriel with 2% noise added, with fminsearchbnd and all upper bounds set to infinity

the MSE is $1.30 \cdot 10^5$.

From these two disturbances, there can be concluded that the fits with *fminsearchbnd* are more robust than the fits with *lsqcurvefit*. This is the case for similar merit functions. Still, the *fminsearchbnd* function is sensitive to noise and changes in the values of the initial parameters. Changing the algorithm for *lsqcurvefit* from trust-region-reflective to Levenberg-Marquardt does not influence the fit. Another advantage of *fminsearchbnd* over *lsqcurvefit* is that the merit function can be changed. This is not possible for *lsqcurvefit*. Changing the merit function can be useful when high values of the low-frequency range dominate the low values of the high-frequency range.

To find the best fits for both of these functions, optimal design settings must be chosen. Different design settings that can influence the fitting are for example the choice of initial parameters, the part that the least squares are taken of, the algorithm tolerances (such as the step size and the maximum number of function iterations) and the algorithm type.

E

Benchmark model fit

A benchmark fit to the data of Gabriel (1996) is performed to verify the fitting method of this Master Thesis [34]. Gabriel (1996) has performed measurements on many tissue types, among which heart tissue [34]. These measurement data and the fit with the Cole-Cole model, see figure E.1, are well documented in her articles [10]. The data can also be found online in the IT'IS database [74]. The data that is used in this chapter is extracted from this database and is similar to the data that is used in the articles of Gabriel (1996) [10][34]. As these data and the Cole-Cole model are widely used, the best fitting parameters are mentioned in some articles. Therefore, the study from Gabriel (1996) is used as a benchmark for the model fits that are performed in this thesis.

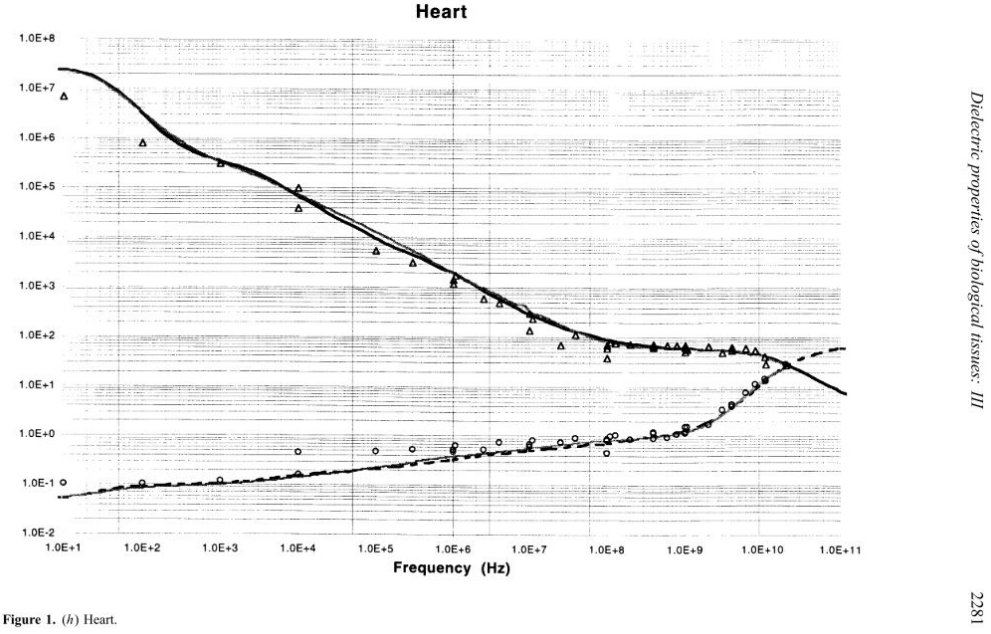

Figure E.1: The permittivity and conductivity of heart muscle against the frequency as measured by Gabriel (1996) together with a fit of the 4 pole Cole-Cole model [10]

Measurement method of Gabriel

The data of Gabriel is roughly comparable to heart data that is measured according to the methods in this Master Thesis. The data of Gabriel is measured in the frequency range from 10 Hz to 10 MHz with an HP4192A impedance analyzer. This frequency range is overlapping with the range in this

Master Thesis and the impedance analyzer used is similar. The total frequency range that Gabriel measured is larger but these are measured via different methods. An open-ended co-axial probe with sputtered platinum electrodes is used because this material moves the electrode polarization to a lower frequency. In this Master Thesis, two-needle electrodes are used. This difference influences the measured tissue area and the electrode polarization formation. Freshly excised (within two hours after death) bovine heart muscle tissue is measured in vitro. The specific places that are measured are not specified.

Effects such as electrode polarization and stray impedance are taken into account in the following way. First of all, the capacitance and conductance are normalized against the parameters of the probe measured in salt concentrations of a similar conductivity. The electrode polarization effect is said to play a role below 1 kHz and is significant below 100 Hz. However, from the EP correction method there cannot be concluded that it is completely removed. This can result in a difference in the low-frequency range between the two data sets. The values of the capacitance and conductance are also compensated for stray inductances by measurements on standard salt solutions. However, the greatest effects of these inductances are present in the MHz range.

Fit by Gabriel

Gabriel (1996) uses a four pole Cole-Cole model to describe the spectrum of heart tissue in the frequency range from 10 Hz to 100 GHz [10]. Four poles are used while there are only three main dispersions as these provide a better fit. The formula for the Cole-Cole model is shown in equation E.1. The parameter ϵ_∞ is kept at 4.0 during the fitting process because heart tissue is a high water content tissue [10]. Gabriel fits the Cole-Cole model to the measurement data by hand with the use of an Excel sheet. According to Sasaki (2014), the best-fit parameters that are calculated 'by hand' (via the Excel sheet) do not provide a good fit during a fitting method that uses a least squares method [75].

$$\hat{\epsilon} = \epsilon_\infty + \sum_{n=4} \frac{\Delta\epsilon_n}{1 + (j\omega\tau_n)^{(1-\alpha_n)}} + \frac{\sigma_i}{j\omega\epsilon_0} \tag{E.1}$$

Gabriel (1996) mentions that the fit with the Cole-Cole model can be used with high certainty in the high-frequency range [10]. But it must be used with more caution in the low-frequency range below 1 MHz. This is due to larger uncertainties in this frequency region that are caused by electrode polarization and rare literature data [10]. The following conclusions are drawn about the parameters of the Cole-Cole model by Gabriel [10]. The parameter ϵ_n is related to the water content of the tissue, whereas the α parameter is negligible for body fluids. The value for τ in tissue is higher than for pure water, which indicates that the water molecules are restricted in tissue by their environment.

Repetition of the fit

The fit is performed in accordance with the method discussed in chapter 3. The function that is used is *fminsearchbnd* with the Nelder-Mead simplex algorithm. As initial parameters, the best-fit parameter values of Gabriel are taken. This resulted in a good fit. The choice of initial parameters is very important for the correctness of the fit, even a slight change can result in a large error.

Fit over desired frequency range

The measured data of Gabriel span a frequency range from 10 Hz to 100 GHz, while the frequency range of this thesis ranges from 100 Hz to 1 MHz, see figure E.2. This range might be described

with a two or three-pole Cole-Cole model instead of one with four poles as the frequency range covers fewer dispersion regions. However, the limited frequency range can be described with a four and three-pole Cole-Cole model but not with a two-pole Cole impedance model. The models also describe the electrode polarization that is left in the impedance spectrum.

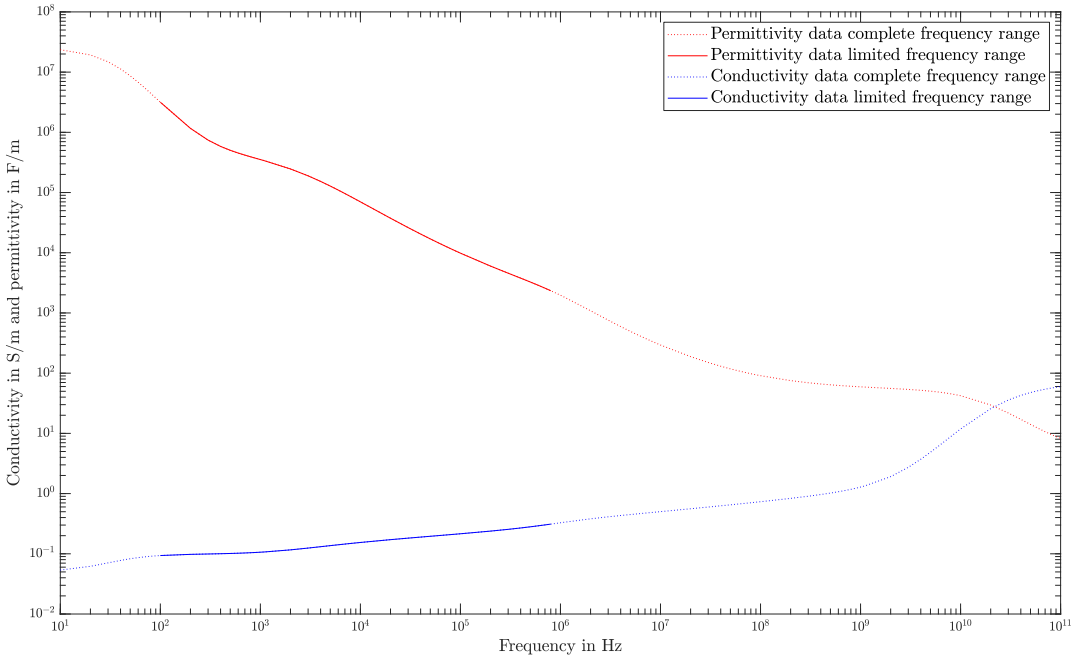

Figure E.2: Indication of the complete and limited frequency range in the data of Gabriel (1996) [10]

F

Classification measures

Measure	Formula	Explanation
PPV	$\frac{TP}{TP+FP}$	Proportion of positive predictions that are truly positive
NPV	$\frac{TN}{TN+FN}$	Proportion of negative predictions that are truly negative
Sensitivity	$\frac{TP}{TP+FN}$	Ability to correctly detect the ablated tissue
Specificity	$\frac{TN}{TN+FP}$	Ability to correctly detect healthy tissue
Accuracy	$\frac{TP+TN}{TP+TN+FP+FN}$	Ratio between the number of correctly classified samples and the total number of samples
MCC	$\frac{TP \times TN - FP \times FN}{\sqrt{(TP+FP)(TP+FN)(TN+FP)(TN+FN)}}$	A general measure for the quality of the classification

Table F.1: Overview of the measures for the evaluation of the classification performance. TP = true positive, TN = true negative, FP = false positive, FN = false negative, PPV = positive predictive value i.e. the precision, NPV = negative predictive value and MCC = Matthews correlation coefficient [59][60][76]

G

Impedance spectra for parametric model evaluation

This appendix shows the impedance spectra that are used for the evaluation of the parametric models in chapter 4.

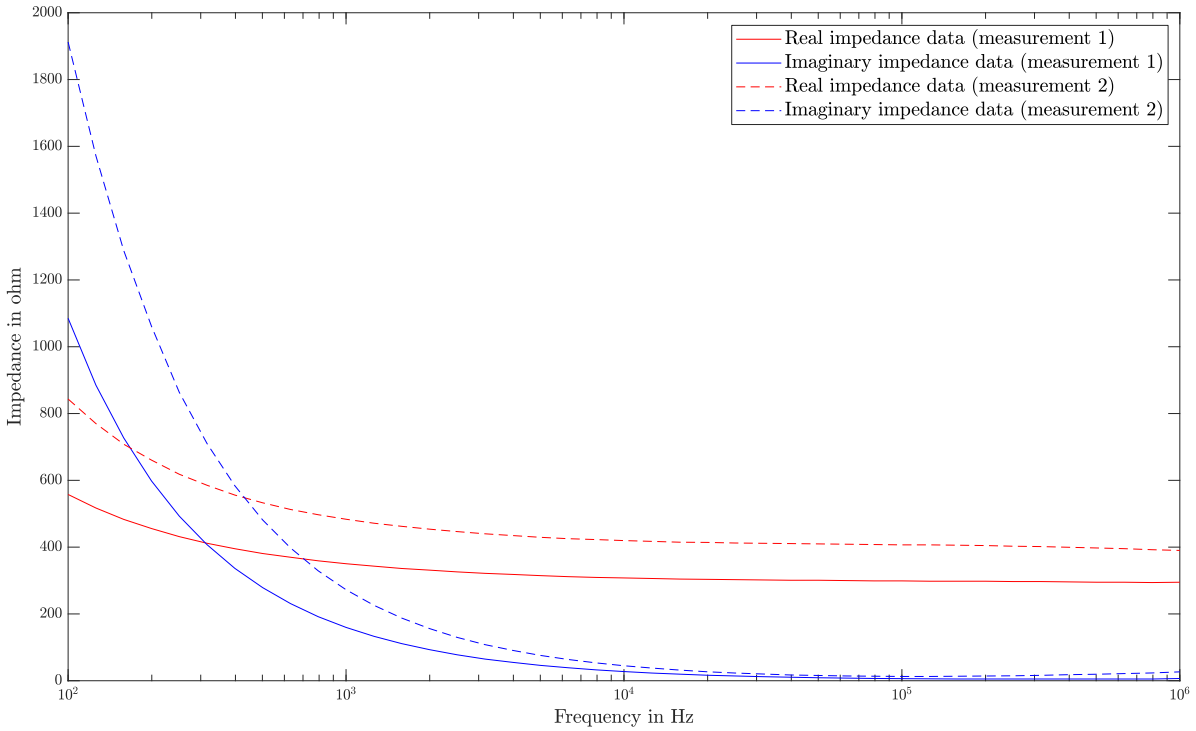

Figure G.1: Impedance spectra of measurements 1 and 2

H

Ablation depth

In this appendix, the ablation depths of the created lesions are displayed per heart in table H.1. Also, lesions created with fulguration mode and lesions created with pure cut mode are shown in figure H.1.

Heart H1

Measurement	Ablation depth	Measurement	Ablation depth	Measurement	Ablation depth
15	4mm	19	2mm	23	2mm
16	2mm	20	1mm	24	2mm
17	Superficial	21	1mm	25	Superficial
18	1mm	22	2mm		

Heart H2

Measurement	Ablation depth	Measurement	Ablation depth	Measurement	Ablation depth
11	1mm	15	2mm	19	2mm
12	1mm	16	1mm	20	Superficial
13	2mm	17	Superficial		
14	1mm	18	1mm		

Heart H3

Measurement	Ablation depth	Measurement	Ablation depth	Measurement	Ablation depth
6	2mm	8	1mm	10	5mm
7	2mm	9	2mm		

Table H.1: Ablation depths of measurement locations of hearts H1, H2 and H3

Figure H.1: Ablation effects of the fulguration (**a**) and the pure cut (**b**) modes

Results - Differences between locations

In this appendix, the results of the distinction between different locations and different hearts are displayed. This is done by a visualization of the three locations for hearts H1 and H2 per parameter in a boxplot. The three locations are the sidewall of the left ventricle (sw LV), the inside of the left ventricle (ins LV) and the inside of the left atrium (ins LA). Furthermore, the impedance spectra of the outside of the left ventricle of heart H3 are shown in comparison to spectra of the sidewall of the ventricle of the same heart.

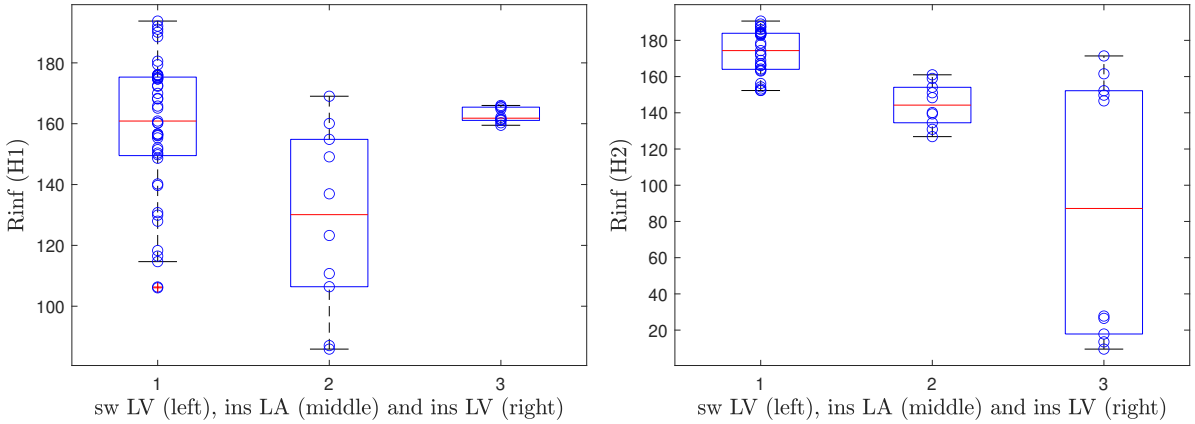

Figure I.1: Boxplots of R_∞ for the different locations of hearts H1 and H2

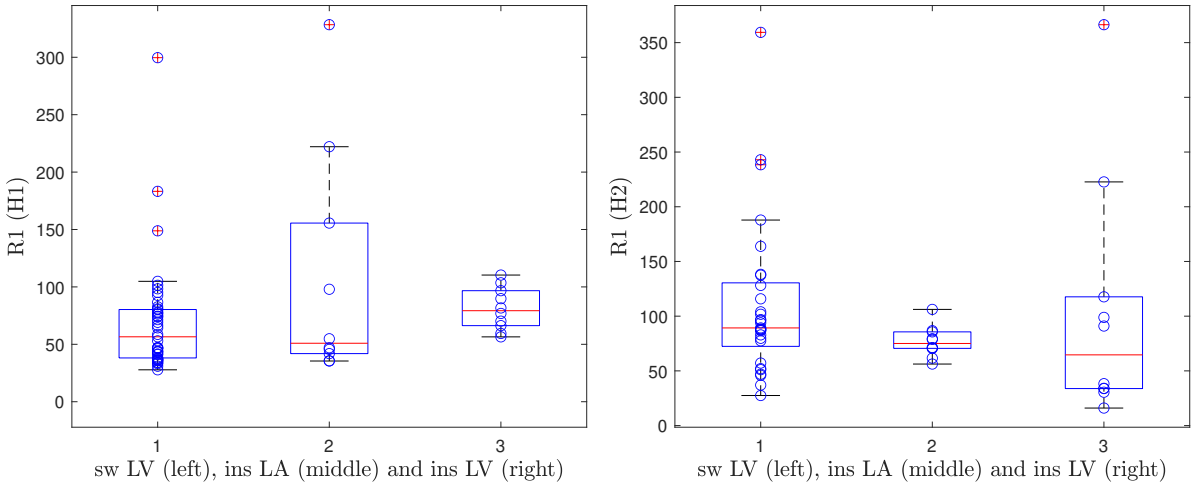

Figure I.2: Boxplots of R_1 for the different locations of hearts H1 and H2

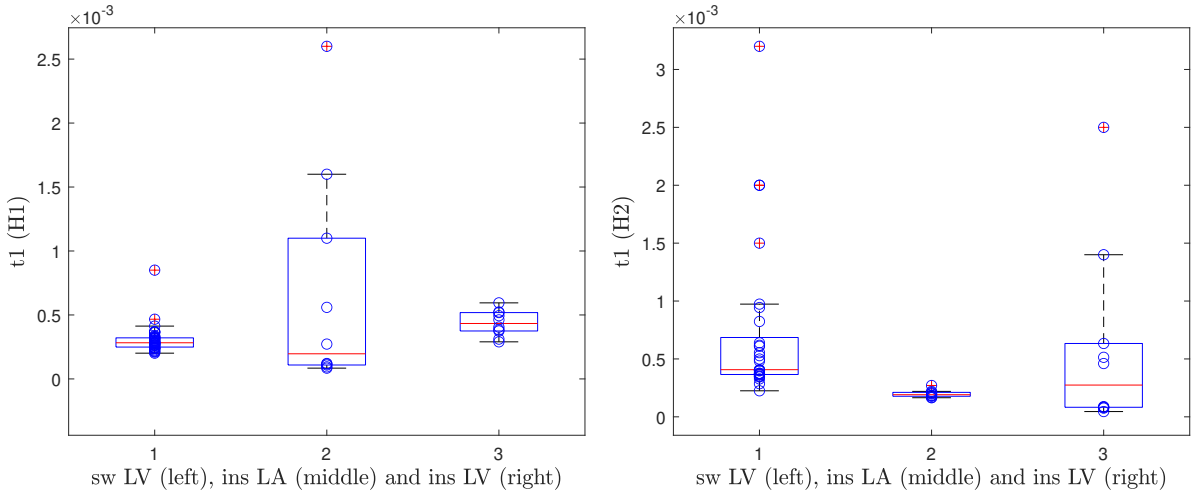

Figure I.3: Boxplots of t_1 for the different locations of hearts H1 and H2

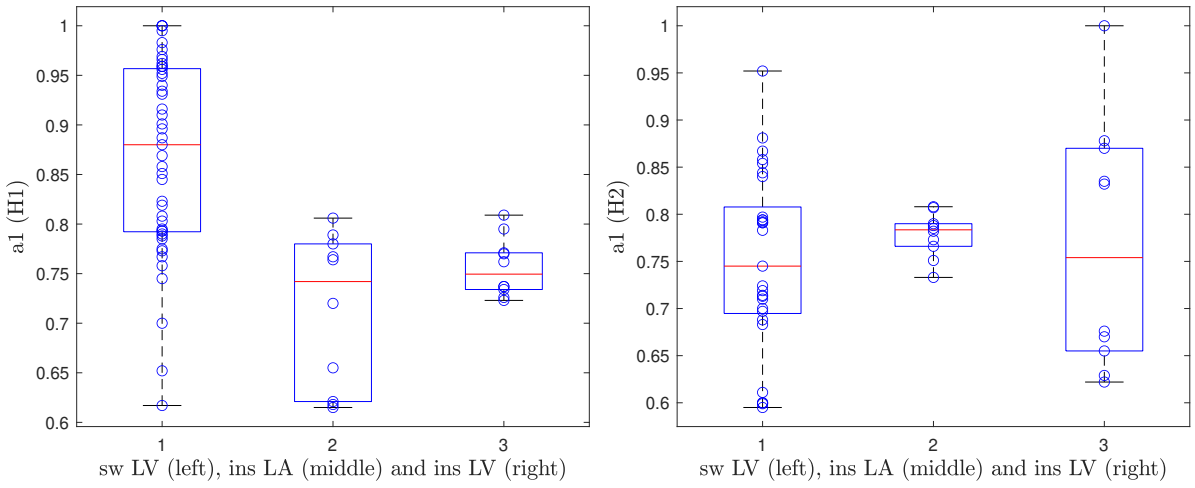

Figure I.4: Boxplots of a_1 for the different locations of hearts H1 and H2

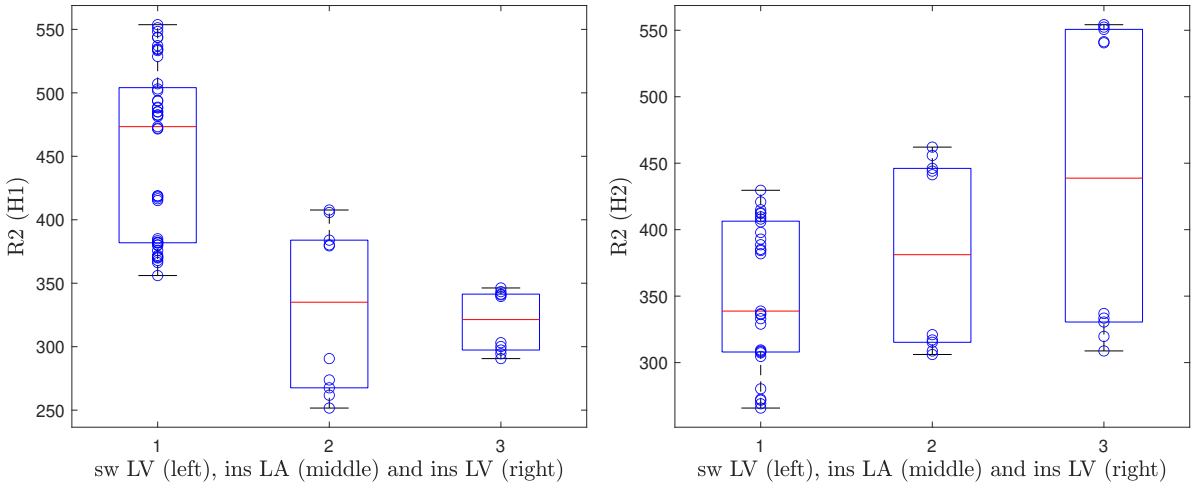

Figure I.5: Boxplots of R_2 for the different locations of hearts H1 and H2

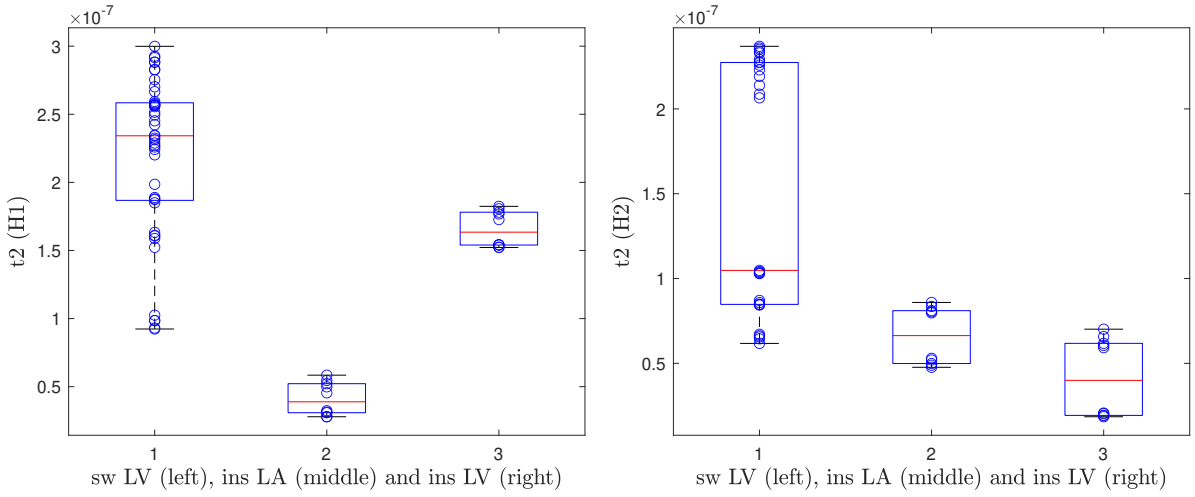

Figure I.6: Boxplots of t_2 for the different locations of hearts H1 and H2

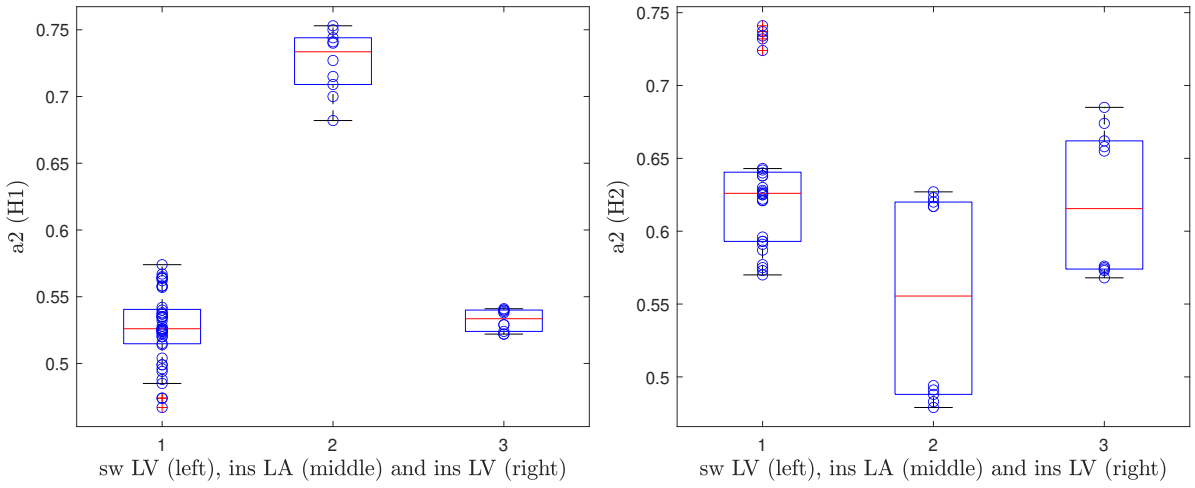

Figure I.7: Boxplots of a_2 for the different locations of hearts H1 and H2

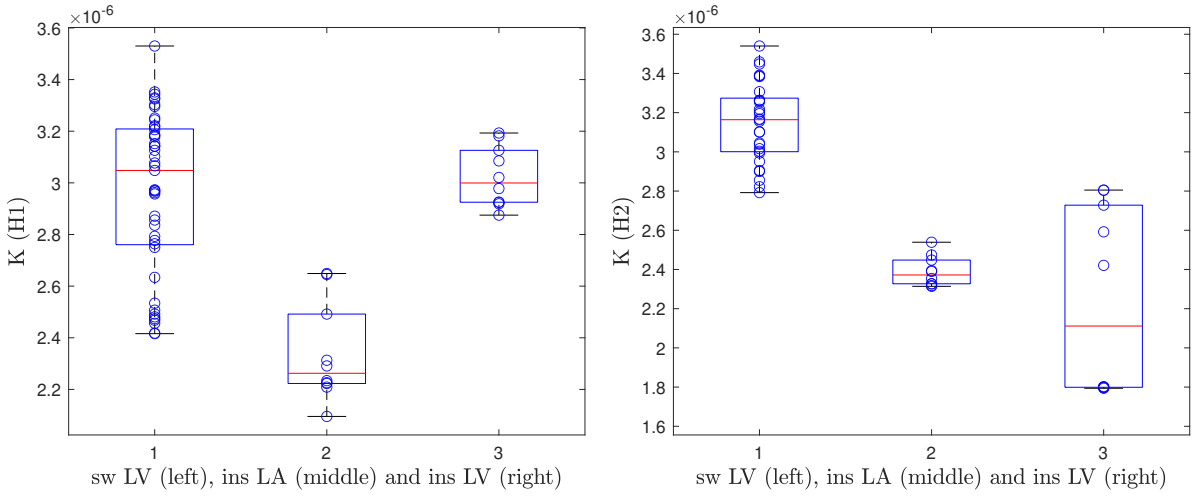

Figure I.8: Boxplots of K for the different locations of hearts H1 and H2

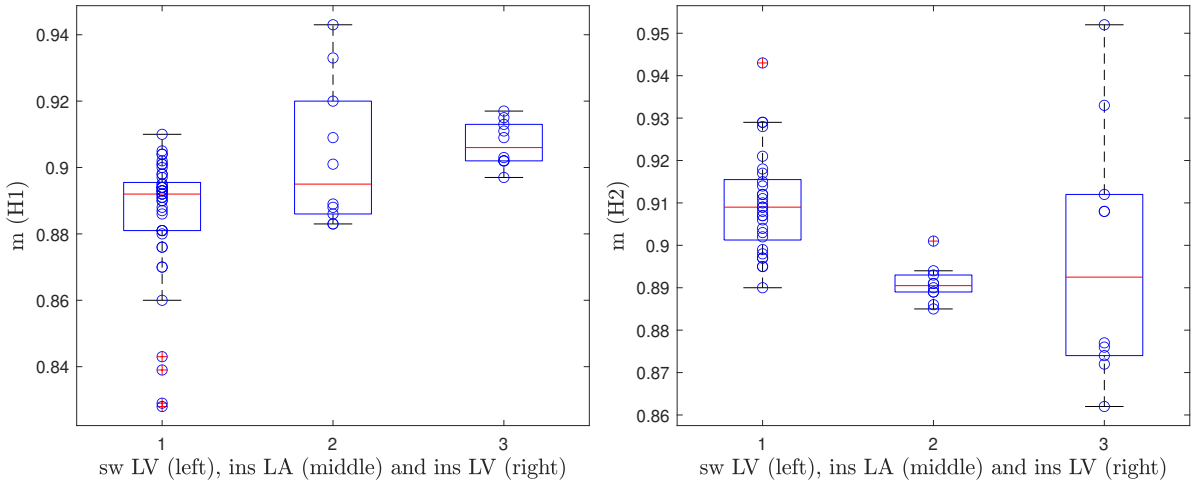

Figure I.9: Boxplots of m for the different locations of hearts H1 and H2

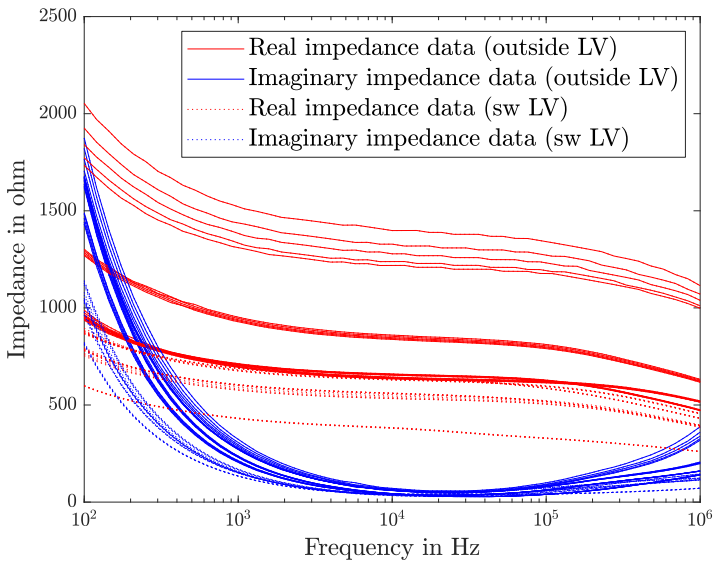

Figure I.10: Impedance spectra of the measurements on the outside of the LV of heart H3 (solid lines) and of the measurements on the sidewall of the LV of heart H3 (dotted lines)

J

Results - Differences between healthy and ablated tissue

In this appendix, the results of the distinction between healthy and ablated heart tissue are displayed. First of all, an overview of the changes in parameters before and after ablation per measurement location is given in figure J.1. Then the boxplots that display each parameter individually for both the healthy and ablated measurements are given for each measurement location. Also, the p-value of the Wilcoxon signed-rank test is indicated.

	sw H1	**sw H2**	**sw H3**	LA H1	LA H2	ins LV H1	ins LV H2	Outs LV H3
R_∞								
R_1								
t_1								
a_1								
R_2								
t_2								
a_2								
K								
m								

Figure J.1: Changes in parameters before and after ablation. An increase in parameter value after ablation is indicated in green and a decrease is indicated in red. The changes in parameter values are calculated based on the median

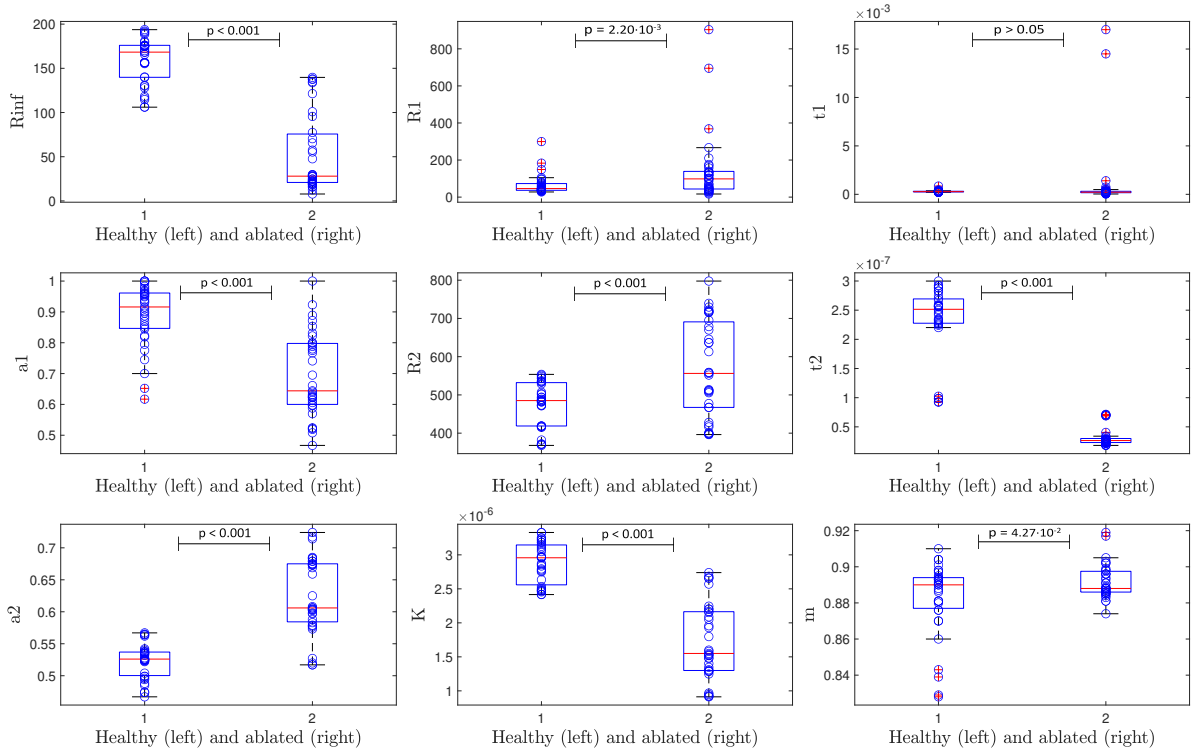

Figure J.2: Boxplots of the parameters of healthy and ablated tissue of the sidewall LV of heart H1

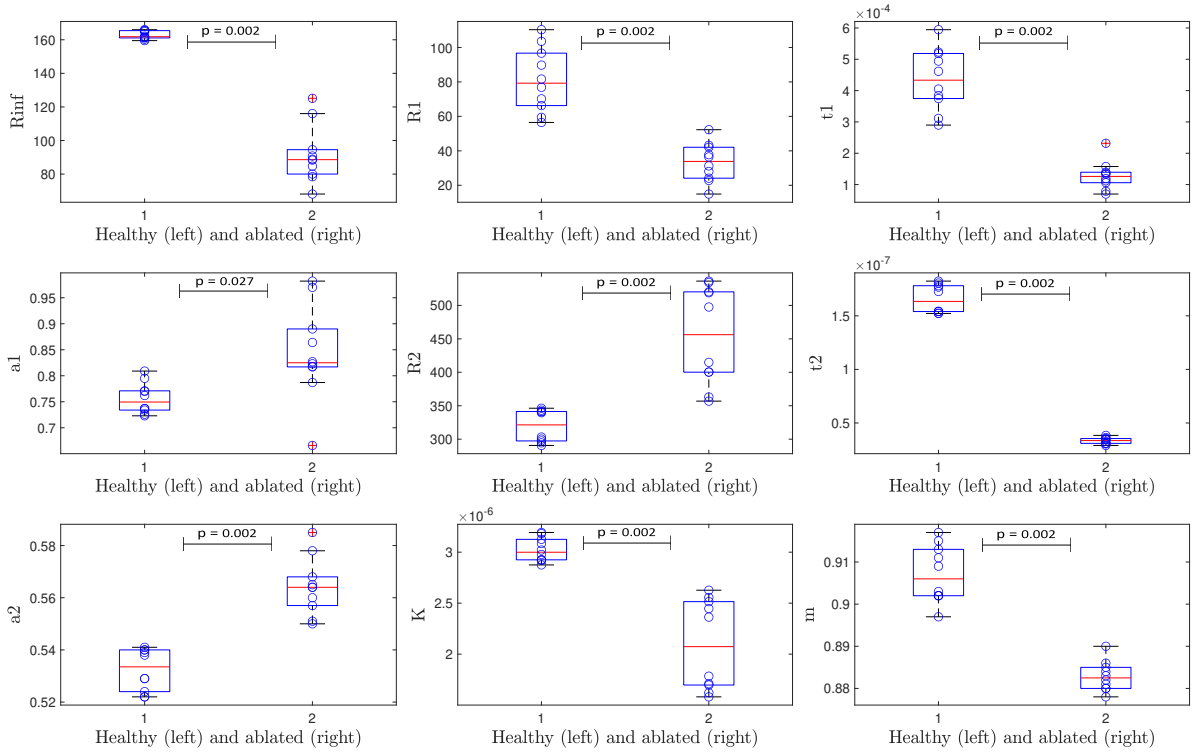

Figure J.3: Boxplots of the parameters of healthy and ablated tissue of the inside LV of heart H1

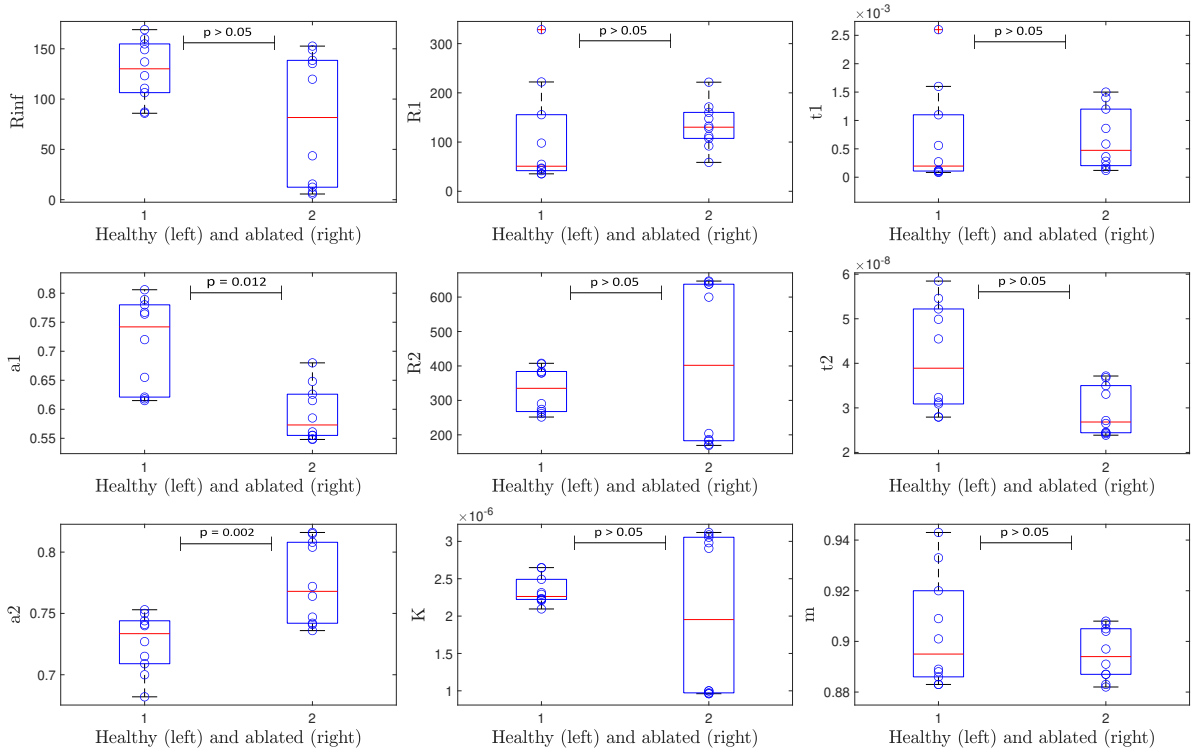

Figure J.4: Boxplots of the parameters of healthy and ablated tissue of the LA of heart H1

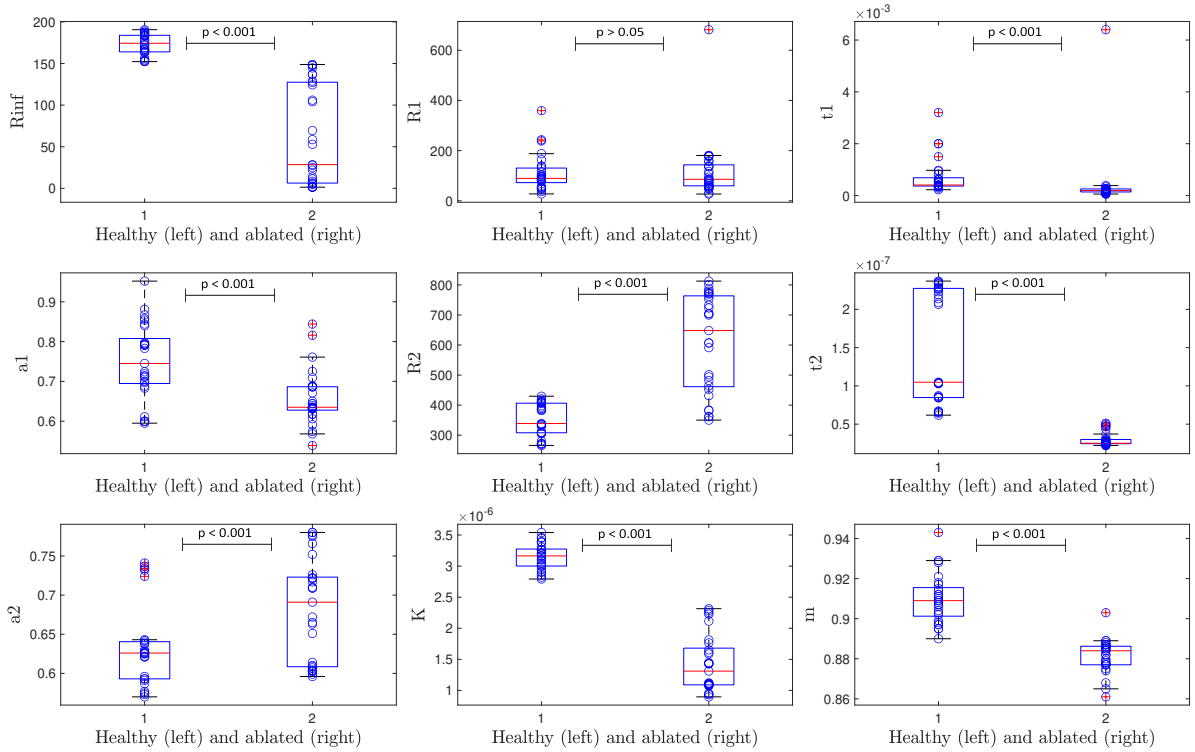

Figure J.5: Boxplots of the parameters of healthy and ablated tissue of the sidewall LV of heart H2

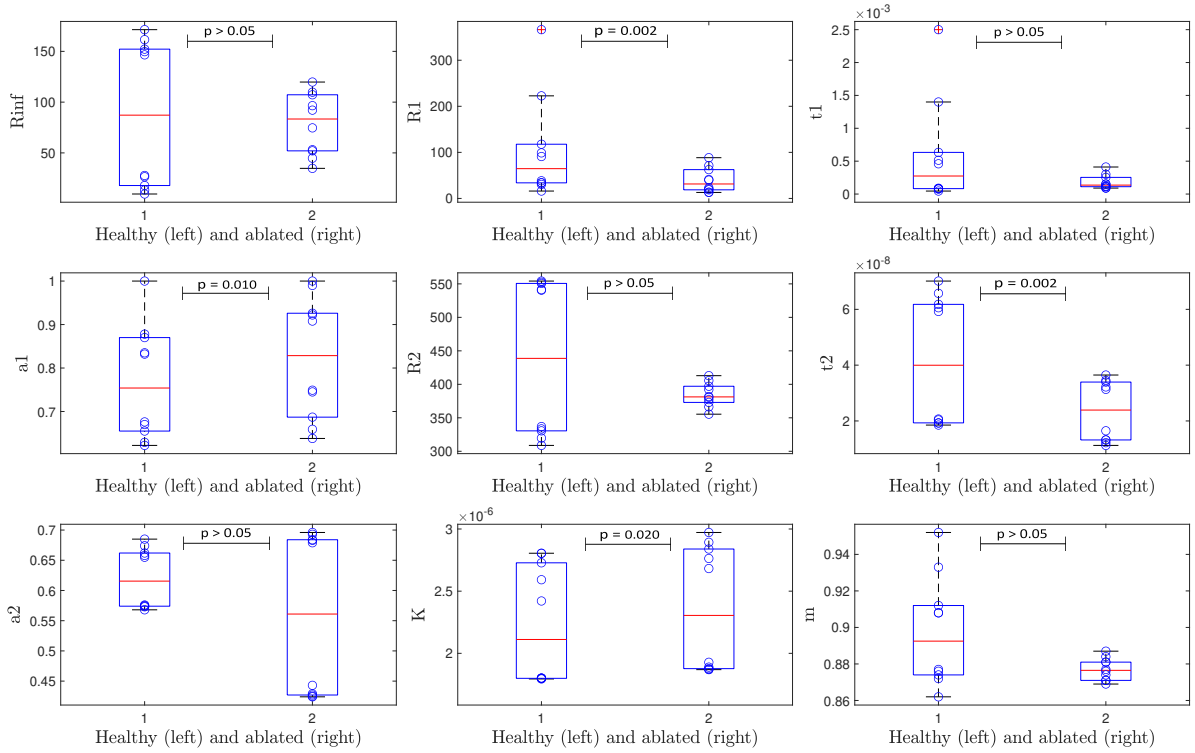

Figure J.6: Boxplots of the parameters of healthy and ablated tissue of the inside LV of heart H2

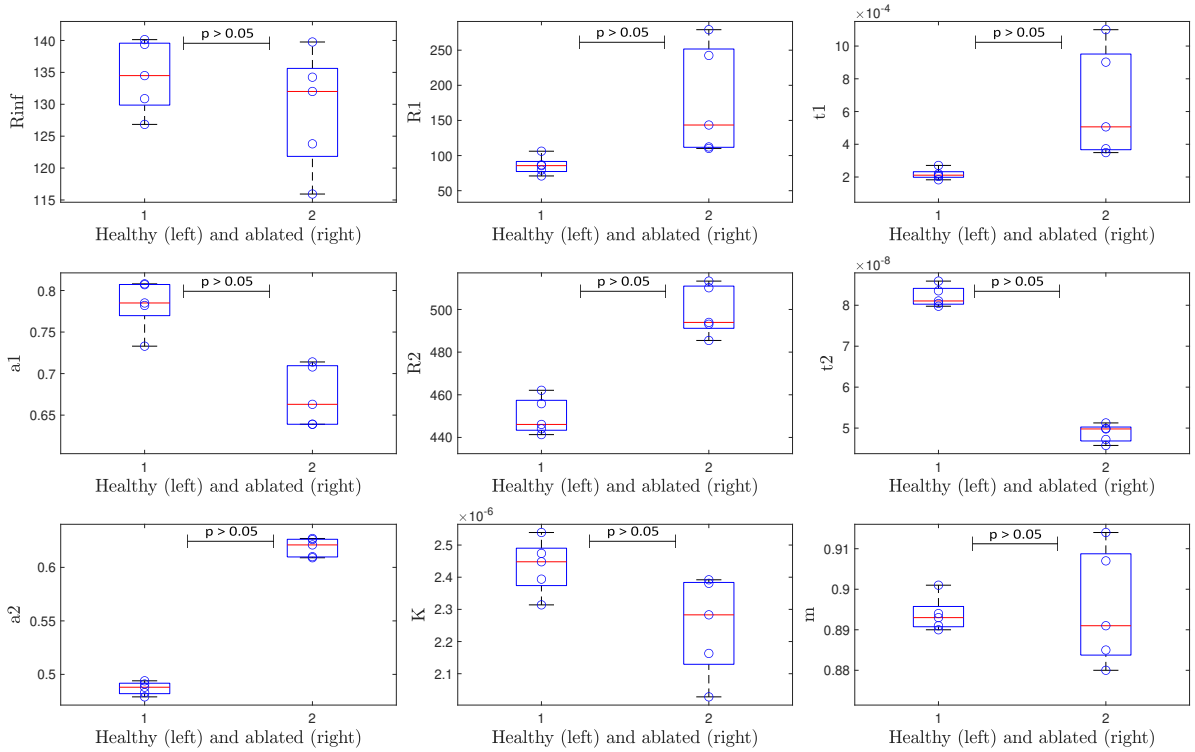

Figure J.7: Boxplots of the parameters of healthy and ablated tissue of the LA of heart H2

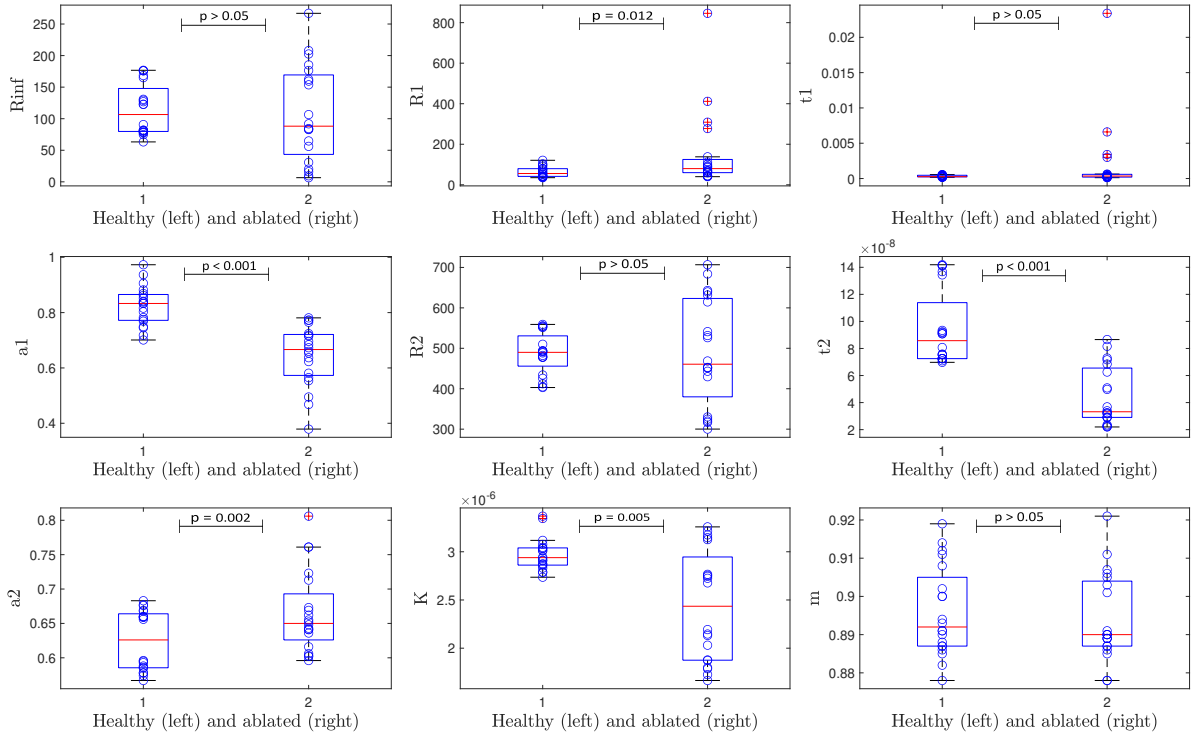

Figure J.8: Boxplots of the parameters of healthy and ablated tissue of the sidewall LV of heart H3

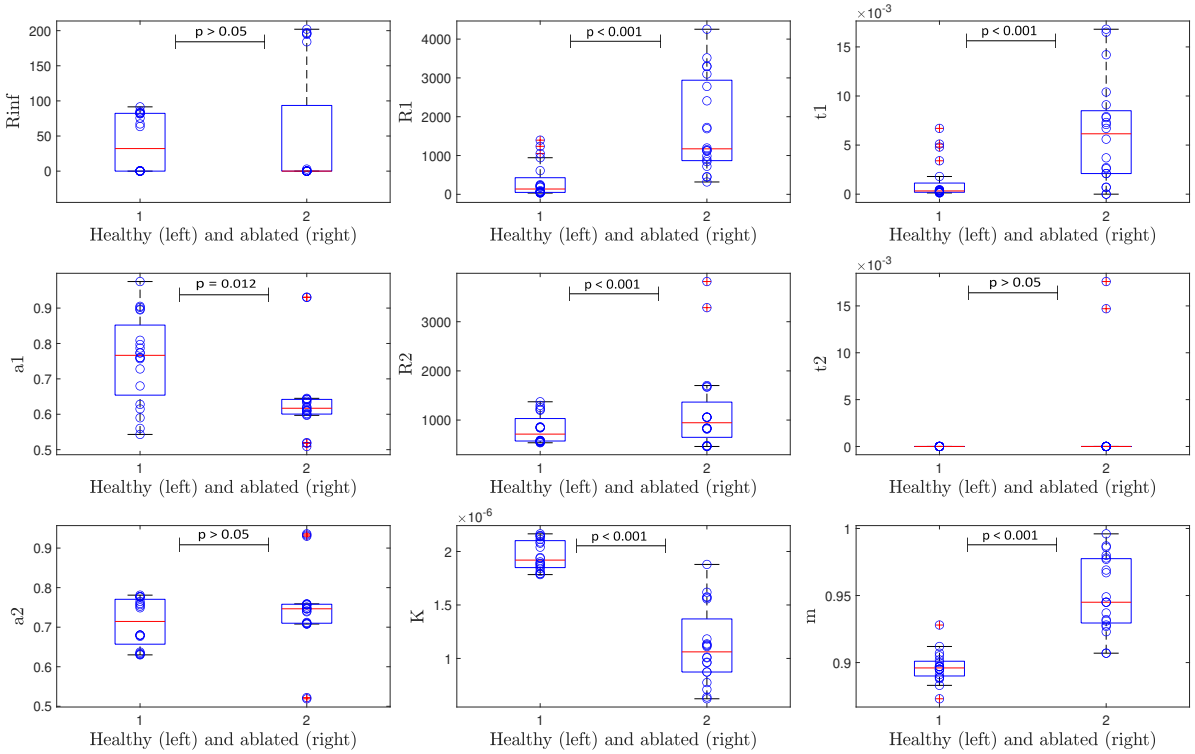

Figure J.9: Boxplots of the parameters of healthy and ablated tissue of the outside LV of heart H3

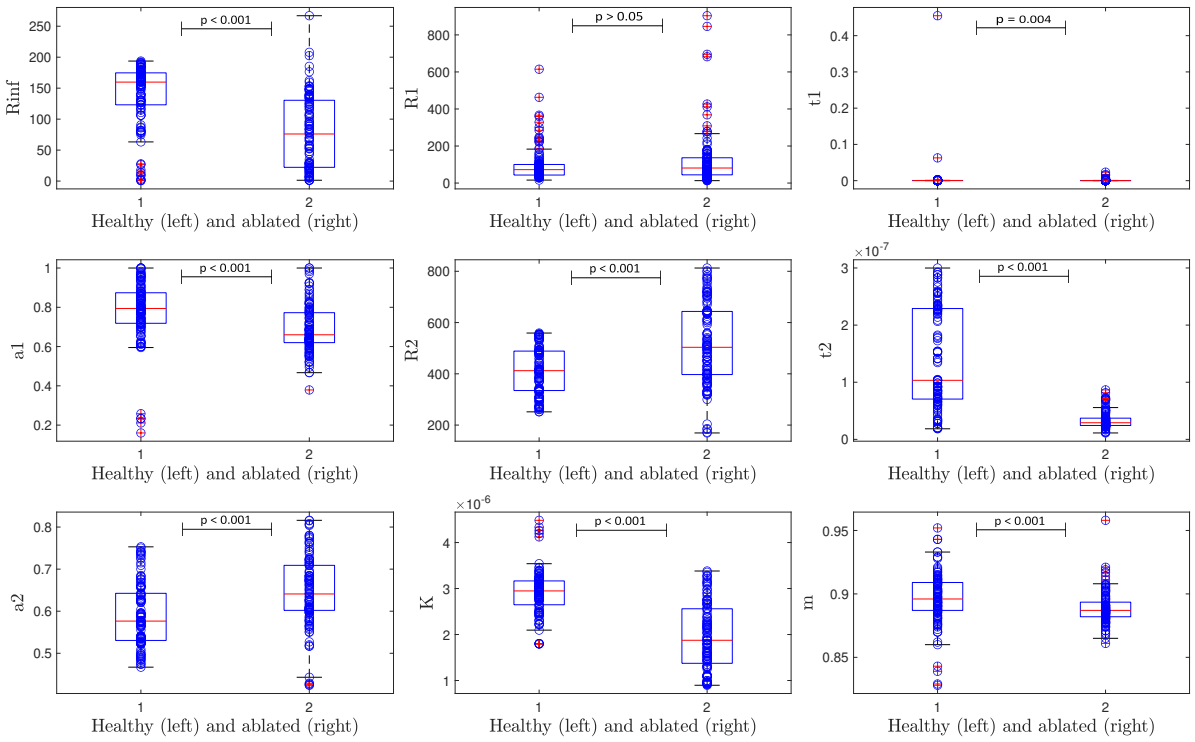

Figure J.10: Boxplots of all parameters of healthy and ablated tissue for all measurements of hearts H1, H2 and H3 (except the measurements of the outside of the LV of heart H3)